THE USE OF CHEMILUMINESCENCE FOR THE DETECTION OF TEMPERATURE AND FUEL-TO-AIR RATIO IN TURBULENT PREMIXED FLAMES

by

James E. Reaney

Thesis submitted to the Graduate Faculty of Virginia Polytechnic Institute and State University in partial fulfillment of the requirements for the degree of

MASTER OF SCIENCE
in
Mechanical Engineering

APPROVED:

Richard J. Roby,
Chairman

Walter F. O'Brien, Jr.

Larry A. Roe

August 1992
Blacksburg, Virginia

C.2

THE USE OF CHEMILUMINESCENCE FOR THE DETECTION OF TEMPERATURE AND FUEL-TO-AIR RATIO IN TURBULENT PREMIXED FLAMES

by

James E. Reaney
Committee Chairman: Dr. Richard J. Roby
Mechanical Engineering

(ABSTRACT)

A fast response method for the determination of temperature and equivalence ratio has been developed for turbulent premixed flames. This method utilizes chemiluminescent signals to make correlations with flame temperature and equivalence ratio. Emissions from two radical groups are used for the correlations: an OH system at 309 nm and a CH system at 431 nm. The experimental apparatus consists of a turbulent burner, an optical system (lenses, monochromator, and photomultiplier tube), and a data collection system (digital oscilloscope and computer). An optical system using fiber optics and band pass interference filters was also investigated. The spectra of turbulent, premixed methane flames of known stoichiometry were recorded. A high temperature Pt-Pt10%Rh thermocouple was used to establish flame temperature. The ratio of signal width to signal height of the OH spectra was used to correlate flame temperature. The ratio of OH to CH signal heights was used to correlate equivalence ratio. Turbulent correlations were compared to laminar correlations developed in previous studies. The effect of increasing turbulence on correlations was investigated. Applications for this technology and recommendations for future work are discussed.

ACKNOWLEDGEMENTS

I would like to express my gratitude to Dr. Rick Roby for providing me the opportunity to pursue graduate studies and especially for his confidence in my abilities. If not for his sponsorship and professional endorsements, I would never have gotten the chance to write this thesis. His guidance and considerable knowledge were of invaluable aid throughout this project. I am proud to be one of Rick's students and hope to continue our association on both academic and professional levels. I will never forget the opportunity he afforded me.

I would also like to thank Dr. Walter O'Brien for his assistance during the time leading to my graduate career. His attitude towards students willing to pursue graduate studies was refreshing. In many ways, he helped to open the door to my graduate career. I hope I have the opportunity to work with him again.

My mother I thank for doing a terrific job of raising a difficult child into manhood. My father I thank for preparing me to meet the challenges of life and to succeed in a challenging world. The love and support of my mom, dad and sister Jennifer give me the strength and courage to achieve my goals. My family will be proud to know I have made it this far.

I would like to thank the members of the Wednesday Afternoon Combustion Seminar, both students and faculty; their input and patience were extremely helpful. And for the graduate students of the spacious office suite that is 117 Randolph Hall, the combustion mecca of Virginia Tech, I thank you all for the conversation, advice, company, and good times. Linda Blevins, Michelle Peatross, Jim Hunderup, Dan Gottuk, and Doug Wirth, I wish you all good fortune and success.

TABLE OF CONTENTS

LIST OF FIGURES

1. INTRODUCTION

1.1 Background and Motivation

As the gas turbine engines of today try to meet the performance goals of tomorrow, every area of the machine has come under the close scrutiny of the engineer in the hopes that even the smallest of improvements can be made. Historically, compressor and turbine blade aerodynamics were the first areas optimized for performance. The desire for higher specific power engines drove the search for gains in these systems. As the principles which governed airflow were understood and put to use, the search for better performance in the form of increased fuel efficiency was initiated. The economic pressures of the commercial airline and power generation industries demanded that advances be made to reduce fuel consumption. Cycle efficiencies increased, specific power output remained equal to or better than past models, and fuel consumption was cut drastically. Now, in the modern era of gas turbines, emissions are the third factor that influences the design of today's machines. One system being investigated to produce gains in the fuel consumption and emissions areas is the combustor. The combustor systems in tomorrow's gas turbine engines must control when, where, and how much fuel is added, monitor fuel/air mixing, distribute heat addition evenly to the turbine, and optimize the combustion process to produce more power with less fuel and little if any harmful emissions. The technology is indeed complex; it needs to be if tomorrow's gas turbines will continue to push performance to higher levels.

To meet the needs of increasingly more complex gas turbine combustors, a sophisticated combustor diagnostic system needs to be developed. Ideally,

the system would be inexpensive to install and maintain, non-intrusive, highly accurate, and operate in real time. The system should be able to deliver information about the two parameters most important to the combustion process: temperature and fuel-to-air ratio. The system response should be immune to the effects of high pressure and fluctuating turbulence. And the system should be able to be integrated into an intelligent combustor control package that could modify the combustor system to meet changing operating conditions. The development of such a diagnostic and control system would facilitate research for advances in combustion technology, with benefits to all facets of the gas turbine industry and other internal combustion engine technologies as well. This thesis investigates the development of one such diagnostic system; an optical probe based on the chemiluminescent signals of combustion.

The research for the chemiluminescent combustion diagnostic and control system began as research for the development of a flame light-off detector [1]. The primary problem addressed was flame blowout in afterburning gas turbine engines. Flame blowout problems usually occur during ignition and shutdown of the afterburner system -- the transient operating conditions. The consequences of afterburner blowout are severe: compressor and/or fan stall or surge can be induced by combustion conditions at the afterburner. See Appendix A for details of the application of the chemiluminescent detector to afterburner operation.

Besides being used in the development of a flame light-off detector, it became clear that the chemiluminescent signals of combustion could also be used to monitor temperature and fuel-to-air ratio as well -- a topic of considerable interest to the stationary gas turbine industry. The need for a gas

turbine combustion diagnostic and control system has become urgent in recent years. According to Walsh [2]:

> "The gas turbine, in general, is a low emitter of exhaust pollutants because the fuel is burned with ample excess air to ensure complete combustion at all but the minimum load conditions or during start-up. However, regulations passed during the past 6 to 12 years have made it necessary to reduce the level of certain pollutants by more than a factor of three."

Some of the "certain pollutants" Walsh speaks of are oxides of nitrogen (NO_x), oxides of sulfur (SO_x), carbon monoxide (CO), unburned hydrocarbons (UHC), and particulate matter (soot). Of these unwanted pollutants, NO_x is perhaps the least desirable and its production the most difficult to control. The difficulties associated with NO_x suppression highlight some of the various problems involved with pollutant control and show how the chemiluminescent detector could provide solutions. Although there are several methods that will suppress NO_x formation, many are unusable because they may result in the increased production of other unwanted pollutants or adversely affect engine performance. Likewise, attempts to reduce CO or UHC emissions may result in increased NO_x production, poor performance, or both. To develop methods for reducing all these emissions without sacrificing performance, the complex chemical kinetics involved in the production of the pollutants needs to be understood.

NO_x production is a strong function of temperature. Reducing the combustion temperature will result in lower NO_x emissions, to a point. (Studies have shown that there may be fundamental limits to the reduction of NO_x through lowered combustion temperatures; other less-temperature dependent

processes may govern NO_x production as well [3]). In addition to sensitivity to combustion temperature, NO_x production is also sensitive to the concentration of oxygen (particularly atomic oxygen). NO_x emissions peak at equivalence ratios of about 0.9 and quickly fall off for more fuel-rich mixtures (which contain less and less oxygen) [4]. Therefore, the best strategies for controlling NO_x emissions involve reducing combustion temperatures and lowering the concentration of oxygen in the mixture.

Burning fuel-rich mixtures is the easiest method of reducing NO_x emissions. Not only do rich mixtures have low oxygen concentrations (relative to the fuel concentration), but rich mixtures burn cooler as well. Combustion temperature is a function of fuel-to-air ratio; it always peaks near the stoichiometric fuel-to-air ratio (see Figure 1.1). However, burning excessively fuel-rich mixtures greatly increases fuel consumption, decreases power output, and results in higher CO and UHC production.

Burning an excessively fuel-lean mixture can also reduce NO_x emissions by lowering combustion temperatures. Power output is again reduced with lean combustion (power output is directly proportional to combustion temperature). Lean flames are also difficult to stabilize, particularly highly turbulent flames (the type used in most gas turbine combustors). However, the benefits of lean combustion include increased fuel economy and lowered CO and UHC emissions; strong motivation for burning fuel-lean mixtures (see Figures 1.2 and 1.3).

Dilution of the fuel/air mixture can also reduce NO_x emissions by lowering combustion temperatures without significantly changing the fuel-to-air ratio of the

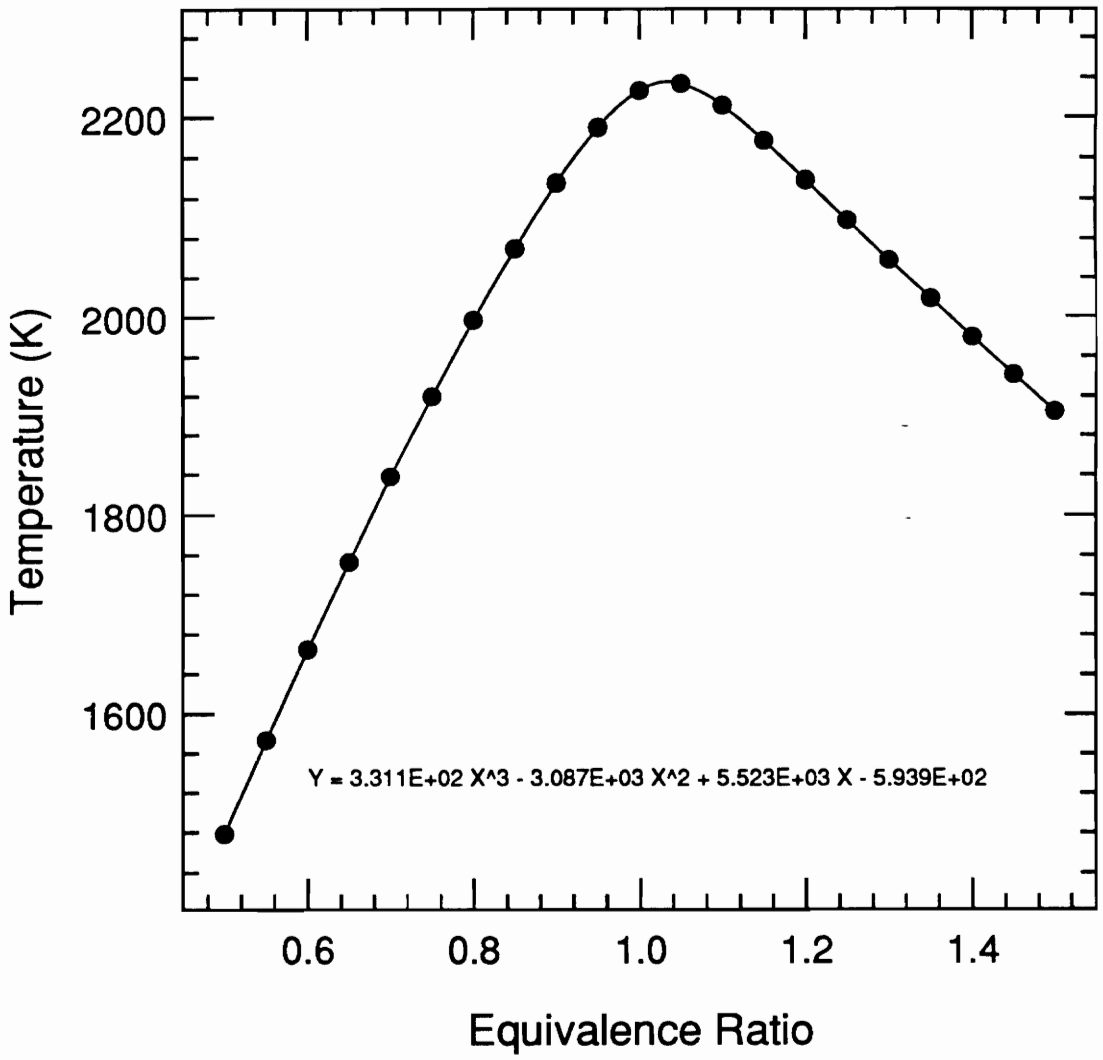

Figure 1.1: Adiabatic flame temperature as a function of equivalence ratio for a premixed methane-air flame.

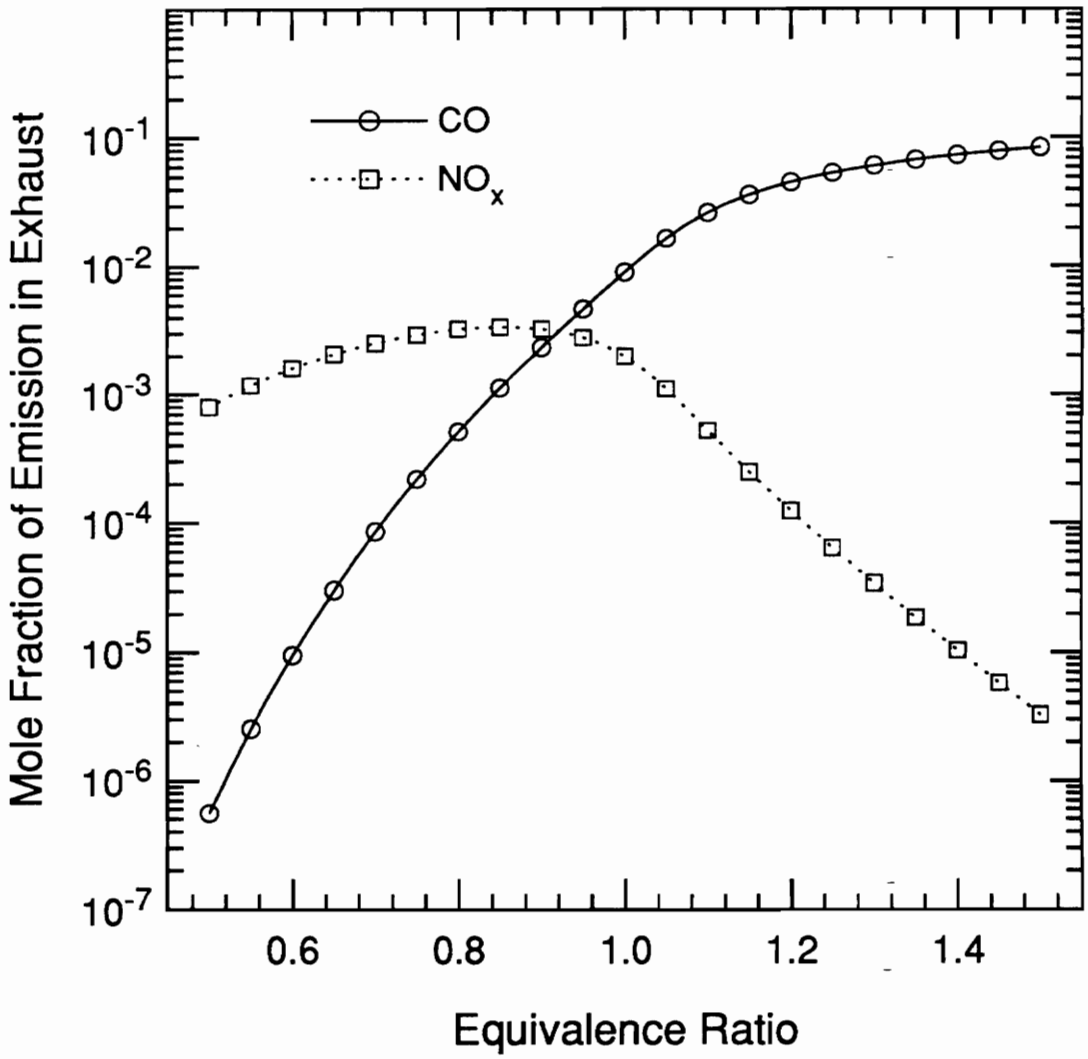

Figure 1.2: Equilibrium CO and NO_x emissions from a premixed methane-air flame as a function of equivalence ratio.

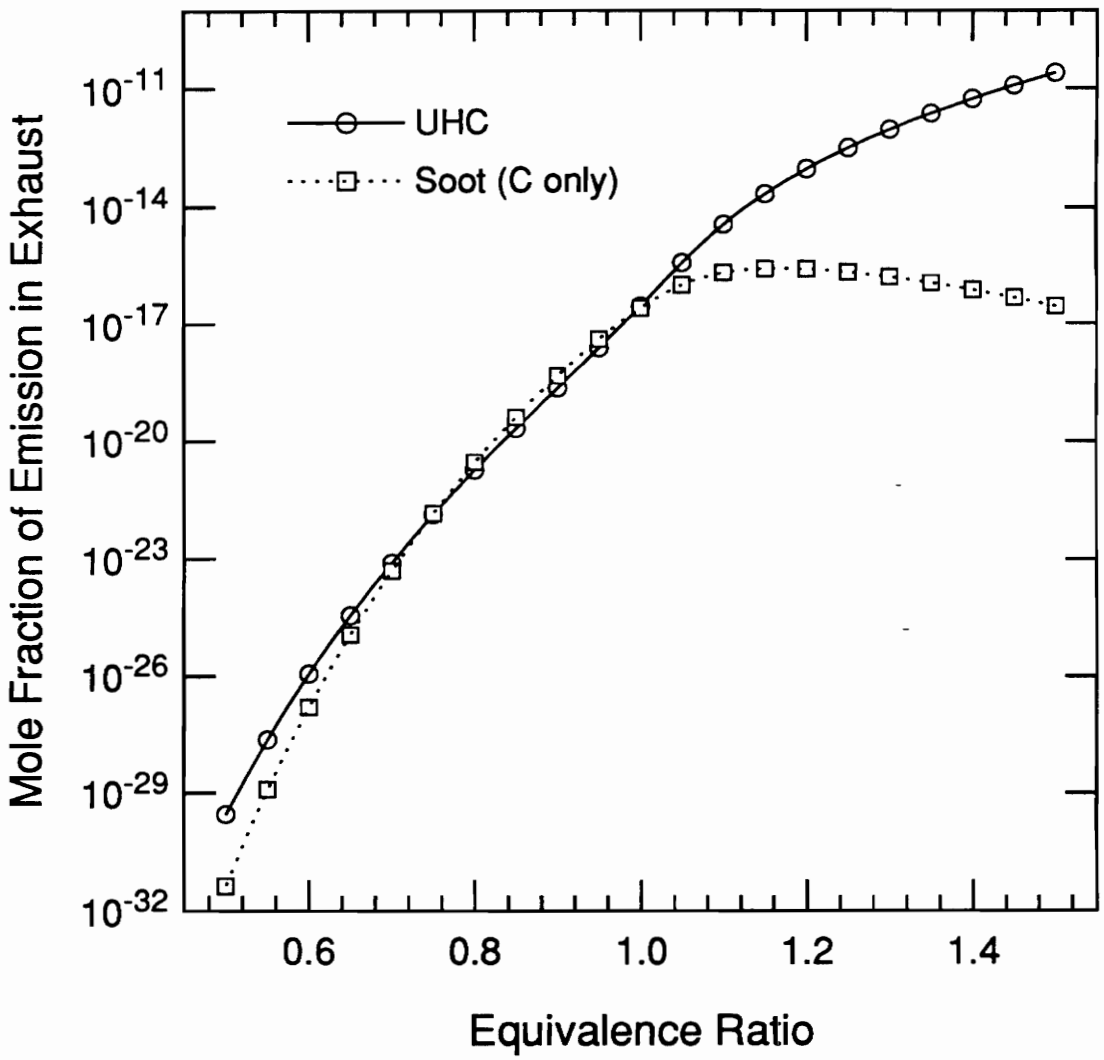

Figure 1.3: Equilibrium UHC and soot emissions from a premixed methane-air flame as a function of equivalence ratio.

mixture. The diluent acts as a heat sink, absorbing the kinetic energy of combustion without being greatly involved in the chemistry. Typical diluents are water and steam (in the stationary gas turbine industry), excess air (commercial airline gas turbines), and exhaust gases (automotive industry).

The accurate monitoring of fuel-to-air ratio and combustion temperature is absolutely critical to the control of unwanted pollutants. An intelligent combustion control system must be responsive to minute changes in operating conditions. No detector sensitive enough, fast enough, and cheap enough exists to use in such a control system. Low emissions technology *is* the next generation of gas turbines; there is a need for a system to control the operation of the combustor and optimize its performance for varying conditions. The heart of such a system is a detector that can provide accurate and reliable information about temperature and fuel-to-air ratio quickly and cheaply. The primary motivation for this research is the knowledge that the chemiluminescent probe can be used to fill this need.

A single chemiluminescent detector, such as described in this thesis, can respond quickly to changes in combustion conditions -- giving rise to a control system with an extremely fast response time. It can detect flame blowoff, detect unstable combustion, provide information on rich or lean mixtures, measure the temperature of combustion accurately and precisely, even possibly be used to diagnose anomalous combustion problems without disassembling the combustor. It can do all of this using current, rather mundane technology; meaning a system that is inexpensive and quite reliable.

1.2 Existing Combustion Chamber Monitoring Technology

To get an idea of the performance parameters of combustor probes, the capabilities and limitations of existing combustion chamber monitoring devices need to be understood. For instance, the Geiger-Mueller Phototube, by far the most widely used flame detection sensor in the gas turbine industries, has both advantages and disadvantages. The tube contains an easily ionized gas that produces a small current when ultraviolet (UV) light excites the gas. Light with a wavelength from 180 to 260 nm will ionize the gas and is abundant in combustor flames. The current from the tube charges a capacitor, which discharges with a frequency proportional to the stability of the flame. A pulse rate of over 120 Hz is considered a stable flame signal. The response time of this device, including associated signal processing, is on the order of 100 milliseconds. The Geiger-Mueller Phototube's frequency response is far too slow to be of use in an active control combustor system; changes in combustion conditions at the chemical level (e.g., NO_x formation) take place over a period of only a few milliseconds. And because the Geiger-Mueller Phototube samples ultraviolet radiation over a relatively broad range, it is susceptible to background UV radiation "noise" in the combustor (the spark kernel is a particularly noisy source). However, the Geiger-Mueller Phototube is inexpensive, and can withstand the rigors of the combustion chamber environment quite well [5].

Morey, Quentin and Angello have developed a probe that can be used to monitor the combustor chamber process directly [6]. A water-cooled fiber-optic image guide is used to transfer the image of the combustion process from inside the combustor to remotely located video and film cameras. Used on a General

Electric 7001 stationary gas turbine, the probe was able to deliver observations on ignition delays, flame bistabilities and flame detachments. While this system could be useful in detecting flame blowout, other diagnoses rely on a human operator to interpret the data. Response time of the system is quite good because of the nature of the luminous signal, but the equipment is bulky, cumbersome and expensive. However, the investigators believed that such a system could play an important diagnostic role in maintaining peak engine performance.

Cohen, Gat and Witte developed a somewhat complex probe for monitoring of ignition in automotive diesel engines [7]. It was hoped the probe would fulfill a need for reliable sensing of diesel ignition to more precisely control fuel injection parameters. The probe consisted of both an ionization sensor (Langmuir gauge) and a luminosity sensor and was tested in both Oldsmobile and Volkswagen diesel engines at various RPM and load conditions. They concluded:

> "The noticeable and repeatable delay of the ionization signal which is encountered at higher engine speeds, is accompanied by a variable rate of rise. [However,] the luminosity sensor has an easily characterized and repeatable signal making it a better ignition marker. The luminosity sensor 'sees' all radiant emission from the combustion event occurring anywhere in the prechamber and so accurately indicates the start-of-ignition."

Other automotive combustion probes have been developed as a result of Cohen, Gat and Witte's preliminary research. Texas Instruments Incorporated has developed a piezoelectric pressure transducer for use in automotive engines that monitors peak combustion pressure and allows for optimization of spark

timing according to prevailing operating conditions. Hitachi Limited has developed a combustion chamber probe which utilizes fiber-optics and spectra sensing equipment. The fiber-optic cable fits through the center of a spark plug and transmits visible light to an engine control unit. If light is detected with substantial UV components (i.e., shifted towards the ultraviolet), a high spark energy is indicated and well-developed combustion results. If, however, light shifted towards the infrared is detected, a low spark energy is indicated and poor combustion may result. Corrective action in the form of varying fuel-to-air ratios (cylinder by cylinder, as the system is intended for fuel-injected engines only) can then compensate for low spark energy [8].

All the sensors discussed thus far have proven their value towards a combustion control system designed to optimize engine performance. All the sensors are non-intrusive so as to be able to mitigate the problem of the harsh combustor environment and all but one of the sensors rely on visible or UV light for their signal. Two of the sensors use fiber-optics to transmit combustion signals. Yet none of the sensors has been designed or tested for the sensing of combustion chamber temperature or fuel-to-air ratio -- two quantities intricately linked to the combustion chemistry.

Present gas turbine designs monitor combustor temperatures with thermocouples in the turbine exhaust gases. The actual combustor temperature is extrapolated from exhaust temperatures and information on the work done by the turbine and the operating parameters of the engine. It is an inexact science at best. There can be large errors involved with the extrapolation. Most current gas turbines employ multiple combustor "cans" in an annular arrangement.

Resolution of individual combustor temperatures with thermocouples placed in the exhaust *after* the turbine is impossible. Even with specialized pre-turbine thermocouples, the exhaust gases still mix and individual combustor can temperatures cannot be distinguished. With an ever-increasing emphasis on low emissions technology, it is important to know the temperatures of the *individual* combustor cans. Often, a single can operating off-design can contribute to the majority of the pollutants produced by the entire gas turbine. Currently, only disassembly and manual inspection of the individual combustors will reveal any problems. Because of the especially harsh nature of the gas turbine combustor environment and the inability to get reliable information from the turbine exhaust gases, optical techniques are the only logical choice for combustion temperature monitoring.

Like temperature monitoring devices, the state of fuel-to-air ratio monitoring technology is poor. Present gas turbine designs use overall fuel and air flow ingestion rates to determine the fuel-to-air ratios for the different operating modes of the combustor. Individual fuel and air flow rates for each combustor (some designs have as many as fourteen combustor cans) are often not taken into account. Considering that small changes in the fuel-to-air ratio of even a single combustor can increase pollutant production many fold for the entire machine (especially if running fuel-rich), the benefits of an individual combustor fuel-to-air monitoring device can be appreciated. Monitoring individual fuel and air flow rates for each combustor is possible, but the hardware involved is cumbersome. Here, it is the simplicity of a fiber-optic system to monitor fuel-to-air ratios which makes it a desirable choice, especially since the same system can monitor temperatures as well.

Because of the harsh environment, an optical sensor is a must for the gas turbine combustor. Fiber-optics are useful in that they can transfer the signal to a remote area, away from the rigors of the engine compartment. Chemiluminescence is an especially practical method of detecting flame ignition, blowoff, temperature and fuel-to-air ratio quickly and reliably. Power and emissions both can be improved with such a system. Thus, a chemiluminescent detector using fiber-optics is a very logical choice for the design of a combustion control system. And in the design of such a system, it is important to understand the uses and limitations of the technologies involved. Therefore, it is vital that the processes involved in chemiluminescence be understood, so that its potential can be fully explored.

1.3 Chemiluminescence

Chemiluminescence is the light released by electronically excited molecules as they return to their equilibrium ground state. There are many methods of inducing a given species to an electronically excited state. The formation of new chemical bonds between molecules can result in an excited species (a process called chemi-excitation). Many exothermic reactions result in excited species; combustion reactions are particularly strong producers of excited species. These excited species return to their preferred ground state by energy transfer; a kinetic energy transfer results in charged species and/or free electrons (chemi-ionization) while the emission of a quantum of light is the process of chemiluminescence. For many combustion reactions, the amount of energy released in the form of chemiluminescence far exceeds the thermal energy released by the reaction. For detailed information on

chemiluminescence and the spectra of flames please refer to Gaydon's book, *The Spectroscopy of Flames* [9].

There are three types of spectra emitted from flames. The first, line spectra, are emitted by free atoms in electronic transition. Each line emitted corresponds to a transition from one electron energy state to another (e.g., from an electronically excited state to the ground state). Energy is conserved when a quantum of light is released; this is the chemiluminescent signal. Line spectra are usually not obtained from pure flames; only the hottest fires can achieve dissociations to such a degree that monatomic gases are in abundance and their emissions are the most prevalent. It is possible, however, to seed a flame with metallic impurities, such as sodium, so that line spectra can be readily observed.

The second type of flame spectra are band spectra. These are electronic transitions by molecules, accompanied by simultaneous changes in the internal vibrational and rotational energy of the molecule. In effect, a system is created; each electronic transition gives rise to a number of possible vibrational and rotational energy changes, each change resulting in the emission of a discrete line spectrum. Thus, molecular electronic transition systems are band spectra; the bands themselves contain a finite number of discrete line spectra. Simple, diatomic molecules show regularity in both their band and line structures; their bands usually have a sharp peak or "head"; the wavelength of which can be precisely measured. More complex molecules show no such regularity; their bands are somewhat diffuse and heads are difficult to pinpoint. Band spectra in the infra-red are usually the result of vibrational and/or rotational changes alone; there are no electronic transitions to mark these spectra. Band spectra are the

most prominent feature of air-hydrocarbon flames, with free radicals like CH, OH, C_2, CN, and NH providing the strongest band systems.

The third type of flame spectra are called continuous spectra. These emissions are associated with solid particles or liquid droplets within the flame; there may be other sources, however. Gas-phase processes such as dissociation of molecules, atom ionization, or recombination reactions of atoms into molecules can also give rise to continuous spectra. Continuous spectrum emissions from gaseous flames are not usually of the same intensity of band or even line spectra, but they may occur over a broad range of wavelengths, often masking or obscuring the more important band spectra.

Because of their intensity, band spectra are the most useful for diagnostic purposes. The strongest chemiluminescent signals from air-hydrocarbon flames come from the excited free radicals CH^*, OH^*, C_2^*, CN^* and NH^* returning to their ground states. Because the energy required for the transition from the ground electronic state to the lowest excited state is relatively high, the chemiluminescent bands of these radicals are quite abundant in the visible and ultra-violet wavelengths.

In the first portion of this research, the development of the chemiluminescent flame light-off detector by Hamer [1], the flames of several hydrocarbon fuels were investigated to determine the intensities of band spectra emissions (see Figure 1.4). A spectral scan was performed for each flame, from the UV into the visible light range (280 to 540 nm). In each case, there were three band spectra that were prominent. The OH^* band emission was the strongest, a system with its main head at 306.4 nm, two other strong heads at

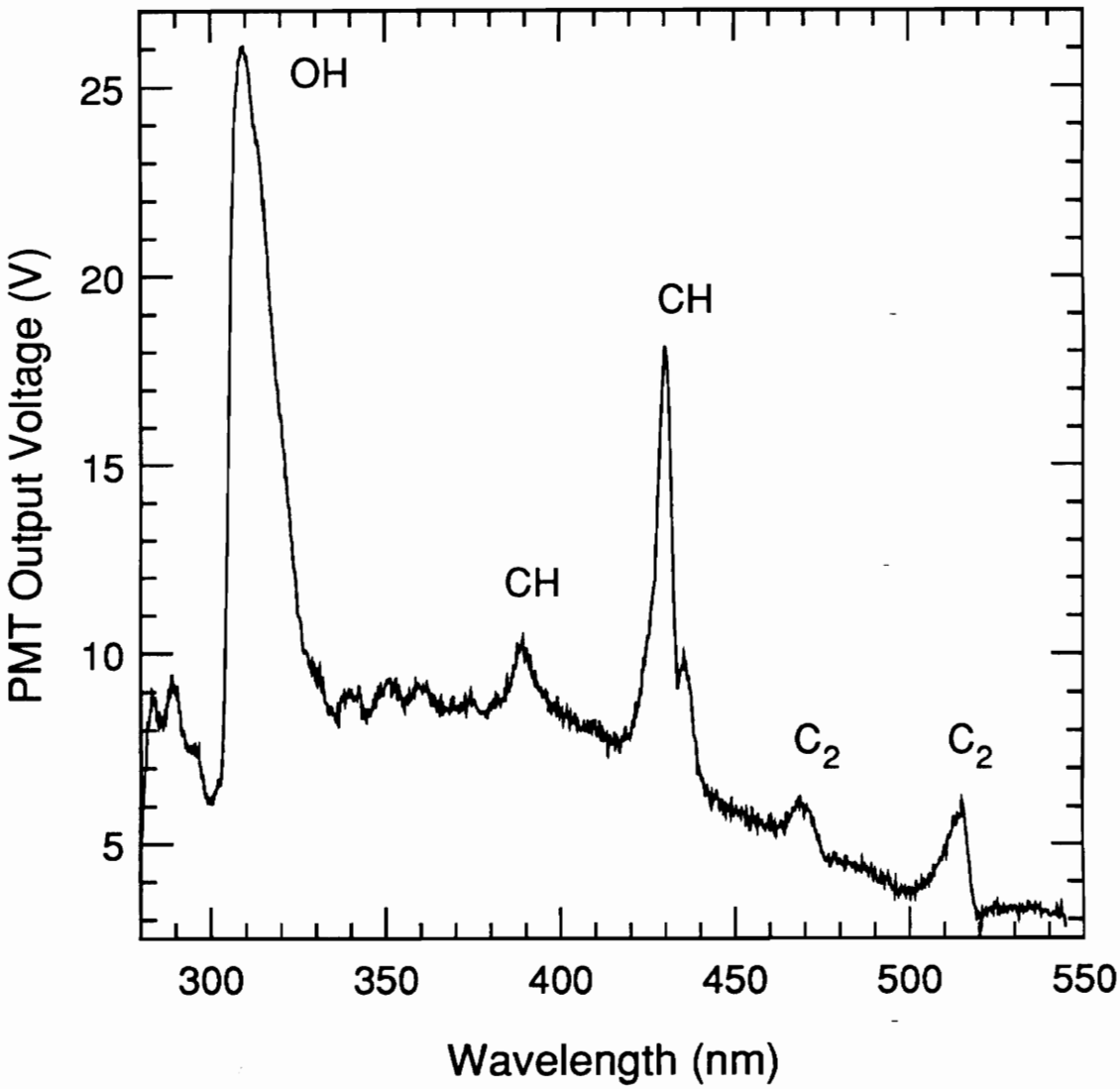

Figure 1.4: Band spectra emissions from a methane-air flame, captured with a scanning monochromator and photo-multiplier tube. From Hamer [1].

306.8 nm and 309 nm, and a fourth weaker head at 307.8 nm [9]. CH* band spectra occur at both 390 nm and 431.5 nm with the latter emission being much stronger (about 40% of the OH* signal in a stoichiometric methane-air flame). Two C_2* bands, both of relatively low intensity (less than 10% of the OH* signal in the methane-air flame), occur at 473.7 and 516.5 nm. The two strongest band spectra, OH* at 309 nm and CH* at 431.5 nm were chosen for study.

The system at 309 nm was identified by Gaydon [9] in the following manner:

> "Detailed analysis of the rotational structure shows the bands are due to a $^2\Sigma$-$^2\Pi$ transition in a diatomic molecule with a small moment of inertia. This at once limits us to a hydride with an odd number of electrons and the hydroxyl radical is the only possibility."

To identify the CH system at 431.5 nm, Gaydon states [9]:

> "Three systems of CH are observed in flames, all having a common $^2\Pi$ final level. The systems all show that the open rotational structure characteristic of a diatomic hydride, and the branches are double, indicating a molecule with an odd number of electrons. They are also obtained readily from discharges through pure hydrocarbon vapours, and the emitter can only be CH."

The OH* excited radical is formed mostly by one process common to all air-hydrocarbon flames:

$$CH + O_2 \rightarrow CO + OH^* \qquad [10]$$

The CH* excited radical is formed by two competing reactions:

$$C_2 + OH \rightarrow CO + CH^* \qquad [10]$$

$$CH + OH + H \rightarrow CH^* + H_2O \qquad [11]$$

Note that the OH^* chemiluminescent reaction $OH^* \rightarrow OH + h\nu$ is a provider of the hydroxyl radical necessary for the formation of the CH^* excited radical. The latter of the two CH^* reactions is a three-body reaction and as such does not produce as much CH^* as the former reaction.

The use of chemiluminescence for the study of combustion systems is not new. In *The Spectroscopy of Flames*, published in 1957, Gaydon himself suggests that chemiluminescence can be used to determine the nature of a flame, concentrations of its constituent species, kinetic rate information, and so forth [9]. In 1960, Schott used chemiluminescent techniques to study OH concentration maxima in hydrogen-oxygen detonations [12]. In 1961, Lyon and Kydd studied chemiluminescent C_2, CH and OH absorptions in acetylene flames [13]. Since the early 1970's, the use of chemiluminescence for flame analysis has proliferated. Chemiluminescence was applied to the study of many combustion topics from NO_x analysis to upper-atmospheric ozone experiments to detectors of phosphorus and sulfur compounds. Glover [14], Stedman and Fraser [15], and Fontjin [16] have produced reviews of gas-phase chemiluminescent analytical techniques. Many other researchers have studied the chemiluminescent process itself in hopes of understanding more about the nature of flames [17-24]. In the 1980's, Beyler [25] used chemiluminescent emissions to examine flame structure and the mechanism of flame stabilization in a premixed, swirl-stabilized combustor. Beyler's work is particularly noteworthy in that he suggests the chemiluminescent emissions be used as a signature of the combustion reaction zone.

Chemiluminescence has indeed found broad applications in combustion research these last few decades. However, the use of chemiluminescence for the simultaneous detection of temperature and fuel-to-air ratio of flames remains unique to the research conducted for this thesis.

1.4 Scope of Thesis

The need for flame diagnostic sensors in the gas turbine industry has been discussed. The benefits of an accurate temperature and fuel-to-air ratio detector are undeniable. This thesis presents the results of research into a system that can be used to address the needs of ignition detection, flame blowout, unstable combustion, anomalous combustor operation, and temperature and fuel-to-air ratio information. The detector examines the intensity and wavelengths of specific chemiluminescent signals of combustion.

The formation of the CH^* and OH^* excited radicals that leads to chemiluminescent signals takes place in the earliest stages of combustion. The reactions involved occur on a time scale of several hundred microseconds to a few milliseconds [1]. Therefore, monitoring the wavelengths specific to CH^* and OH^* emissions provides an extremely fast flame sensing signal. The work of Hamer [1] and Johnsson [26] has already shown that chemiluminescent signals can be used for ignition and flame blowoff detection for various fuels. The experimental apparatus consisted of, in Hamer's case, fixed optics, a monochromator and photomultiplier tubes. Johnsson employed this set-up as well, but went on to investigate the use of fiber-optics, filters and photodiodes. (The fixed optics and monochromator system is too bulky and too costly for practical applications.) Both researchers used laminar flow burners to simplify

experiments in the preliminary stages. Johnsson concluded that reliable and accurate temperature and fuel-to-air ratio information could be obtained by the chemiluminescent method from laminar, pre-mixed methane-air flames [26].

The goals of this thesis were to determine if the results of Hamer and Johnsson's work were applicable to more realistic gas turbine flames and if not, why not. A key component missing from Hamer and Johnsson's flames was turbulence. Turbulence affects many flame parameters, most notably reaction zone sizes and locations, flame speeds, and in diffusion flames, mixing rates. Real gas turbine flames are extremely turbulent. If the conclusions reached by Hamer and Johnsson can be safely applied to turbulent flames as well, the concept of a chemiluminescent flame diagnostic system is that much closer to practical application.

The underlying structure of the research conducted in this thesis was to isolate the experimental variables and determine each variable's effect on the method of chemiluminescent detection. The effects of turbulence, flame temperature, fuel-to-air ratio, and equipment changes were separated and investigated independently. The experimental procedure had four main components: verification of the turbulent burner design, isolation of experimental variables, evaluation of different experimental set-ups, and simulation of actual gas turbine conditions.

The first phase involved the building and testing of the turbulent burner (described in detail in section 2.2). The laminar flame experiments of Johnsson were repeated with the turbulent burner. The performance of the burner were evaluated in terms of flow capacity and flame stability.

The second phase was a primary focus of the research conducted for this thesis. Correlations of temperature and fuel-to-air ratio with chemiluminescent signals were developed separately for turbulent flames. Comparisons between laminar and turbulent correlations were made. The effects of increasing turbulence on these correlations was also investigated.

The third phase was of a more practical, as opposed to theoretical, nature. The set-ups employed by Hamer and Johnsson (fixed optics, a monochromator, and a photomultiplier tube) are not applicable to harsh gas turbine conditions. The use of fiber-optics, filters, and photo-diodes would be investigated to determine their effects on the accuracy and reliability of the chemiluminescent method. Different correlations would no doubt be made with the new equipment. However, it was important to gather experimental data with hardware which more accurately simulates actual application equipment to determine if similar trends were observed and whether similar conclusions could be reached.

The final phase involved making any equipment modifications necessary to more completely simulate the actual gas turbine combustor environment. These modifications included high-pressure combustion (ten atmospheres is a typical combustor pressure), high temperature operation (combustor feed air is usually compression heated by the compressor to much higher than ambient conditions), various fuels (liquid fuels in particular), addition of various diluents (water or steam, exhaust gas, etc.), and the addition of accompanying hardware to simulate the presence of compressor and turbine systems of an actual gas

turbine. Clearly, the best way to simulate actual gas turbine conditions is with an actual gas turbine fitted for experimentation.

In practice, the experimental plan was not fully implemented. Steps one and two were completed with moderate success, step three only on a rudimentary level, and step four was not investigated. Unforeseen pitfalls forced some adaptations to the overall plan. However, the data gathered from the experiments that were performed prove that the concept of the chemiluminescent detector system does work for turbulent flames, does work over a range of temperatures, fuel-to-air ratios, and turbulence levels, does work with fiber-optics and filters, and therefore holds much promise.

2. Experimental Apparatus

2.1 Introduction

The chemiluminescent detector system features four main components. The burner, in this case designed specifically for burning turbulent, pre-mixed gas-phase combustibles, is the first component. Second is the optical hardware, used for imaging, magnifying, and/or transporting the light signal away from the flame. The third component is the detection apparatus: a two-fold system responsible for isolating specific wavelengths of the chemiluminescent signal and converting that energy into useful electrical impulses and for determining reference flame temperatures. The last feature of the system is the recording device, typically a digital oscilloscope, used for recording, analyzing and storing the electrical data for further study. Every incarnation of the experimental set-ups used by Hamer, Johnsson and in this research incorporates these four basic components. The details of each component are detailed below.

2.2 Burner System

2.2.1 Introduction

The function of the burner system is to provide a completely homogeneous gas mixture for combustion and to burn that mixture in a controlled manner. In this research, methane and air were completely premixed prior to combustion. The design of the burner allowed high flowrates necessary for turbulent combustion. A small, annular hydrogen diffusion flame was used to keep the methane-air flame attached to the burner lip. High precision rotameters

controlled the flowrates of the gases. A two-axis translator allowed for measurements to made across the entire height and width of the flame.

2.2.2 Turbulent Flame Burner

The burner used in this research was built at the Virginia Tech Mechanical Engineering Shop and based on a design first used by Vandsburger [27]. It consists of a central mixing chamber where the methane, air, and nitrogen diluent (if any) come together and mix thoroughly before being burned. The mixture exits the chamber through a perforated disc and into a tube (similar to a Bunsen burner) where, upon exit, it is burned. Atmospheric air does not come in contact with the mixture at any time before burning (unlike a Bunsen burner, where the fuel and ambient air mix before burning). A larger tube, concentric with the main tube, forms an annular area through which small amounts of hydrogen are passed. The hydrogen enters the burner through a completely separate orifice and does not come in contact with the combustible mixture until it exits the annulus. The hydrogen is used to attach the flame to the burner in cases of high turbulence; flame blow-off is a common and annoying consequence of burning highly turbulent, fuel-lean flames. The amount of hydrogen used for flame attachment is surprisingly small -- less than half a percent of the total volume flowrate for these experiments. Although the hydrogen does contribute to the fuel in the mixture, the flowrates involved are so small that its contribution to chemiluminescent emissions is negligible and can be safely ignored. See Figure 2.1 for a schematic of the turbulent flame burner.

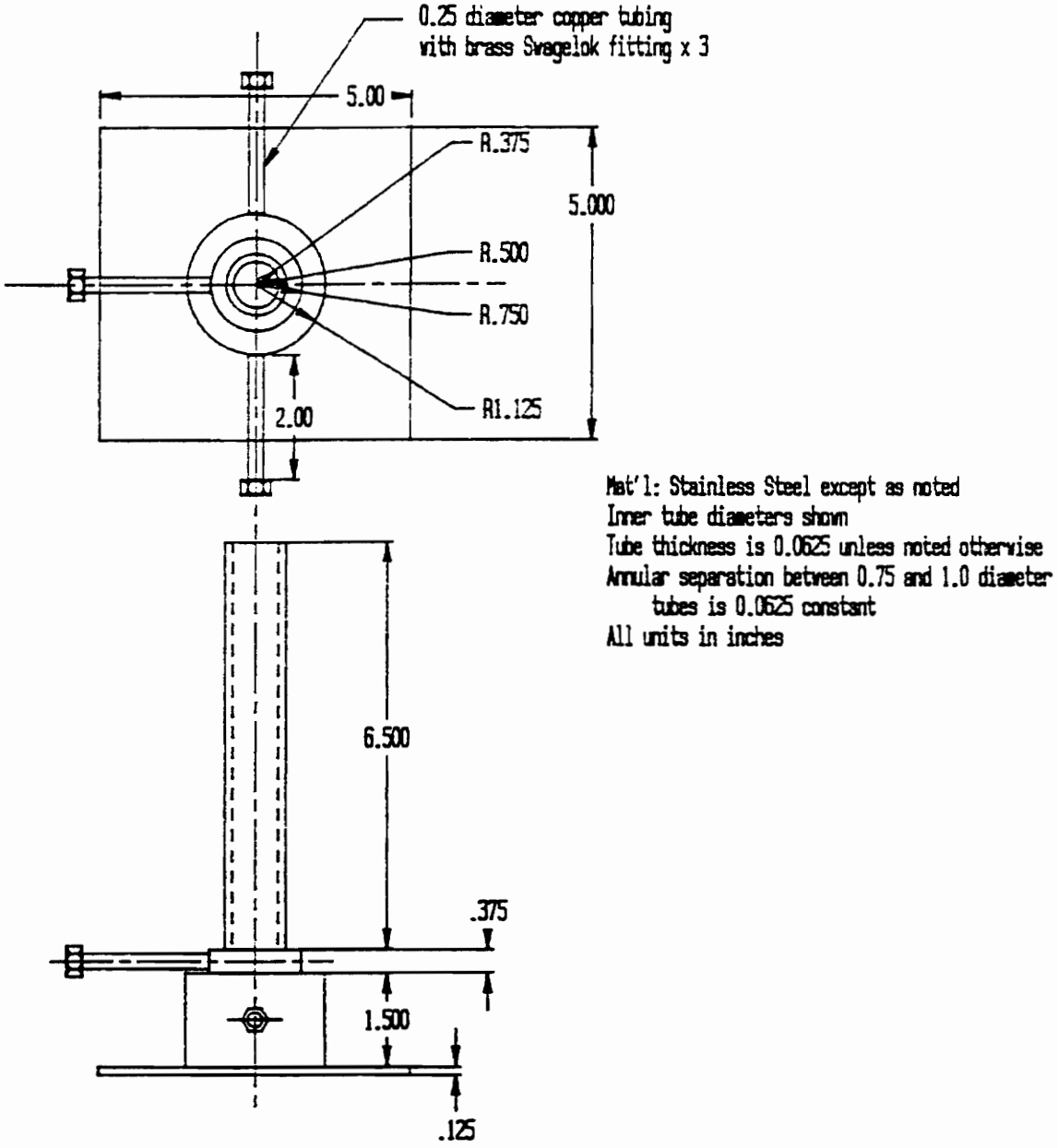

Figure 2.1: Turbulent burner schematic.

2.2.3 Fuel, Oxidizer, and other Gases

Methane was the only fuel investigated in this study, chiefly because it is a simple hydrocarbon that easily forms excited radicals and burns "cleanly", i.e., without an excessive amount of soot. (Soot formation would have complicated temperature measurements due to the high amount of radiative heat transfer of the soot particles from the flame to the surroundings.) More importantly, natural gas (which is mostly methane) is the fuel of choice for industrial gas turbines because of its low cost and availability. Methane was also used exclusively by Johnsson in his temperature and fuel-to-air ratio experiments. Comparisons with Johnsson's results were a major consideration in the choice of fuels. Also, earlier work by both Hamer and Johnsson had already revealed that similar correlations between OH^* and CH^* signal intensities could be drawn for methane, liquid hexane, and liquid Jet-A fuels. (The determining factor appears to be the H/C ratio of the fuels, as might be expected; see [1] and [26]). It is anticipated that any conclusions drawn for methane-air flames can be extended, with reasonable considerations, to other gaseous and liquid hydrocarbon fuels.

2.2.4 Rotameters

Controlling the flowrates of methane, air, nitrogen, and hydrogen was accomplished with Matheson rotameters. Series 605 rotameters (now designated series E-800) were used for the methane and the air; low flow, fuel-lean flames sometimes used a series 604 (now series E-700) for control of the methane. A series 604 rotameter was used in all cases for control of the nitrogen flowrates and a series 602 (now E-500) for the hydrogen. High-accuracy Matheson needle valves, series HA6 (part number FM-1051-HA), were

used with all rotameters for precise control of flowrates. With 40 psig of gas cylinder pressure (monitored by Matheson single stage pressure regulators, part number 3112) feeding the rotameters, the series 604 was capable of delivering about 325 scc/s (standard cubic centimeters per second) of methane or 450 scc/s of nitrogen; the series 605, over 670 scc/s of methane or 815 scc/s of air. Twenty psig fed the series 602, which could put out 70 scc/s of hydrogen. For the high turbulence experiments, 80 psig was used to supply the series 605 rotameter for controlling air flow. At 80 psig supply pressure, the series 605 can deliver more than 1660 scc/s of air. All gas lines were Nycoil polyethylene tubing, 1/4 inch outside diameter, 0.040 inch wall thickness; rated at 120 psig (at 75° F) working pressure. High turbulence experiments used 3/8 inch O.D., 0.062 inch wall thickness Nycoil polyethylene tubing (rated at 200 psig at 75° F). All fittings were of the Swagelok variety, 1/4 or 3/8 inch brass elbows and unions, where appropriate. The rotameters were calibrated with a Singer DTM-115 gas volume meter from American Meter Company and a digital stopwatch. Calibration curves for the rotameters used in this research are given in Appendix B.

2.2.5 Mounting Assemblies

The turbulent flame burner was mounted on a two-axis translator from Velmex, Inc. (Unislide part numbers A4015W1, A4021W1, and A4001XZ.) Vertical travel was about nineteen inches with a 0.1 inch pitch screw translator. Horizontal travel was about thirteen inches, also with 0.1 inch resolution. The two-axis translator was in turn mounted on a rigid support attached to a Melles-Griot breadboard tabletop on which the optical hardware and light detection

systems were mounted. See Figure 2.2 for details on the complete burner setup.

2.3 Optical System

2.3.1 Introduction

The function of the optical system is to focus the light of the flame onto the monochromator entrance slit, screen out any stray ambient light, and maximize the intensity of the chemiluminescent signal in the process. To accomplish these goals, lenses and polyvinyl chloride (PVC) ductwork were used (experiments were conducted in the dark and all light sources and reflective surfaces were covered with either flat black paint or black electrical tape, as a precaution against unwanted ambient light). In later experiments where wavelength specific filters were used in place of the monochromator, fiber-optic cables and collimating lenses were used to transmit the chemiluminescent signal to the photo-detector.

2.3.2 Lenses

Hamer's experiments showed that as the image magnification of the flame increased, the intensity of the chemiluminescent signal decreased [1]. This was believed to be caused by the fact that high magnification imaged only a small portion of the flame on the photo-detector. Lower magnifications would image more of the flame onto the photo-detector and the chemiluminescent signal would be correspondingly stronger. Johnsson chose a magnification of one for his experiments, citing the larger database already collected by Hamer at this magnification as the primary reason [26]. At a magnification of one, the

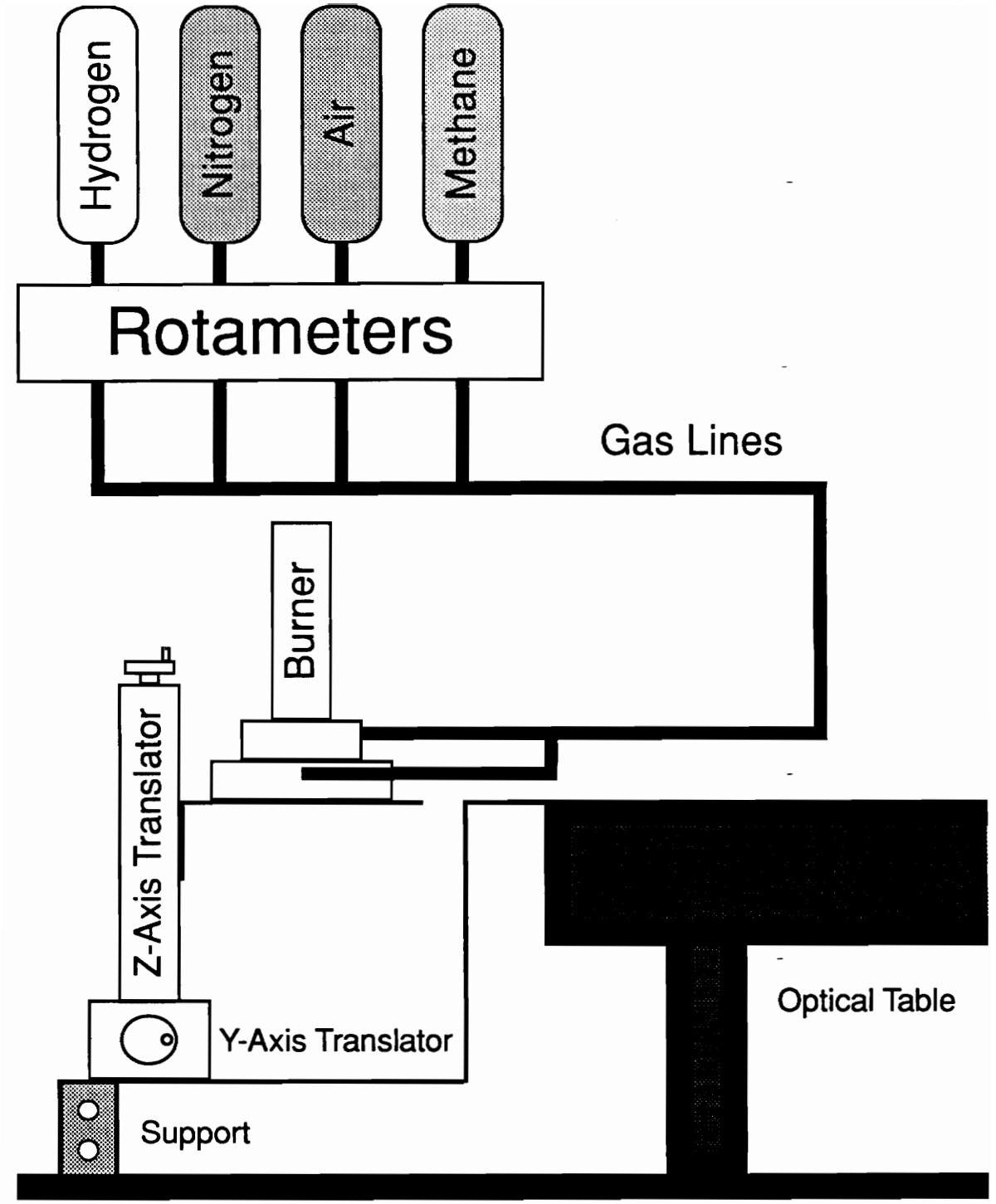

Figure 2.2: Burner system set-up.

chemiluminescent signal was deemed strong enough by both Hamer and Johnsson. In the research conducted for this thesis, Hamer and Johnsson's advice was followed, and all experiments were performed with a magnification of one.

The relationship between object, lens, and image is given by the Gaussian lens formula:

$$\frac{1}{F} = \frac{1}{S_i} + \frac{1}{S_o} \qquad [28]$$

where F is the focal length of the lens, S_i is the distance between the effective refracting surface (ERS) of the lens and the image, and S_o is the distance between the ERS of the lens and the object. Focal length is the length from the principal point of a lens (the intersection of the ERS and the optical axis) to its focal point (the point at which paraxial light rays entering the lens converge). The ERS is roughly halfway between lens surfaces.

For practical considerations, it was necessary that the monochromator and photo-detecting hardware be placed away from the flame. A one meter separation distance was deemed adequate. To maintain the magnification factor of one, the distances between object, lens, and image had to be calculated using the Gaussian lens formula. Magnification factor is simply the ratio of the distances involved:

$$M = \frac{S_i}{S_o} \qquad [28]$$

Therefore, with a magnification of one, the two distances needed to be equal and thus a lens with a 250 mm focal length would be needed. Image quality would be somewhat compromised with a single lens, as the image is not at the plane of focus (the image is 250 mm before the plane). A lens with a 500 mm focal length would keep the image at the plane of focus, but the magnification would not be unity (it would be zero, as the object would be imaged as a point of light). Additionally, the requirement that light from the flame be maximized forced some other considerations to be made in the choice of lens set-ups. See Figure 2.3 for details on the single lens set-up.

The F/# (read "F-number") is a non-dimensional parameter that measures the light gathering capability of the lens. The F/# is the ratio between the effective focal length (EFL) of the lens and the diameter of light (D) on the entrance pupil of the lens:

$$\mathrm{F/\#} = \frac{EFL}{D} \qquad [28]$$

The effective focal length differs from the back focal length (the distance from the back of the lens to the focal point) by roughly half the thickness of the lens. Effective focal length is simply the focal length for a single lens system, but is a function of individual lens focal lengths and lens separation distances in a multiple lens system. Effective focal lengths are necessary for calculations, back focal lengths for positioning of the hardware (it is easier to measure from the lens surface than from a point inside the lens). The diameter of light on the entrance pupil of the lens is not always the lens diameter. Collimated laser light,

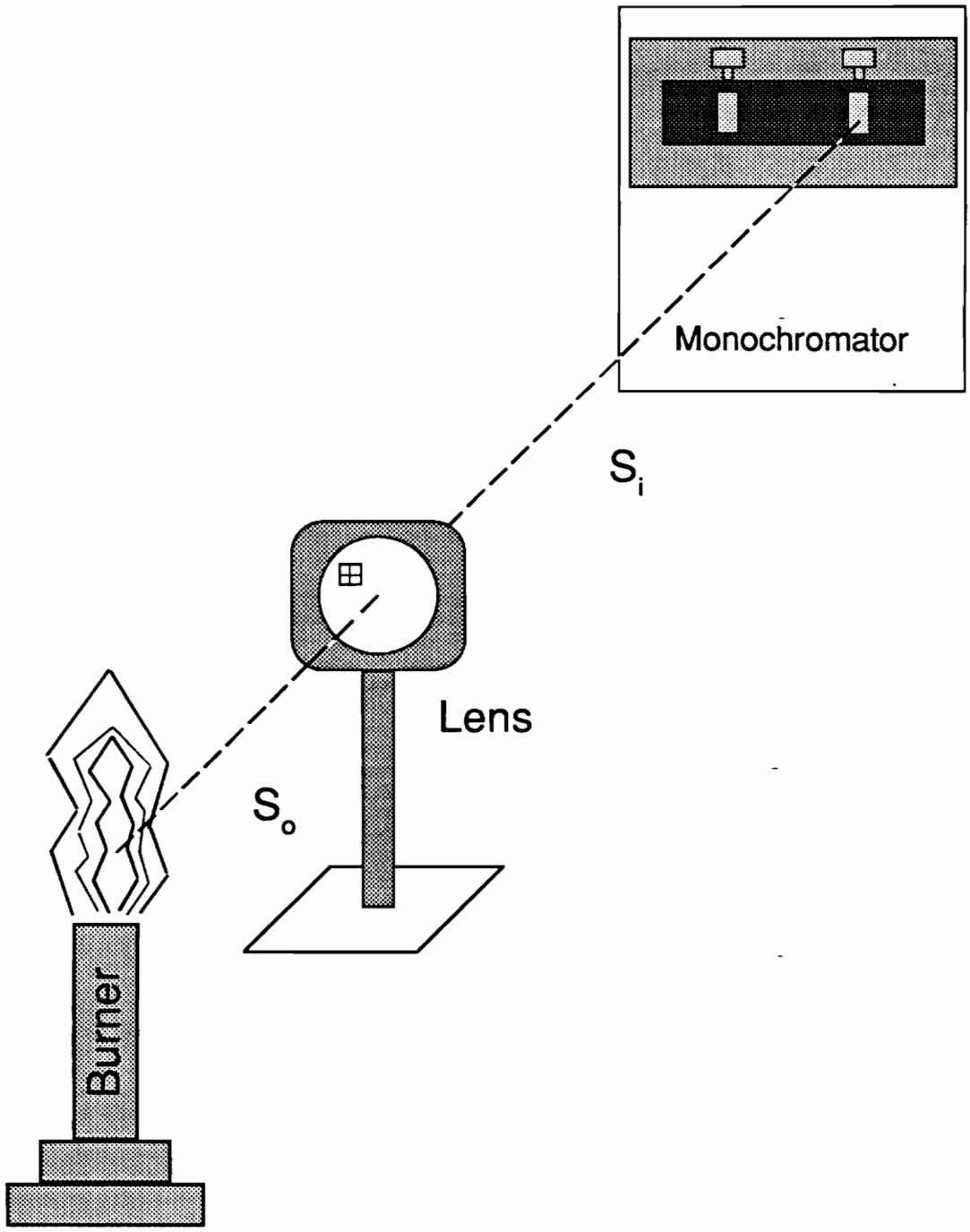

Figure 2.3: Single lens optical system set-up.

for instance, would produce an entrance pupil diameter only as wide as the laser beam.

The brightness of the image is inversely proportional to the square of the F/#. The lower the F/#, the brighter the image is. Thus, an F/2 image is four times as bright as an F/4 image. Clearly, the light from the flame to the detector is maximized by using a lens with a low F/#. But, as shown by the formula above, F/# is directly proportional to the focal length of the lens; a low F/# would mean a short focal length lens. However, F/# is also inversely proportional to the diameter of the lens. Thus a large diameter could offset a long focal length to produce a lens with a low F/#. (This is the reason early telescopes had enormous diameters.) Here the available inventory of lenses in the laboratory was the constraint. There was an assortment of lenses in one inch and inch-and-a-half diameters. Most of the larger diameter lenses had extremely short focal lengths, however. Two one inch diameter, plano-convex fused silica lenses (Oriel #40390 and #41390) were the only lenses available with 250 mm focal lengths. These lenses had an F/10 rating. A one inch diameter, plano-convex fused silica lens (Oriel #41410) was also available; it had a 500 mm focal length and an abysmal F/20 rating.

However, the Gaussian lens formula shows us that the focal length of a two-lens system depends on the distances between the object, image, and each of the two lenses. For the lens closest to the image, S_o is infinite (light from the object reaches the lens as essentially parallel lines, thus the object is imaged as if it were infinitely far away). For the lens closest to the object, S_i is infinite. Therefore, the focal length of the lens closest to the object is simply the distance

to that object and the focal length of the lens closest to the image is simply the distance to that image.

The magnification of a two-lens system is therefore the ratio of the two focal lengths:

$$M = \frac{F_2}{F_1} \qquad [28]$$

where F_2 is the focal length of the lens closest to the image and F_1 is the focal length of the lens closest to the object. Obviously, to maintain unity magnification, a two-lens system would require that both lenses be of the same focal length and that the distances on either side of the lens system be equal as well.

The solution to the focal length/image brightness trade-off was to use a system of shorter focal length lenses that were comparatively larger in diameter. The best lens available in terms of low F/# was the Oriel #39323: a 1.5 inch diameter, bi-convex, fused silica lens with an excellent F/1.3 rating, but unfortunately a focal length of 51 mm (besides which, it was the only 51 mm focal length lens available). It was possible, however, to use two lenses of equal focal lengths to form a compound lens system that would not only achieve longer effective focal lengths but maintain unity magnification. For a two-lens system, the compound lens formula is:

$$\frac{1}{EFL} = \frac{1}{F_1} + \frac{1}{F_2} - \frac{S}{F_1 F_2} \qquad [28]$$

where F_1 and F_2 are the focal lengths of the first and second lenses, respectively, and S is the distance between the effective refracting surfaces of the two lenses. Since we are required to keep the magnification factor of one, F_1 and F_2 will be equal and the compound lens formula reduces to:

$$S = 2F - \frac{F^2}{EFL}$$

Using this formula, the separation distance between two lenses having focal lengths of 150 mm would be 255 mm, for a system with an effective focal length of 500 mm. Two Oriel #41570 (1.5 inch diameter, plano-convex, 150 mm focal length, F/3.9 fused silica) lenses were combined to form a compound lens system. This compound lens system would have an F/13 rating, 2.25 times brighter than a single 500 mm focal length lens of the same image quality. This lens set-up was implemented for some of the initial experiments. See Figure 2.4 for details on this lens configuration.

Early experiments revealed that sections of the turbulent flame did not shed a strong chemiluminescent signal. These "dark zones" invariably occurred at the base of the flame, within the first inch of the tip of the burner. It was theorized that the finite amount of time needed for the chemiluminescent reactions to take place and the velocities of the gases exiting the burner were the causes of the dark zones. Gas velocities were on the order of three m/s for these early experiments, and if a particular chemiluminescent reaction required five ms to complete, the gas molecules would travel 1.5 cm above the burner. The solution to the problem of the dark zones was, of course, to move the lens system so as to image farther up on the flame.

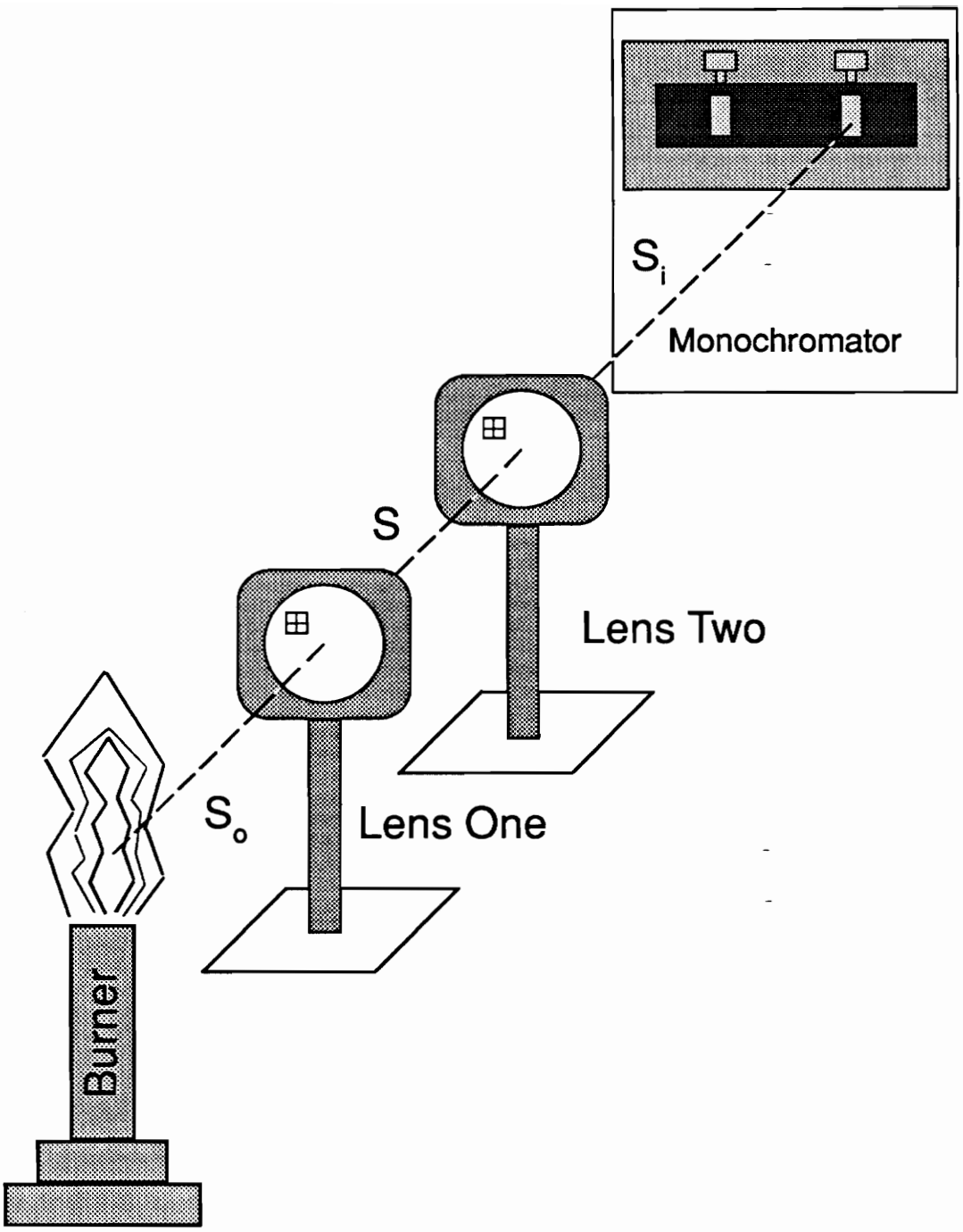

Figure 2.4: Compound lens optical system set-up utilizing two plano-convex lenses.

Experiments were carried out to determine if the nature of the chemiluminescent emission changed over the height of the flame. Hamer [1] had concluded that imaging different portions of the flame would yield different data, but only because the number of chemiluminescent signals reaching the detector was changing. Johnsson [26] also reached the conclusion that different magnifications were also contributing to the changes in data. In both sets of experiments, however, nearly the entire flame could be imaged onto the detector, as the laminar flames were very small. In contrast, the turbulent flames were on the order of six to sixty inches high, depending on the stoichiometry and turbulence level.

Sections along the height of the flame were imaged and the results compared to determine if the chemiluminescent emissions varied with flame height. Flames with different stoichiometries and Reynolds numbers were tested. A set of data for each flame was generated. The data sets showed no correlation between chemiluminescent signals (which remained similar for the same flames) and flame height. Therefore, the decision was made to image the detector a few inches above the burner lip (so as to eliminate the problem of the dark zones) and no consideration was made concerning keeping the height of the detector imaging area constant from flame to flame.

There was also a concern that in the early experiments, the section of the flame that was being imaged onto the monochromator was not an adequate representation of the entire flame front. To determine how much of the flame was actually being imaged, calculations concerning angular field of view were performed. Field of view is the angle subtended by the source (the flame in this

case) producing the maximum usable image size. The formula for calculating field of view is:

$$FOV = 2\tan^{-1}\left(\frac{H}{EFL}\right) \qquad [28]$$

where H is the usable image height. In a camera, for instance, field of view is limited by the dimensions of the film or by the size of the viewfinder. In the early experiments, field of view was limited to 15 mm, the height of the monochromator entrance slit. The angular field of view was therefore only 3.4 degrees, which corresponds to a circular segment of the flame 30 mm in diameter or over 700 mm^2 in area.

To further increase the strength of the chemiluminescent signal, an even larger portion of the flame needed to be imaged onto the monochromator entrance slit. Yet, retaining a magnification of one limited the field of view to a 30 mm diameter circle. Greater areas of the flame could be scanned by reducing the magnification still further, but then comparisons with Hamer and Johnsson's experimental database would be less meaningful. The solution to this problem came in the form of a cylindrical lens.

The cylindrical lens is designed to give magnification in only one plane, unlike conventional spherical lenses that give equal magnification in two orthogonal planes. Cylindrical lenses are used to image a point source as a line (a common laser application) or to change the height of an image without altering the width. For example, in this research, a greater portion of the flame height could be imaged than possible with a spherical lens. The lens used for

these experiments was a rectangular cylindrical type (as opposed to a circular cylindrical lens), Oriel #44055: a fused silica, 150 mm focal length lens measuring 2 by 2.5 inches. To maintain unity magnification and a 500 mm effective focal length, some modifications to the initial set-up were necessary. The cylindrical lens was placed closest to the flame, with S_i = 500 mm. One Oriel #41570 lens was retained and placed nearest the monochromator; S_o = 245 mm. As before, the separation distance between the two 150 mm focal length lenses was 255 mm. The cylindrical lens had an F/2.3 rating, based on a 2.52 inch effective diameter. The cylindrical/plano-convex compound lens system had an overall F/13 rating (using the 1.5 inch diameter plano-convex lens as the limiting factor for brightness determination), the same as with the previous set-up, but with more of the flame height being imaged onto the monochromator. Up to a 2.5 inch flame width section could be imaged with the cylindrical lens; now a greater portion of the flame height could be imaged as well. The corresponding flame area being imaged was over 1900 mm^2, an improvement by a factor of 2.7. See Figures 2.5 and 2.6 for details of this later set-up.

It should be noted that the detector sees a relatively small portion of the flame overall, regardless of which equipment set-up is used. If a flame were about twelve inches tall, the total area available for detector imaging is on the order of 24,000 mm^2 (a cylindrical sheet one inch in diameter and twelve inches tall). Keep in mind that the flame sheet is translucent as well; that is, chemiluminescent emissions on the far side of the flame (from the detector) can reach the detector as easily as emissions on the near side.

All 1.5 inch diameter lenses were mounted in Oriel #12720 general

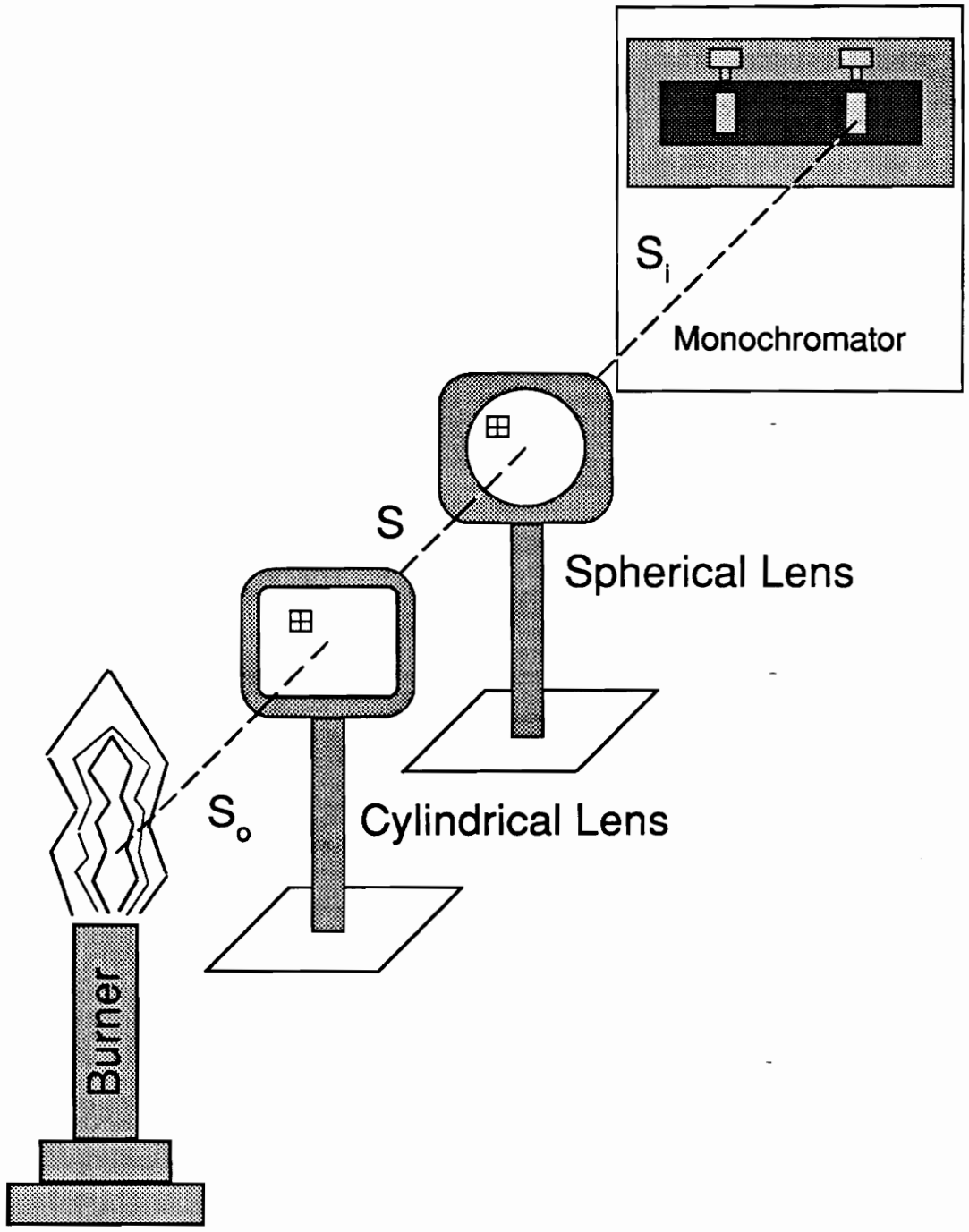

Figure 2.5: Compound lens optical system set-up utilizing a cylindrical lens and a plano-convex lens.

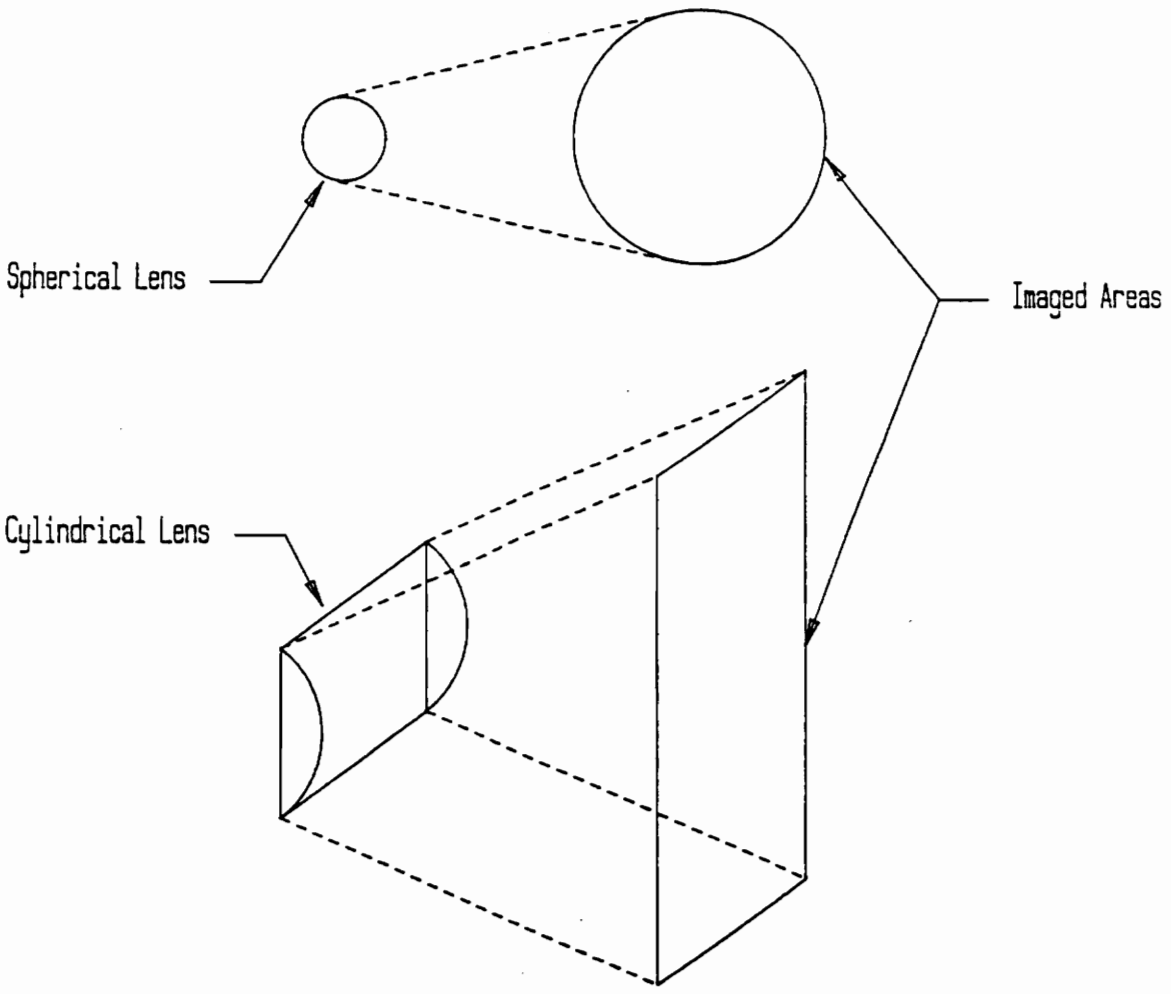

Figure 2.6: Comparison of imaged areas of a spherical and a cylindrical lens. Not to scale.

purpose lens holders that were in turn rod-mounted onto Oriel #11612 table slides. The cylindrical lens was mounted in an Oriel #1311 rectangular lens holder that was also rod-mounted onto a table slide.

2.3.3 Fiber-optics

After initial experimentation with the lens/monochromator system was concluded, the use of fiber-optic hardware was investigated. It was anticipated that any "real-world" application of the chemiluminescent detector system would utilize fiber-optics and filters, primarily because of the harsh nature of the combustor compartment. What was not known was whether the trends observed in the data for the lens/monochromator system would also be observed with the fiber-optic/filter system.

Two fiber-optic systems were considered for the chemiluminescent detector application. The first was the Oriel #77562: a three foot long, 1.6 mm diameter high-grade fused silica fiber bundle of 200 fibers each of 200 micron diameter. The fibers transmitted light from 280 to 2200 nm. Both ends of the fiber were terminated with Oriel #77644 collimating beam probes, containing fused silica lenses with 19 mm focal lengths. Collimating lenses were necessary to collect and focus light onto the fibers and to recollimate light exiting the fibers into parallel rays. The second fiber-optic system consisted of a single strand, high grade fused silica fiber, one meter in length and terminated with standard SMA connectors (type 905). The single strand fibers were obtained from Fiberguide Industries, Inc. (part number SPCMA-2005-PX1)

The fiber bundle system had the advantage of transmitting a stronger signal than the single strand, by virtue of its increased collection area. However, the single strand fibers were more flexible, more easily installed and cost only one-sixth as much as the bundles. If the signal from the single strand fibers were strong enough to use, much of the cost and complexity could be removed from the chemiluminescent detector design.

The fiber bundle was mounted in Oriel #77803 beam probe adapters at either end. The end oriented towards the flame was rod-mounted while the other end was connected directly to the filter. See Figure 2.7 for details on the fiber bundle set-up.

The single strand fibers were terminated with SMA connectors, one end connected to an Oriel #77670 11 mm ferule adapter and in turn connected to the aforementioned collimating beam probe. This end was then connected directly to the filter, as before. The other SMA connector of the single strand fiber was connected to an Oriel #77848 single fiber holder, which was rod mounted and oriented towards the flame. Because of the size of the flame relative to the single strand fiber acceptance area, the flame could be treated as an infinitely diffuse light source (as opposed to a point source, for instance) and as such no collimating beam probe was necessary on that end of the single fiber. See Figure 2.8 for details on the single fiber strand set-up.

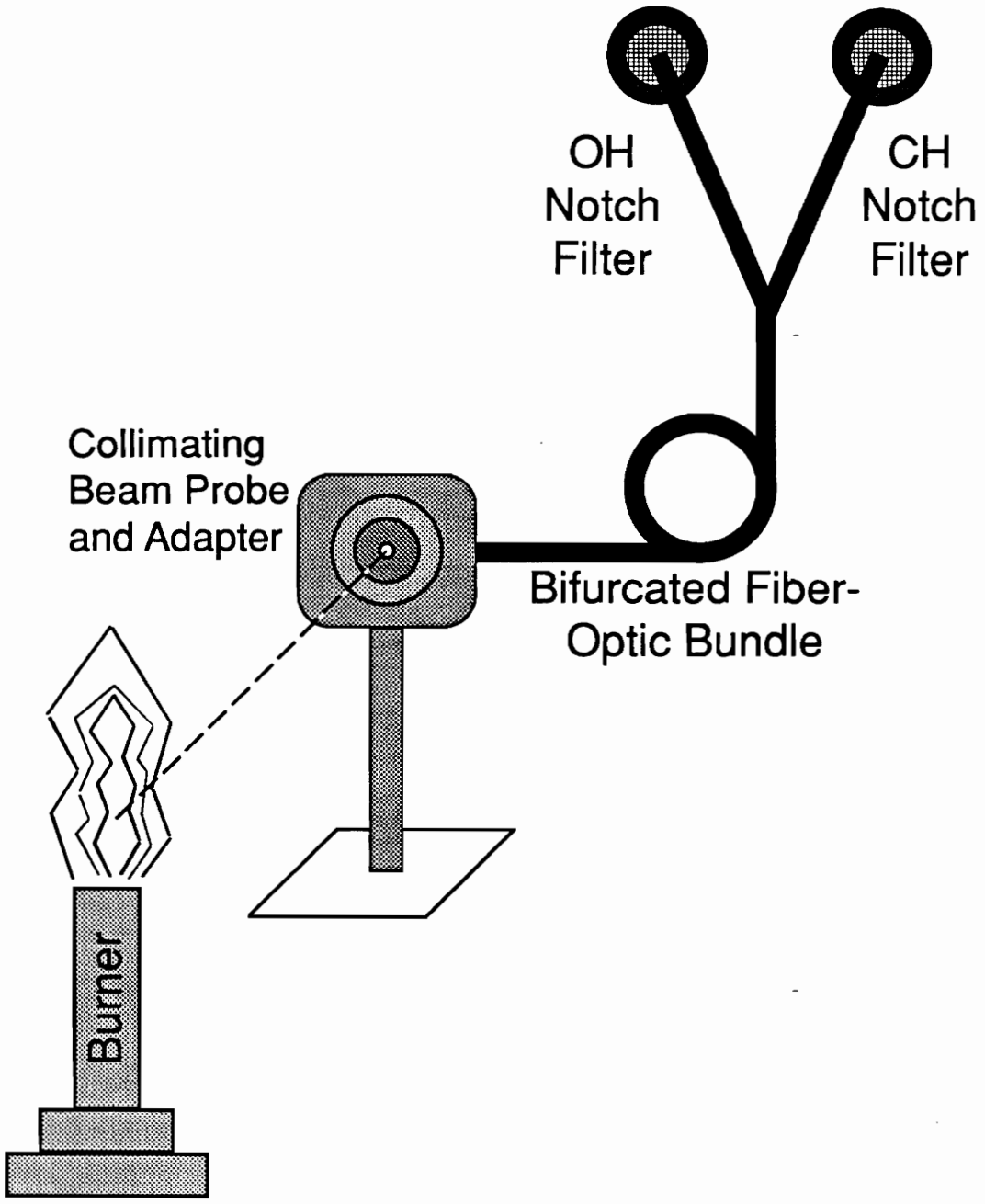

Figure 2.7: Optical system set-up utilizing a bifurcated fiber-optic bundle and two narrow band-pass filters.

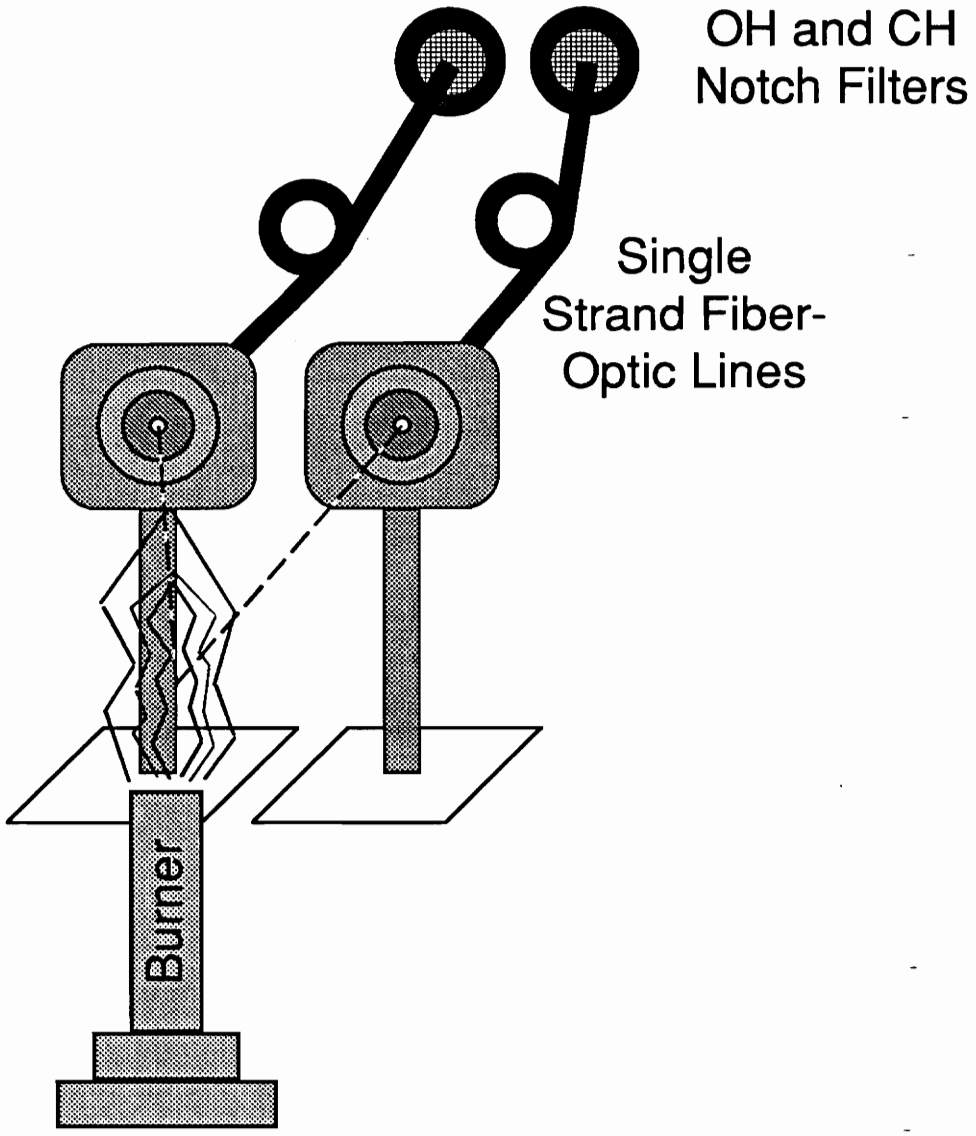

Figure 2.8: Optical system set-up utilizing two single-strand fiber-optic lines each connected to a narrow band-pass filter.

2.4 Detection System

2.4.1 Introduction

The chemiluminescent detector experiments were performed with two different set-ups. The first set-up utilized a monochromator and a photomultiplier tube (PMT). The light was delivered to the monochromator entrance slit by the various optical systems described in section 2.3. The monochromator focused the light at a specific wavelength on the exit slit of the monochromator. Attached to the exit slit was a fast response PMT that produced a current proportional to the amount of light present. By placing the current across a load resistor, a voltage was created which could be monitored and stored by a digital oscilloscope. It was possible for the monochromator to scan across wavelengths at a specified speed, thereby yielding a plot of chemiluminescent signal intensity versus wavelength. The second detector system configuration used band pass interference filters in place of the monochromator. Fiber-optics delivered the light to these filters. The filters were selected to screen out certain wavelengths of the chemiluminescent signal. The intensity of the signal at those specific wavelengths could then be monitored by PMT's, in the fashion of the monochromator set-up.

2.4.2 Monochromator

The monochromator used was a half meter Ebert scanning monochromator (Thermo Jarrell Ash Corp. model 82-020) with a 1180 lines/mm grating. The monochromator's operating range was from 200 to 1100 nm, although for these experiments it was used almost exclusively between 280 and

550 nm. A motor and variable gear drive allowed the monochromator to scan at speeds from 0.2 to 50 nm/min. A scanning speed of 50 nm/min was chosen for all experiments. The gear drive could also be disengaged to permit manual scanning. The resolution of the monochromator was better than one nanometer. Adjustable entrance and exit slits were set to their maximum widths and heights of 10 mm and 15 mm, respectively. Slit height was important in determining angular field of view, as discussed in section 2.3.1. Because the monochromator's reflecting mirror focused selected wavelengths at the center of the exit slit, maximum slit width was needed to allow a greater range of wavelengths (three-quarters of a nanometer on either side of the wavelength of interest) and thus more light intensity to be passed onto the PMT.

2.4.3 Photomultiplier Tube

The photomultiplier tube was a nine stage electron cascade, side window, reflection mode device (RCA model #1P28B). The spectral range of the PMT was from 200 to 660 nm and its response time was 1.8 nanoseconds. A high voltage power supply (RCA model #PF1042) was needed to operate the PMT. The PF1042 required 13.5 volts DC and a potentiometer to control its output voltage. The potentiometer was set at 340 Ω, resulting in approximately 1000 volts as an input to the PMT. In later experiments with the fiber-optic/filter set-up, three identical PMT systems were used. See Figure 2.9 for details on the monochromator/PMT circuits.

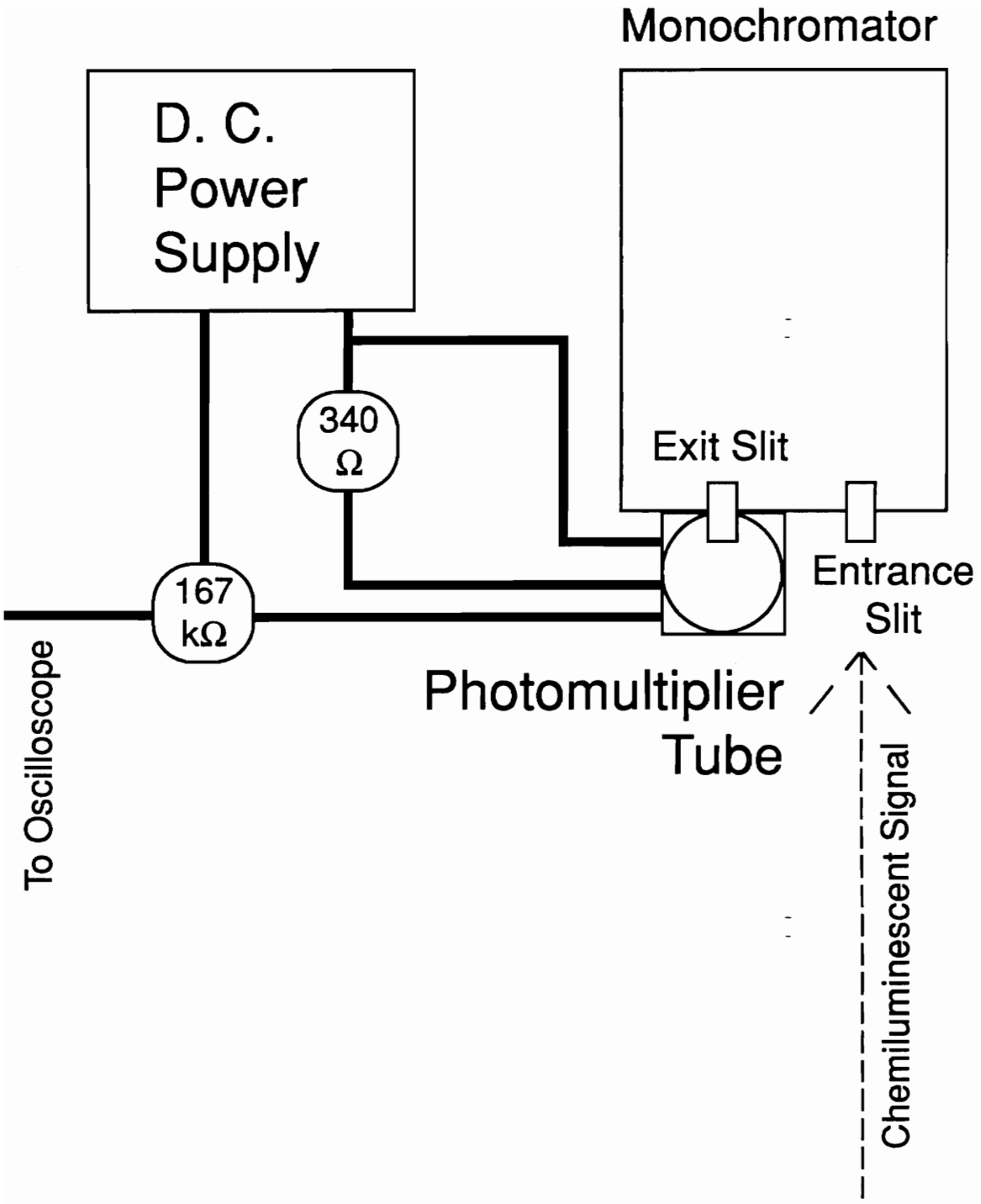

Figure 2.9: Schematic of the monochromator/PMT circuit setup.

2.4.4 Filters

Ideally, three filters would have been used for the fiber-optic/filter set-up. Three filters were necessary to reproduce the correlations made with the monochromator set-up. One-inch diameter narrow band pass or notch filters were used for isolating the OH^* and CH^* chemiluminescent signals, respectively. Oriel #53375 has a center wavelength of 308.5 nm and bandwidth of 11.4 nm at half-peak transmittance; Oriel #53815 has a center wavelength of 429.5 nm and a bandwidth of 8 nm at half-peak transmittance. Peak transmittance for the OH filter was 19 percent and for the CH filter, 50 percent. See Figures 2.10 and 2.11, respectively, for transmittance graphs of the OH and CH notch filters. The remaining filter would have been a special production item, a very narrow band pass or line filter centered on the OH signal wavelength, perhaps with a bandwidth of only two or three nm. This special production filter would have cost several thousand dollars (as it would not have been produced in quantity) and budgetary constraints forced another course. The monochromator was adapted to line filter duty by placing the grating at precisely 309 nm and by using neutral density filters to simulate the twenty percent or so transmission rates of the one inch UV filters. It was not a totally convincing simulation, but worked well enough. See Figure 2.12 for details on the filter/PMT set-up.

2.4.5 Thermocouple

The temperature and fuel-to-air ratio experiments required flame temperatures and equivalence ratios be referenced. For fuel-to-air ratio testing, the referencing procedure was straightforward: the equivalence ratio of the methane and air mixture was determined beforehand using a FORTRAN

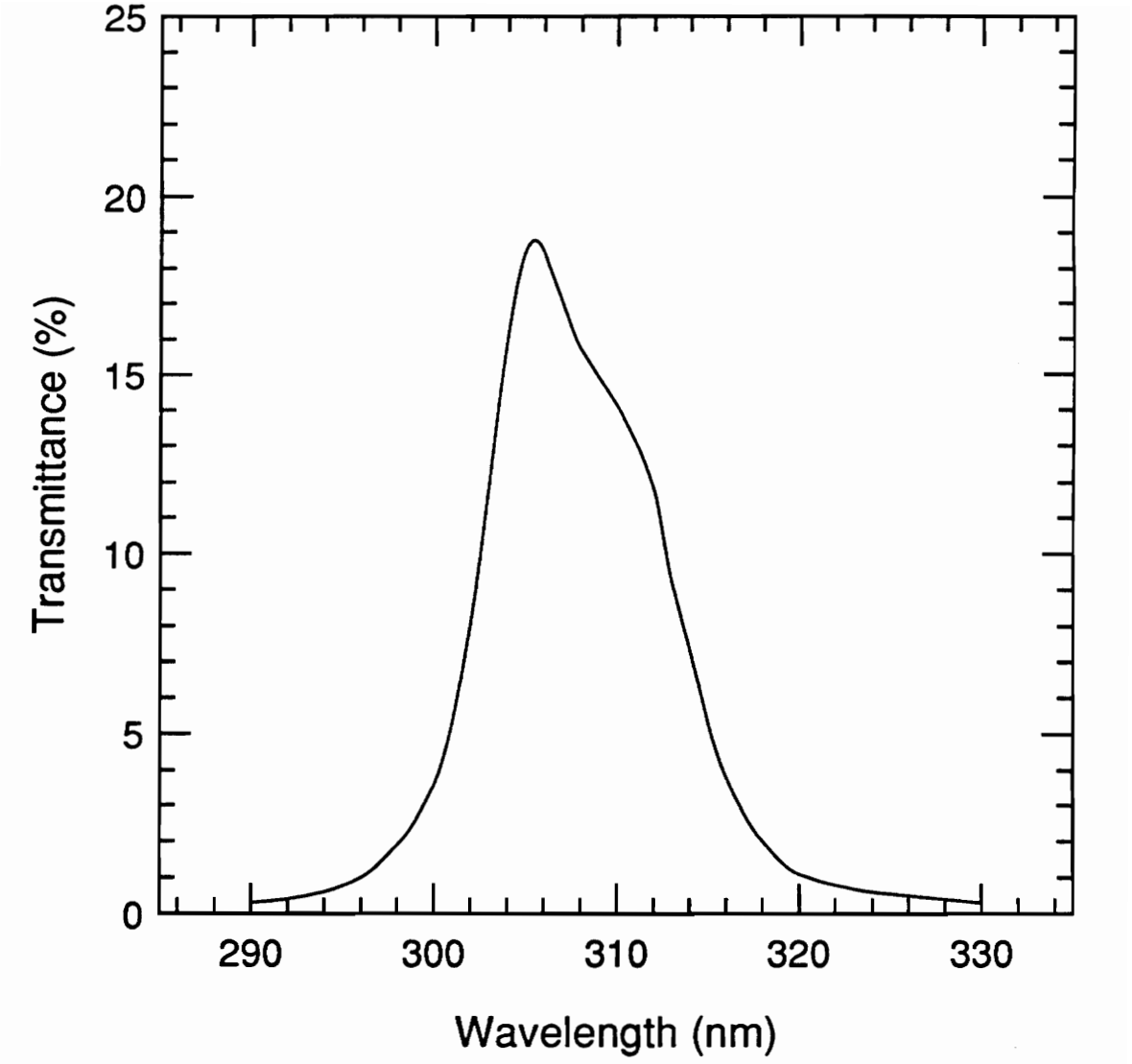

Figure 2.10: Narrow band-pass filter transmittance graph for ORIEL #53375, used to isolate OH radical chemiluminescent signals.

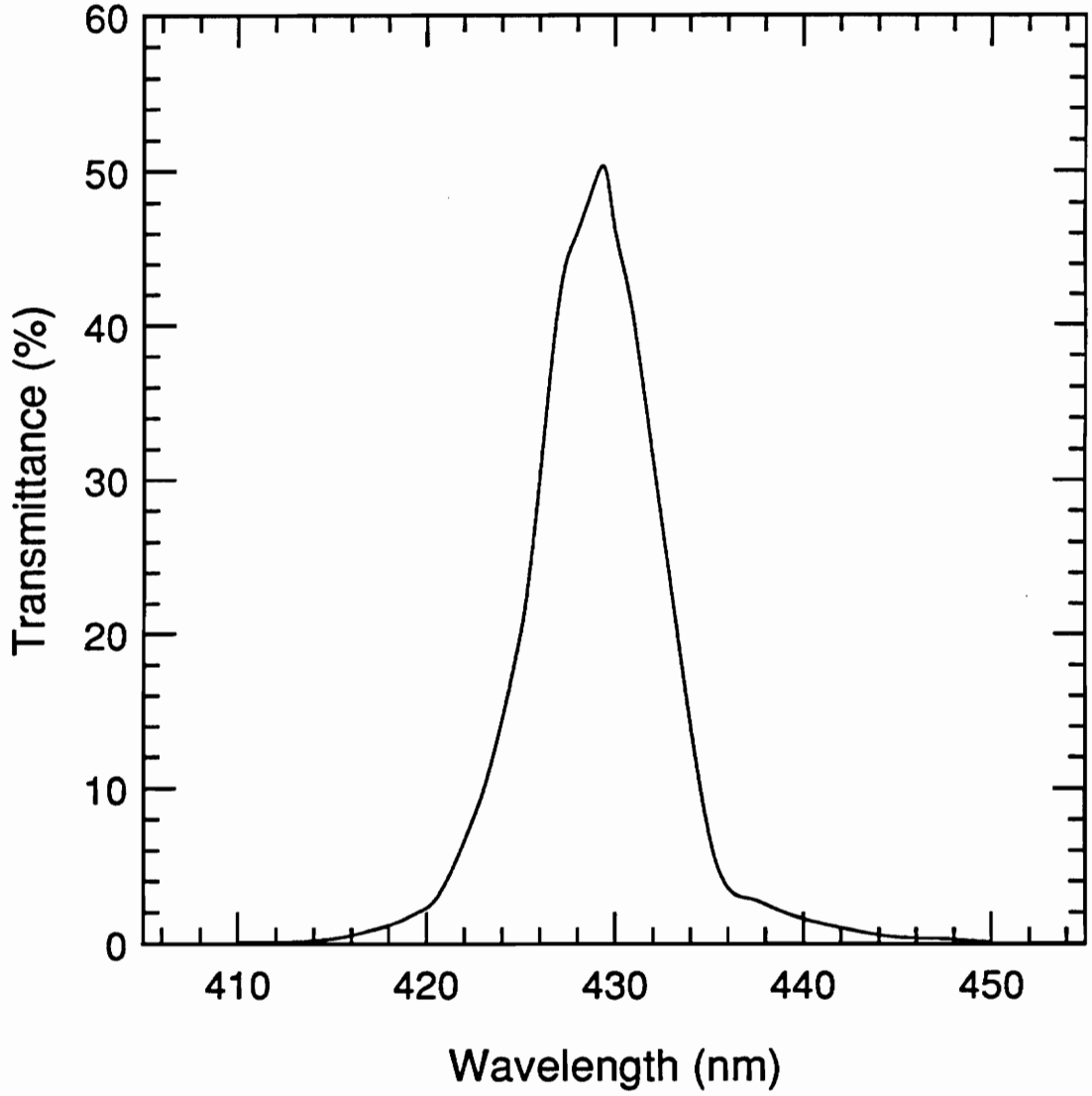

Figure 2.11: Narrow band-pass filter transmittance graph for ORIEL #53815, used to isolate CH radical chemiluminescent signals.

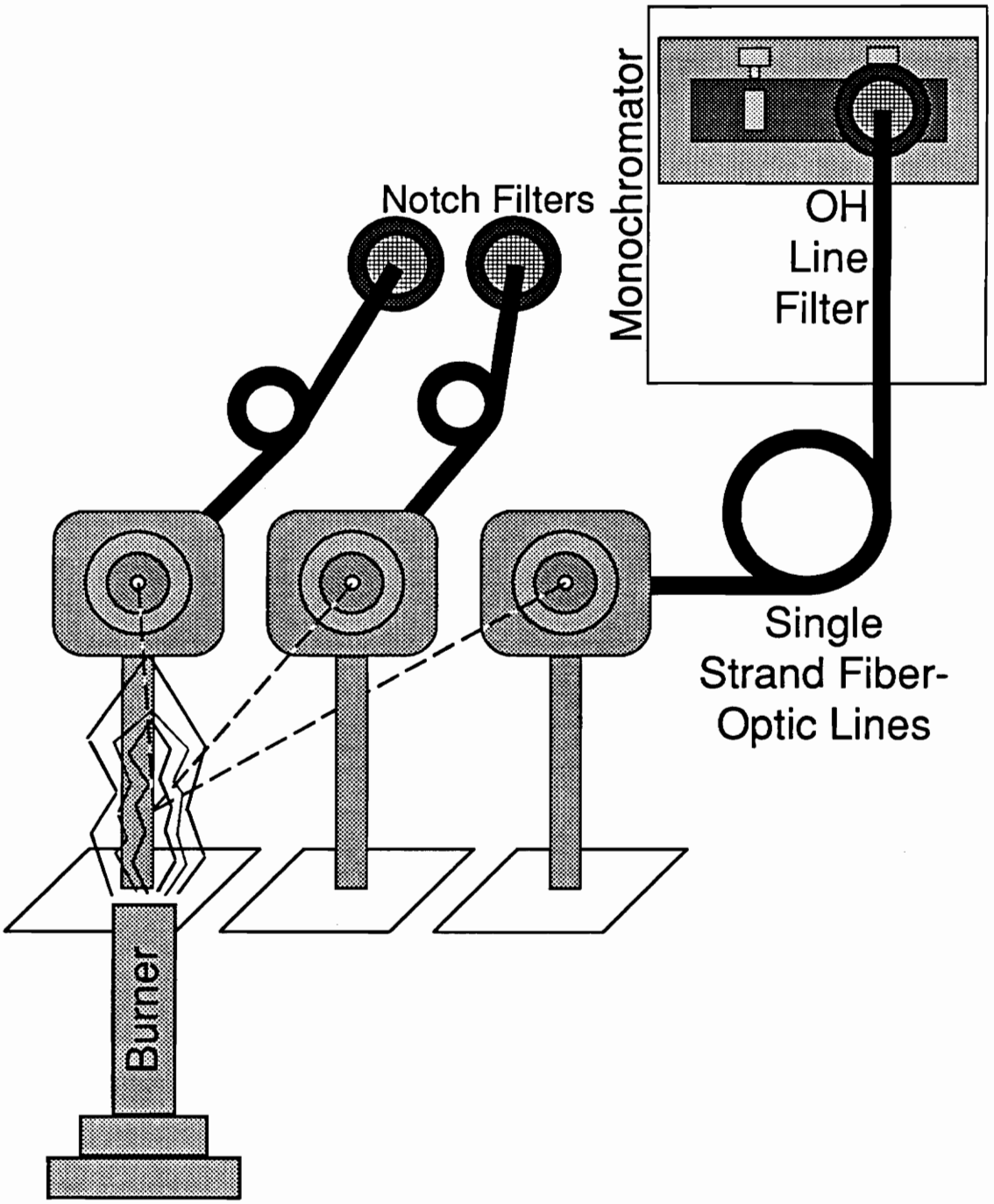

Figure 2.12: Optical system set-up utilizing three single-strand fiber-optic lines, two narrow band-pass filters, and a monochromator/neutral density filter combination simulating an ultra-narrow band-pass filter.

program (reproduced in Appendix C) and the required flowrates set on the rotameters. Flame temperature referencing, however, was another matter entirely. A high temperature thermocouple was placed in the flame both before and after the experiment to determine average flame temperature during the test. The voltage produced by the thermocouple was recorded on the digital oscilloscope on a separate channel along with the PMT output.

The thermocouple used was an uncoated high temperature Platinum and Platinum/10% Rhodium junction model with 5 mil (0.127 mm) diameter wires. The thermocouple wires came prepackaged as Omega #P10R-005-7. Junction bead diameter was typically three to five times the wire diameter (many wires were burned out during experimentation and were replaced with similar, but not identical, junctions). Except for 1.5 cm of exposed wire at the junction end, the wires were encased in a 13.5 cm-long ceramic sheath and a 12.5 cm-long stainless steel annular sheath covering the ceramic. The thermocouple wire connector was Omega type SMP and the cold junction compensator (which eliminates the need for a thermocouple reference temperature) was Omega type MCJ-S. The thermocouple was held in a rod mounted "claw" holder from Coherent Radiation during its use.

Directly converting thermocouple output voltages to flame temperatures is not a simple task. The voltage must be factored into a ninth-order polynomial supplied by Omega [29] to produce a bead temperature. But the bead temperature is not the flame temperature. A good deal of energy is lost at the thermocouple bead through radiation to the surroundings. The amount of energy lost is a function of the surface area of the junction bead; the reason

small diameter wires with small junction beads were used. A FORTRAN radiation correction program [30] was used to correct for the loss of energy by the bead and convert bead temperatures to corrected flame temperatures. This program is reproduced in Appendix D. Since junction bead diameter was an important variable in the radiation heat loss correction program, the beads were measured on a microscope with a magnification of eighty times to more accurately determine their diameters.

2.5 Data Acquisition System

2.5.1 Introduction

The data acquisition system was composed of a digital oscilloscope, data recorder, RS-232C serial interface, and an Intel 80386-based microcomputer. The oscilloscope was used to capture the data and to perform rudimentary analyses on it. The data recorder stored the information for later retrieval. The interface was necessary to transfer the data to the PC, where more detailed analyses and plotting could be performed.

2.5.2 Digital Oscilloscope

A Nicolet model 4562/4094C digital oscilloscope was used in conjunction with a Nicolet F-43 data recorder (a 5.25 inch disk drive) for data acquisition. The time scale was set to 20 ms/point and the voltage scale to 400 mV (100 mV for the thermocouple voltages). The oscilloscope always collected 15,872 points per sweep. Thus, the time scale provided a spectral scan from 280 to 544.53 nm (scan speed was 50 nm/min) lasting 317.44 seconds. The voltage scale provided the full range of operation needed for the PMT and thermocouple

voltage outputs. A diskette of programs supplied by Nicolet allowed many mathematic and statistical operations to be performed on the collected data. Among the more frequently used programs were point smoothing, area integration, arithmetic means, translation along one or both axes, and inversion of voltage values. The operation of the PMT required the use of a 167 kΩ load resistor placed across the output to generate a voltage the oscilloscope could read.

2.5.3 Computer

An 80386-based PC was used to gather data from the oscilloscope and produce graphs with that data. The information was transmitted in 8-bit packets by an RS-232C interface on the back of the oscilloscope to the computer. Transfer was supervised by a compiled BASIC program [31], reproduced in Appendix E, using XON/XOFF protocol and odd-bit parity checking. The data was subsequently translated into ASCII format and graphed using several PROPLOT [32] programs on an Apple Laserwriter II NT laser printer. A typical PROPLOT program is given in Appendix F. After plotting, the data was stored both on hard drive and on 3.5 inch floppy back-up disks.

3. Experimental Procedure

3.1 Introduction

This section details the procedures used to determine relationships between chemiluminescent signals, fuel-to-air ratios and flame temperatures. The effects of turbulence intensity on these relationships are briefly discussed. The reasoning behind the procedures used is explained.

3.2 Fuel-to-Air Ratio Tests

The experiments to determine the relationship between chemiluminescent signals and fuel-to-air ratio for turbulent flame used a methane-air flame with varying amounts of nitrogen added. As mentioned in section 2.2.1, small amounts of hydrogen were added to highly turbulent flames to attach them to the burner. To isolate the effect of fuel-to-air ratio of the chemiluminescent signal, it was necessary to hold temperature and Reynolds number constant for flames with differing fuel-to-air ratio. A FORTRAN program was written (see Appendix C) to calculate the flowrates of methane, air, and nitrogen needed to achieve a given fuel-to-air ratio and turbulence level. Nitrogen was then added to the flame until the desired temperature was reached and the flowrates recalculated to compensate for the additional turbulence caused by the nitrogen addition. This iterative process rarely required more than four steps to achieve a balance between fuel-to-air ratio, temperature and turbulence level.

Actual fuel-to-air ratio was calculated on a molar basis using the equivalence ratio desired and the molecular weights of methane and air. The

equivalence ratio is defined as the ratio of the actual fuel-to-air ratio to the stoichiometric fuel-to-air ratio:

$$\phi = \frac{(F/A)_{actual}}{(F/A)_{stoichiometric}} \qquad [33]$$

The stoichiometric fuel-to-air ratio is that ratio at which the amount of air and the amount of fuel are in the exact proportion for complete combustion. For methane and dry air, the stoichiometric fuel-to-air ratio is 1:9.546 on a molar basis or about 1:9.5 on a volumetric flow basis (the latter figure may change with fluctuations in methane and/or air density).

The level of turbulent intensity was most readily measured by calculating the Reynolds number of the entire flow. The Reynolds number is a non-dimensional coefficient used to estimate turbulence. Reynolds number is defined as:

$$\mathrm{Re} = \frac{4\rho Q}{\pi \mu d} \qquad [34]$$

where ρ is the density of the entire flow, Q is the overall volumetric flowrate, μ is the kinematic viscosity of the entire flow and d is the hydraulic diameter of the passage the through which the gases flow. The density and kinematic viscosity of the entire flow were calculated from the component densities and kinematic viscosities of its constituent parts. For density, a total flow value may be obtained by weighting each component density by its mole fraction in the flow:

$$\rho_{mix} = \sum_{i=1}^{n} x_i \rho_i \qquad [34]$$

For kinematic viscosity, a total flow value is again based on constituent values and can be obtained from the following semi-empirical formula:

$$\mu_{mix} = \sum_{i=1}^{n} \frac{x_i \mu_i}{\sum_{j=1}^{m} x_j \Phi_{ij}} \qquad [35]$$

where $$\Phi_{ij} = \frac{1}{\sqrt{8}} \left(1 + \frac{M_i}{M_j}\right)^{-\frac{1}{2}} \left[1 + \left(\frac{\mu_i}{\mu_j}\right)^{\frac{1}{2}} \left(\frac{M_j}{M_i}\right)^{\frac{1}{4}}\right]^2$$

μ_x = kinematic viscosity of constituent x

M_x = molecular weight of constituent x

By inputting desired Reynolds number, desired equivalence ratio, ambient temperature and barometric pressure into the FORTRAN program, reasonably accurate flowrates could be calculated for methane and air to achieve a desired fuel-to-air ratio.

After the required flowrates were calculated, the corresponding rotameter float positions were calculated from calibration charts prepared beforehand. Appendix B contains the rotameter calibration charts for the rotameters used in this research. The thermocouple was used at this point to ensure that the flame temperature was kept consistent with other experiments. The sequence of

experiments began with a flame with the lowest equivalence ratio feasible (any lower and the flame speed would not overcome the gas velocity and blowoff resulted). The temperature of the lowest equivalence ratio flame was used as the reference temperature for all other flames in the fuel-to-air ratio testing. The logic behind this choice was that flames with fuel-to-air ratios closer to stoichiometric will be hotter, thus the lowest flame temperature is used as the reference and naturally hotter flames are brought down to this reference temperature by nitrogen addition. The lowest equivalence ratio (and hence lowest flame temperature) feasible was $\phi = 0.67$ (it was possible to stabilize a leaner flame but then overly large amounts of nitrogen addition, exceeding the capacity of the 604 rotameter, would be necessary to maintain the reference flame temperature for the richer flames). The corrected flame temperature for this flame was 1636 K. The flame was lit with a hand held butane fireplace lighter, line pressures were adjusted and the experiment was ready to begin.

The monochromator was set to 270 nm and the Nicolet on standby. The monochromator was started, moving across wavelengths at a rate of 50 nm/min. The monochromator emits an audible "click" as it passes every nanometer. When the monochromator reached 280 nm, the oscilloscope was placed on its "Hold Next" position. The synchronization of monochromator and oscilloscope is critical to the accurate translation of scan time on the oscilloscope to wavelength scanned by the monochromator. Therefore, every effort was made to synchronize this operation.

During the experiment, rotameter float positions and line pressures were carefully monitored. Often, fine adjustments were necessary to maintain the

pressures and flowrates throughout the experiment. As mentioned in section 2.5.1, the monochromator scanned from 280 to 544.53 nm over a period of 317.44 seconds. The scan was completed automatically when the oscilloscope filled its databank with 15,872 points.

After the scan was completed data manipulation programs were employed to translate the data from its raw form to a form more useful for analysis. A point smoothing algorithm (provided by Nicolet) was used to screen out noise in the signal and better define the true signal. The algorithm uses a cubic spline curve fit for a specified number of points around a given data point. By specifying a large number of points to be used, noise is greatly diminished but some peak signal information is lost. Specifying too few points to be used will result in lower signal-to-noise ratios, of course. The number of points used is supplied by the user; for these experiments, 25 points on either side of a given data point was determined to be the optimum figure. See Figure 3.1 for an example of the point-smoothing program.

Other programs might be used to translate the data points (as a set) to higher voltage values or to invert the voltages (negative voltages to positive ones) altogether. These procedures were done simply to make comparisons easier and for consistency, they had no effect on the correlations made from the data sets.

Once the data set was translated into a useful form, it was saved on the Nicolet F-43 Data Recorder. The F-43 used 5.25 inch floppy diskettes for recording media. The F-43 could place twenty data sets on one low-density (360 KB) diskette.

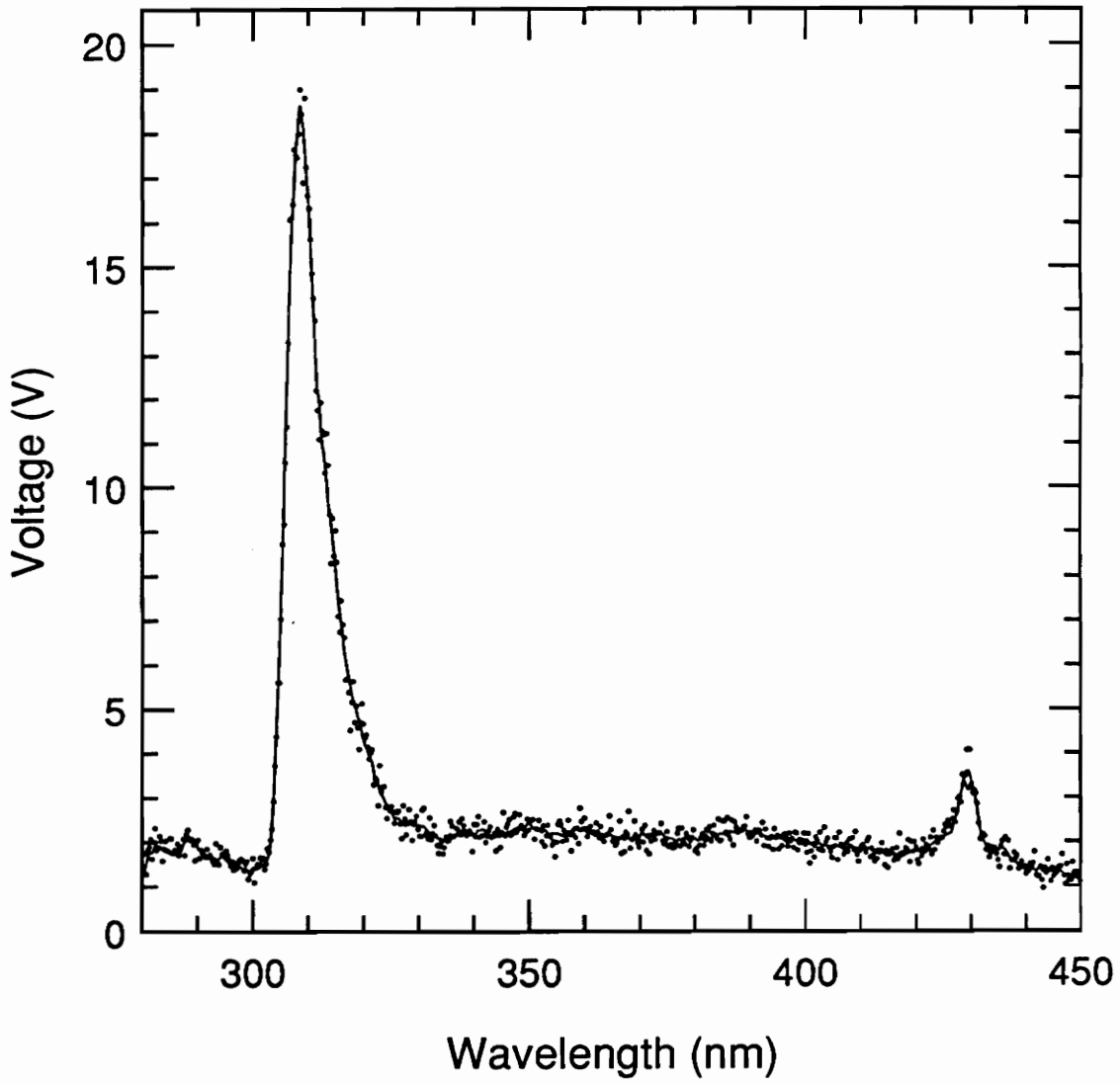

Figure 3.1: Comparison of raw and point-smoothed waveforms for a laminar premixed methane-air flame.

After several data sets were completed and saved, they were then sent to the '386-based PC via an RS-232C connection. The data was then translated into ASCII form and plotted with PROPLOT. The data was saved in its new form on the hard drive of the computer and once more on 3.5 inch, high density (1.44 MB) diskettes.

3.3 Temperature Tests

Temperature testing was performed in much the same manner as the fuel-to-air ratio experiments. The required flowrates of methane, air and nitrogen were calculated with the FORTRAN program and the rotameter floats set to the necessary positions. The thermocouple leads were then attached to a second channel of the oscilloscope and a temperature measurement made. Thermocouple voltage compensation was achieved with an Omega MCJ-S cold junction compensator. The compensation is needed because of the voltage created when the dissimilar metals of the thermocouple wire (platinum or a platinum-10% rhodium alloy) and the thermocouple leads (copper) meet. The corresponding thermocouple compensated voltage is recorded on the oscilloscope and translated into a thermocouple bead temperature by means of the following polynomial:

$$T_{bead} = + 1.695E+20\ V^9 - 1.561E+19\ V^8 + 6.175E+17\ V^7 - 1.372E+16\ V^6 + 1.880E+14\ V^5 - 1.636E+12\ V^4 + 8.991E+09\ V^3 - 3.157E+07\ V^2 + 1.695E+05\ V + 9.278E-01$$

where V is the thermocouple compensated voltage. This bead temperature is then fed into a radiation correction FORTRAN program to account for radiative heat transfer away from the thermocouple bead. Bead diameter and ambient

temperature are also input to this program. The resulting corrected flame temperature is used as the actual temperature of the flame.

For all the temperature experiments, the fuel-to-air ratio was kept at ϕ = 0.875. The logic behind this choice is parallel to the reasoning used in the fuel-to-air ratio tests. The hotter flames are closer to the stoichiometric fuel-to-air ratio, so the hottest flame is used and temperatures are manipulated by adding more nitrogen diluent. Of course, the hottest flames occur not at ϕ = 0.875 but close to ϕ = 1.0 (the stoichiometric ratio). The presence of a secondary diffusion flame that obscured the chemiluminescent signal at fuel-to-air ratios near stoichiometric led to the choice of ϕ = 0.875 as the reference fuel-to-air ratio. A secondary diffusion flame is a sheet of flame in an annulus, surrounding a premixed flame core. The diffusion flame burns by entraining fuel molecules from the premixed flame zone and air molecules from the surroundings. Diffusion flames inherently burn near a stoichiometric fuel-to-air ratio. Thus, the chemiluminescent light from a diffusion flame will always be indicative of a stoichiometric flame. The light from a secondary diffusion flame can therefore obscure chemiluminescent signals from the non-stoichiometric, premixed flame core. The secondary diffusion flame phenomenon only occurred for flames with an equivalence ratio of about ϕ = 0.95 or richer in the experiments performed for this research. The secondary diffusion flame phenomenon could be eliminated entirely with the use of an inert shroud gas such as argon. The shroud gas would envelope the premixed flame core and prevent any ambient oxygen from being entrained into the flame zone. An annular shroud would not be sufficient at high levels of turbulence, however, since the turbulent eddies could very well break through the thin annular shroud. A sealed shroud environment, possibly a

box filled with argon to slightly higher than atmospheric pressure (to prevent ambient air from mixing with the argon) would suffice. However, since the practical application of this chemiluminescent detector deals primarily with fuel-lean flames, no shroud gas experiments were performed to eliminate the effect of secondary diffusion flames. Instead, the research was confined to flames which were lean enough to avoid the secondary diffusion flame phenomenon altogether. To be completely safe, the reference flame was chosen to be ϕ = 0.875.

Temperature measurements were made by manually translating the thermocouple bead inside the flame. Care was taken to ensure the thermocouple bead was exposed to all the flame area and for a sufficient time to develop a response (but not long enough to burn out the bead!). The maximum bead voltage was used to calculate bead temperature. It was assumed that the maximum bead voltage recorded corresponded to the maximum flame temperature (i.e., the hottest part of the flame). Therefore, the temperature correlations developed are in reference to the maximum measured flame temperature and not a spatially or temporally averaged flame temperature. Once temperature measurements were recorded, the experiment was begun. The same procedure used for the fuel-to-air ratio testing was followed: oscilloscope and monochromator were synchronized; flowrates and pressures were monitored and adjusted; the data was smoothed and manipulated into a more useful form; the data was stored on the Nicolet, transferred to the PC, translated into ASCII format, plotted, and saved again. Immediately after the experiment, another temperature measurement was made to ensure that the flame temperature did not vary much during the test. If the maximum

thermocouple voltages did not vary by more than ten percent (which corresponds to a ΔT of 141.7 K to 331.4 K at the thermocouple bead, depending on the stoichiometry of the flame), the arithmetic average of the two maximum voltages was used for flame temperature calculation.

3.4 Turbulence Intensity Tests

Although considered to be a major variable in the relationships between chemiluminescent signal ratios and fuel-to-air ratio and temperature measurements, the effect of increasing turbulence was not investigated fully in this research. Ideally, the fuel-to-air ratio and temperature experiments should be repeated with even higher levels of turbulence. Isolating the effect of turbulence on these correlations would be useful in the development of the chemiluminescent detector.

The turbulence of the flames studied in this research is typified by the term "wrinkled laminar flame". A wrinkled laminar flame is a flame with the least amount of turbulence a flame can have and still be in the turbulent flow regime. The transition from laminar to wrinkled laminar flames occurs at a Reynolds number of about 2300 [4]. Transition from wrinkled laminar flames to the next level of turbulence, intermediate turbulent flames, occurs at Reynolds numbers of about 6000 [4]. The highest levels of turbulence occur in "distributed reaction zone" flames where the turbulence is actually on the scale of the combustion zone and directly affects flame chemistry. These flames occur at much higher Reynolds numbers. Actual gas turbine combustors frequently burn flames with Reynolds numbers upwards of 100,000 and are within the distributed reaction zone regime.

The bulk of the experiments carried out in this research deal with flames with Reynolds numbers of only 3000. A few data points were collected on flames with Reynolds numbers of 7000. The turbulent flame burner and rotameters can possibly handle flames with Reynolds numbers of 10,000 at most. Above this level, the rotameters have overextended their range of operation and the hydrogen attachment flame is no longer sufficient to keep the methane-air flame attached to the burner. It is possible that rod-stabilized flames (where a metal rod or similar bluff body is used to stabilize the flame front by creating recirculation eddies in their wakes) could be burned with this burner and push the Reynolds number limit still higher, but modifications to the rotameters and gas lines would be required as well.

The Reynolds numbers of 3000 and 7000 were chosen because the are well within the wrinkled laminar and intermediate turbulence regimes, respectively. The desired Reynolds number was input to the FORTRAN program used to calculate flowrates and was kept constant by reducing the methane and air flowrates proportionally when nitrogen was added to the flame.

4. Experimental Results

4.1 Introduction

This section presents the results obtained from the fuel-to-air ratio, temperature, and turbulence intensity experiments. The correlations of chemiluminescent signal data to equivalence ratio and flame temperature are described. The effects of increasing turbulence on these correlations are shown.

Figure 4.1 is a point-smoothed oscilloscope waveform of a spectral scan of a turbulent premixed methane-air flame. Quantities determined to be related to equivalence ratio and temperature are labeled. The peaks of the OH and CH emissions are plainly shown. The base values for peak signal height are calculated as the arithmetic averages of the voltage values in a range of specified wavelengths encompassing the chemiluminescent signal. For the OH band emission, baselines are calculated from 298 to 341 nm; for the CH band, 418 to 442 nm. The peak signal height is simply the voltage difference between the peak voltage (maximum signal value) and the reference baseline. Full width at half height (FWHH) is the term used to describe the width of the spectral signal at half-peak intensity. This quantity is correlated with flame temperature. The ratio of OH peak signal height to CH peak signal height (OH/CH Peak Height Ratio, or simply OH/CH PHR) is correlated with the fuel-to-air ratio of the flame. Normalized parameters were necessary because measurements based on intensity alone were dependent on the size of the flame.

4.2 Fuel-to-Air Ratio Test Results

Figure 4.2 shows the OH/CH PHR quantities plotted against equivalence

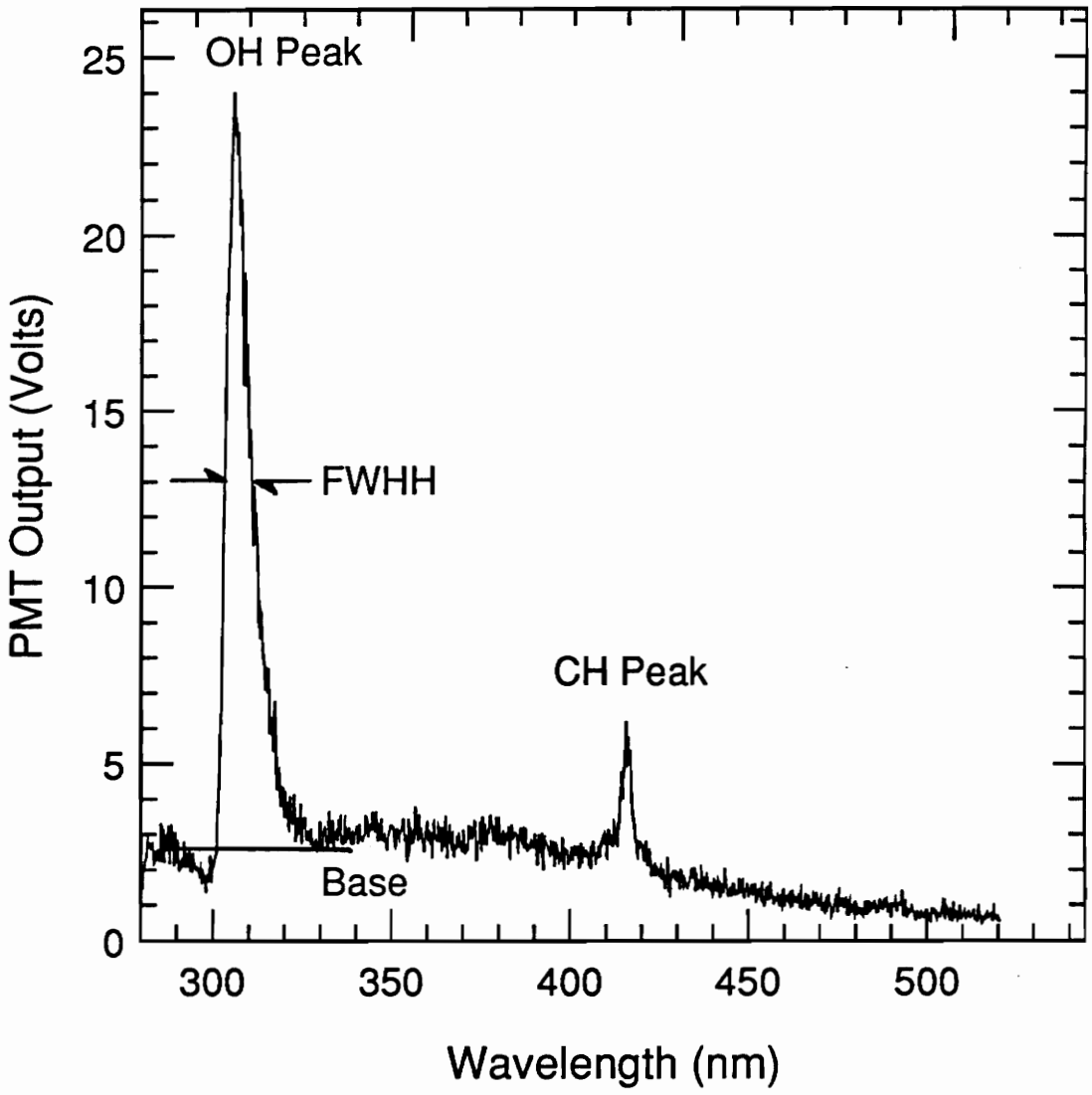

Figure 4.1: Spectral scan of a turbulent premixed methane-air flame, showing labeled quantities.

ratio for turbulent flames. A linear least-squares curve fit is shown along with the data. The regression produced an R^2 (square of the correlation coefficient) value of 0.951. A correlation coefficient of one represents a one-to-one relationship between dependent and independent variables while a correlation coefficient of zero represents no relationship at all. The sign of the correlation coefficient indicates the type of slope the correlation has; negative values indicate negative slopes and positive values indicate positive slopes. The high degree of correlation indicates a nearly linear relationship between OH/CH PHR and flame stoichiometry. The linear correlation with negative slope is in accordance with theory (see section 5.2).

Correlations of other spectral quantities with equivalence ratio besides OH/CH PHR were investigated by Johnsson [26]. None demonstrated a greater potential than the peak height correlation. A comparison of turbulent flame OH/CH PHR and laminar flame OH/CH PHR is given in Figure 4.3.

When the fiber-optic/filter set-up was employed, the OH/CH PHR could no longer be calculated, because there was no monochromator to produce spectral scans. A different correlation involving similar quantities was needed. Since the fiber-optics transmit the intensity of the light received over a broad bandwidth, any correlation developed would have to be based solely on the light intensity information. By using the ratio of OH notch filter signal intensity to CH notch filter signal intensity (OH/CH Notch Filter Ratio, or simply OH/CH NFR), the OH/CH PHR was approximated.

As mentioned in section 2.4, the notch filters used did not transmit all the

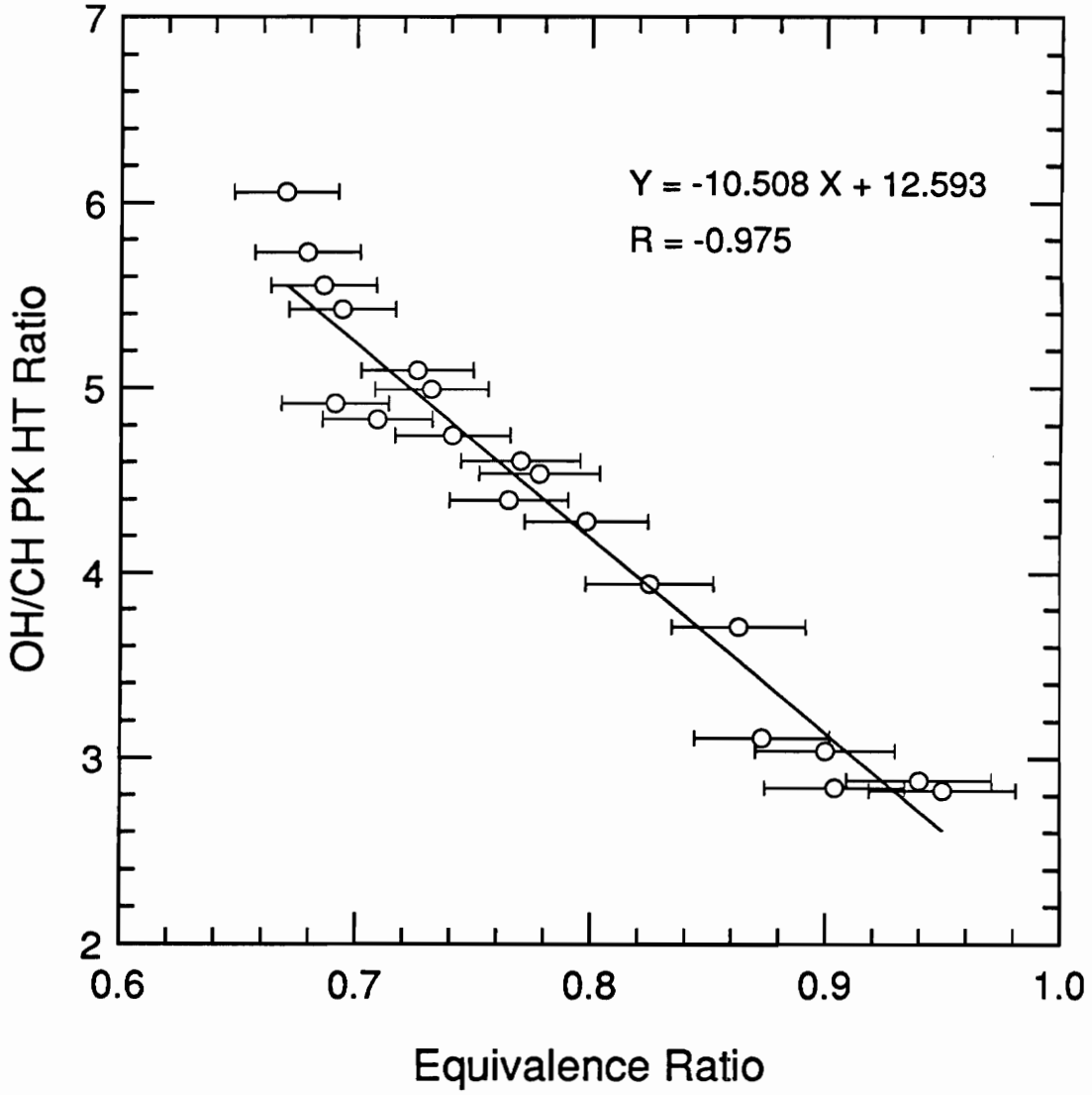

Figure 4.2: OH/CH Peak Height Ratio as a function of equivalence ratio for turbulent premixed methane-air flames.

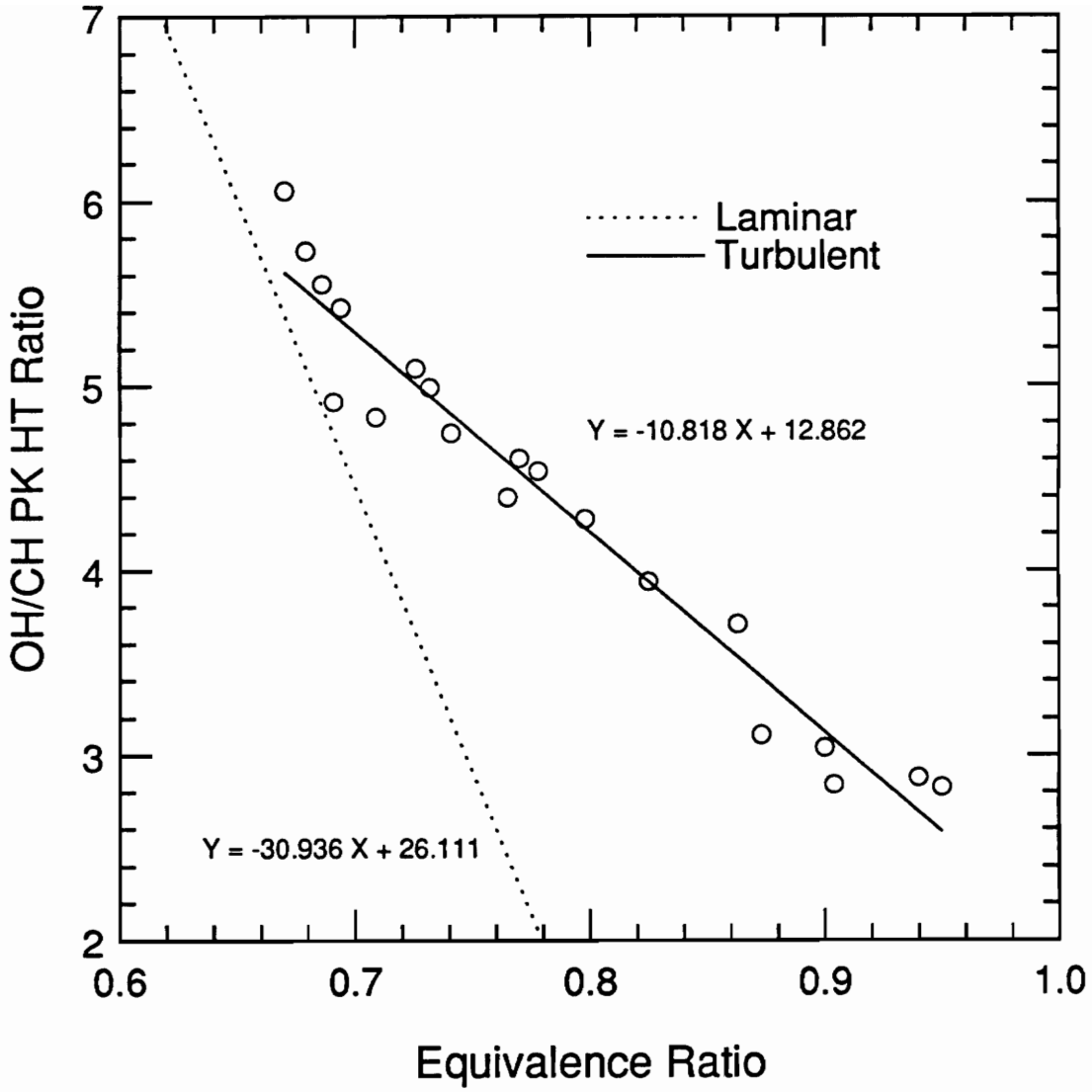

Figure 4.3: Comparison of laminar and turbulent OH/CH Peak Height Ratio correlations for premixed methane-air flames.

light they received, nor did they have a true "notch" profile. The OH notch filter transmitted less than twenty percent of incident light while the CH filter transmitted less than fifty percent. The difference in transmission rates would affect the correlations. Fortunately, the OH signal is the stronger of the two emissions and a loss in OH signal intensity could be easily afforded. Figure 4.4 shows OH/CH NFR plotted against equivalence ratio. Again there is a strongly linear correlation of signal intensity ratio with flame stoichiometry. The slope of the OH/CH NFR correlation is even more negative than the slope of the OH/CH PHR correlation; however, it is believed that the difference in slopes is attributable to different hardware configurations and is not indicative of fundamental changes in the nature of the chemiluminescent signals involved (see section 5.2).

4.3 Temperature Test Results

Figure 4.5 shows the correlation of OH chemiluminescent signal full width at half height (OH FWHH) with radiation-corrected flame temperature. A non-linear correlation is indicated. The resolution of the correlation at lower flame temperatures (less than 1800 K) is poor. Above 1800 K, however, the correlation increases greatly in slope and the ability to distinguish temperatures with OH FWHH information becomes greater. Fortunately, modern gas turbine combustors operate at temperatures above 2000 K (compression heating raises combustion temperatures even with very lean flames).

Figure 4.6 shows the relationship between corrected flame temperature and adiabatic flame temperature. STANJAN, a computer program developed to solve thermochemical equilibria problems, was used to calculate adiabatic flame

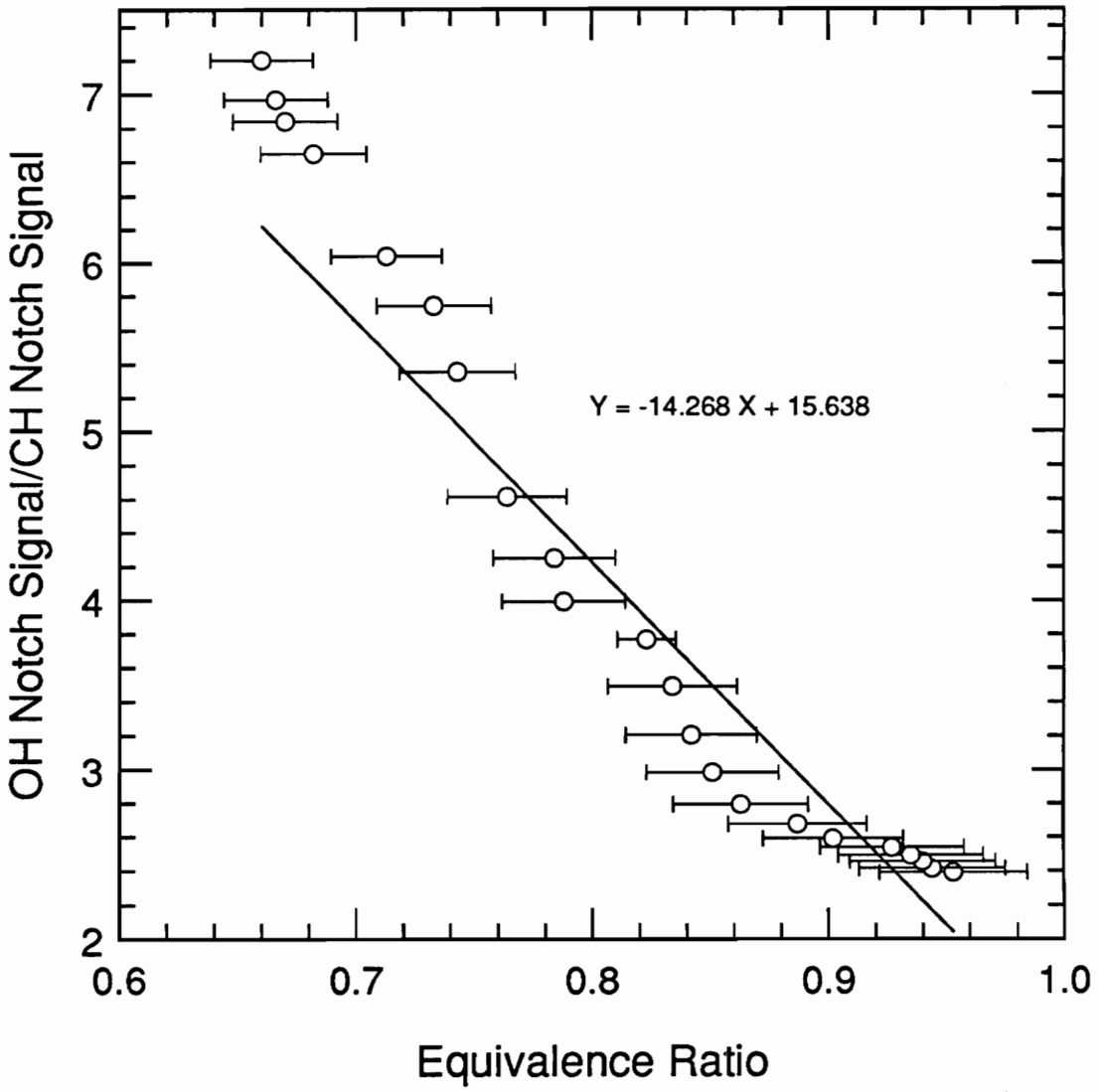

Figure 4.4: OH/CH Notch Filter Ratio for turbulent premixed methane-air flames.

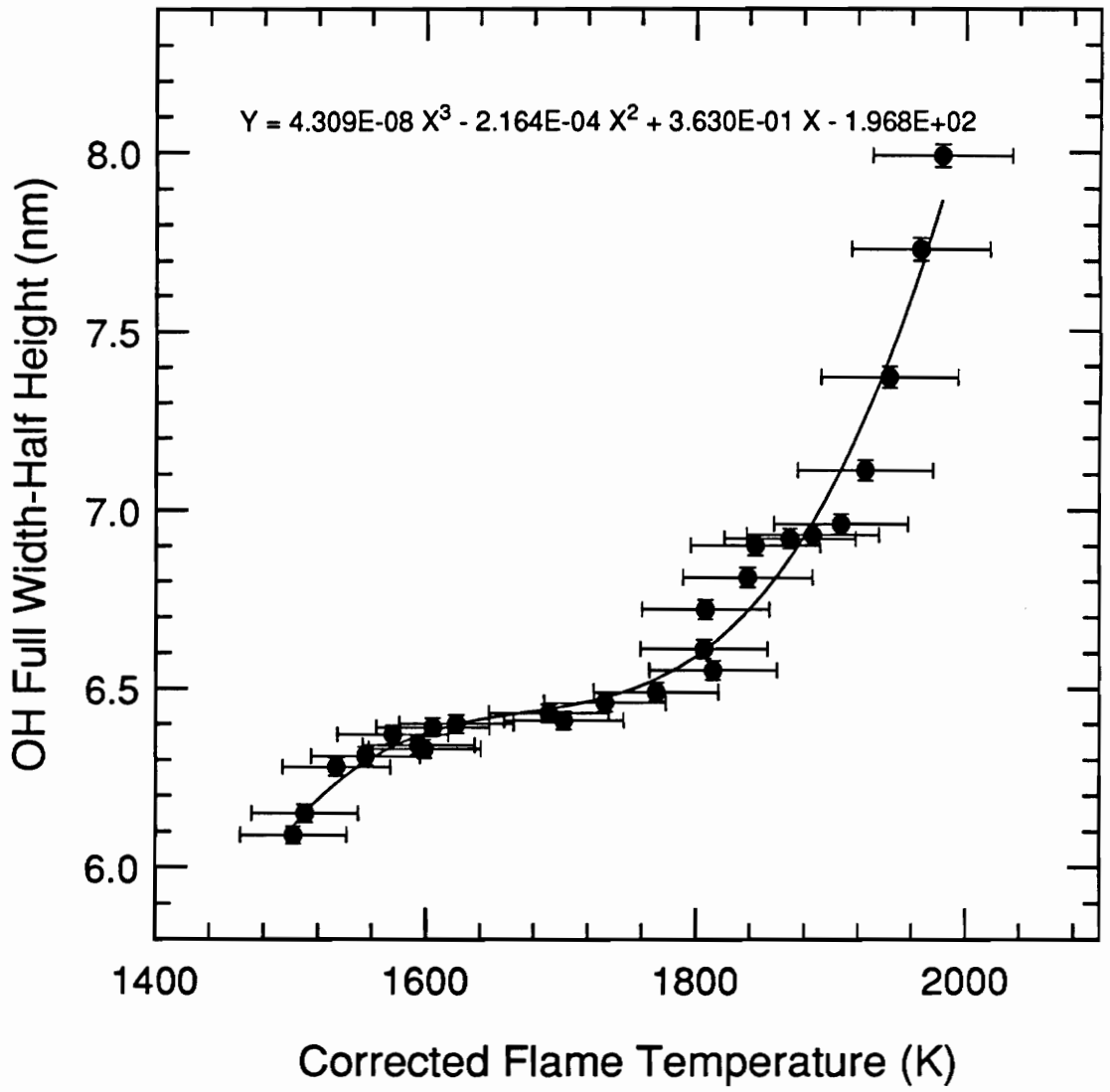

Figure 4.5: OH Full Width at Half Height as a function of corrected flame temperature for turbulent premixed methane-air flames.

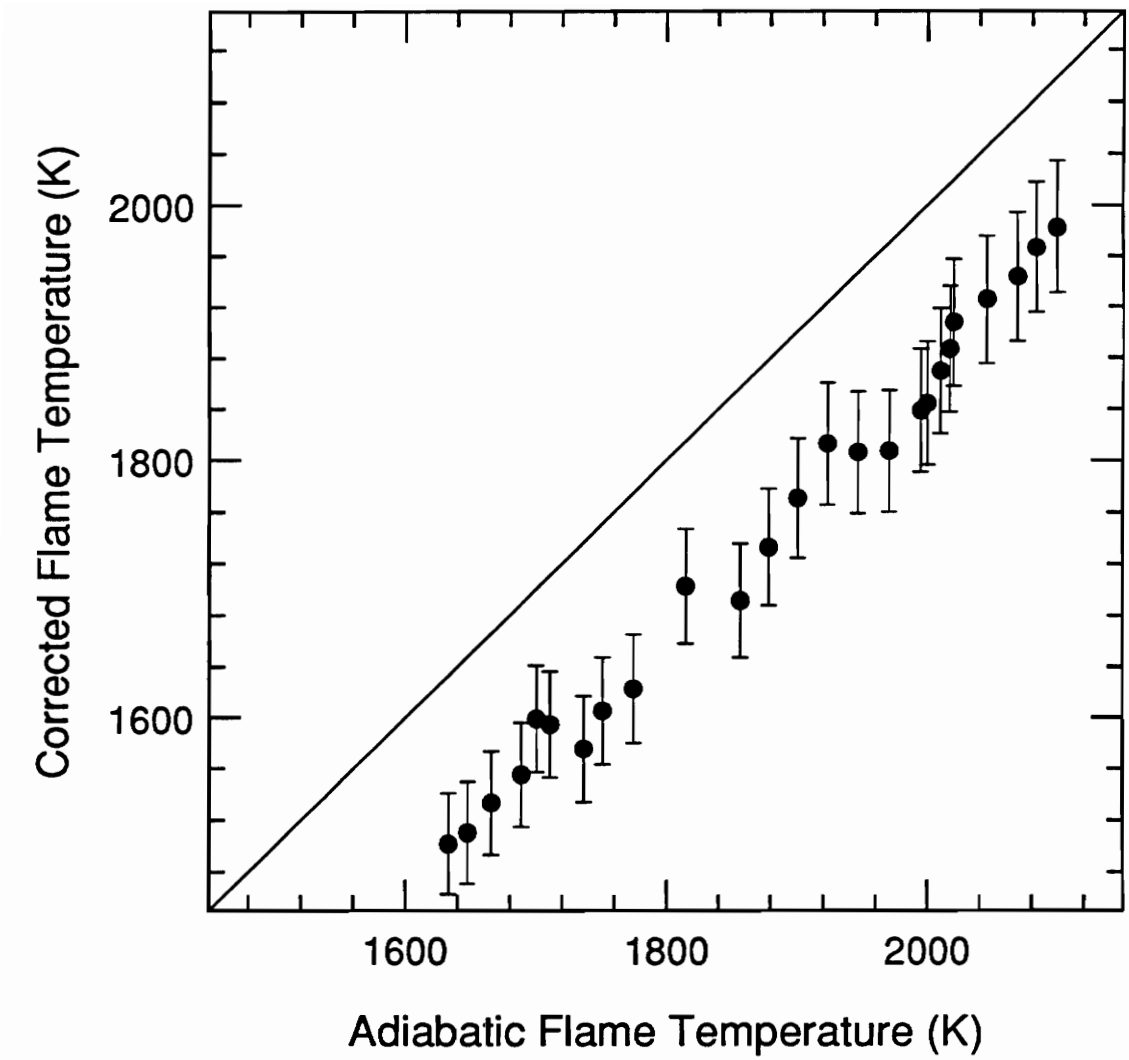

Figure 4.6: Corrected flame temperature as a function of adiabatic flame temperature for premixed methane-air flames.

temperature [36]. The straight line indicates a perfect correlation; the situation where the flame lost no heat. The difference between corrected flame temperature and adiabatic flame temperature could be due to heat conduction to the burner, radiative heat transfer to the surroundings, catalysis of fuel reactions at the thermocouple bead and/or error in the radiation correction program. Figure 4.7 shows OH FWHH plotted against both corrected flame temperature and adiabatic flame temperature. There is a great similarity in the correlations, despite the shift in temperatures.

Correlations of other spectral quantities with flame temperature other than OH FWHH were investigated by Johnsson as well. CH FWHH was expected to show similar broadening with elevated flame temperatures but no noticeable relationship was shown [26]. OH Full width at third height and at full width at quarter height were also investigated, but showed no advantage over OH FWHH.

When the fiber-optic/filter set-up was employed, problems arose as to how the width of the OH chemiluminescent signal could be calculated when no spectral scan was given. As with OH/CH PHR, a different correlation was needed to approximate OH FWHH. The problem was complicated by the fact that the fiber-optics could only transmit information on the intensity of the signals.

The solution was to use the OH notch filter in conjunction with a very narrow band pass or line filter. The characteristics of such a filter are discussed in section 2.4.4. The line filter would give information on the signal intensity at its maximum values -- wavelengths around 309 nm. This information would simulate peak height information. The notch filter would provide a signal

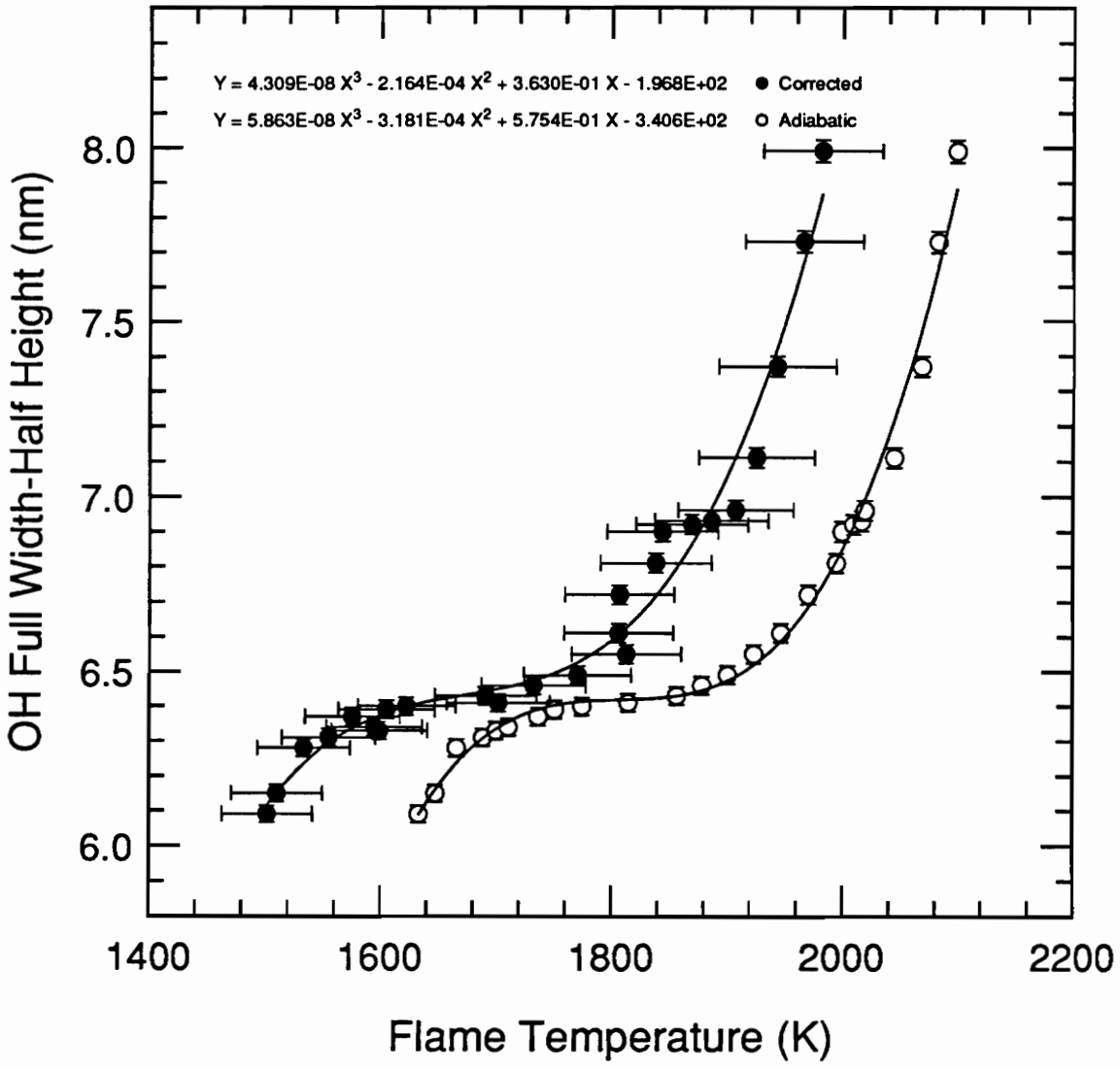

Figure 4.7: OH Full Width at Half Height as a function of both corrected flame temperature and adiabatic flame temperature of turbulent premixed methane-air flames.

proportional to the intensity of light within its wavelengths of operation. This information would simulate area under the peak and could be correlated with the width of the signal. The ratio of notch filter signal to line filter signal (OH Notch/Line Filter Ratio, or simply OH N/LFR) would serve to distinguish hotter flames from physically larger ones and replace the OH FWHH ratio. Again there is a non-linear correlation with a small slope which increases greatly with temperatures above 1800 K. Figure 4.8 shows OH N/LFR plotted against corrected flame temperature and against adiabatic flame temperature. Note that the scale of the OH N/LFR plot is smaller and covers a shorter range than the OH FWHH plot. This indicates that the fiber-optic/filter hardware has a poorer resolution for temperature measurements than the lens/monochromator configuration.

4.4 Turbulence Intensity Test Results

Experiments were performed with flames having Reynolds numbers of 7000. Fuel-to-air ratio and flame temperature correlations were developed with these flames to compare to those developed earlier for flames having Reynolds numbers of 3000. For all turbulence addition experiments, the fiber-optic/filter configuration (shown in Figure 2.12) was used as the hardware was already in place from the latter OH N/LFR tests.

Figure 4.9 shows the OH/CH NFR plotted against equivalence ratio for turbulent premixed methane-air flames with Reynolds numbers of 7000. Comparison with the same plot of flames with Reynolds numbers of 3000 (Figure 4.4) shows almost no difference. The correlation is strongly linear and the slope steeply negative. The laminar flame studies of Johnsson [26] established a

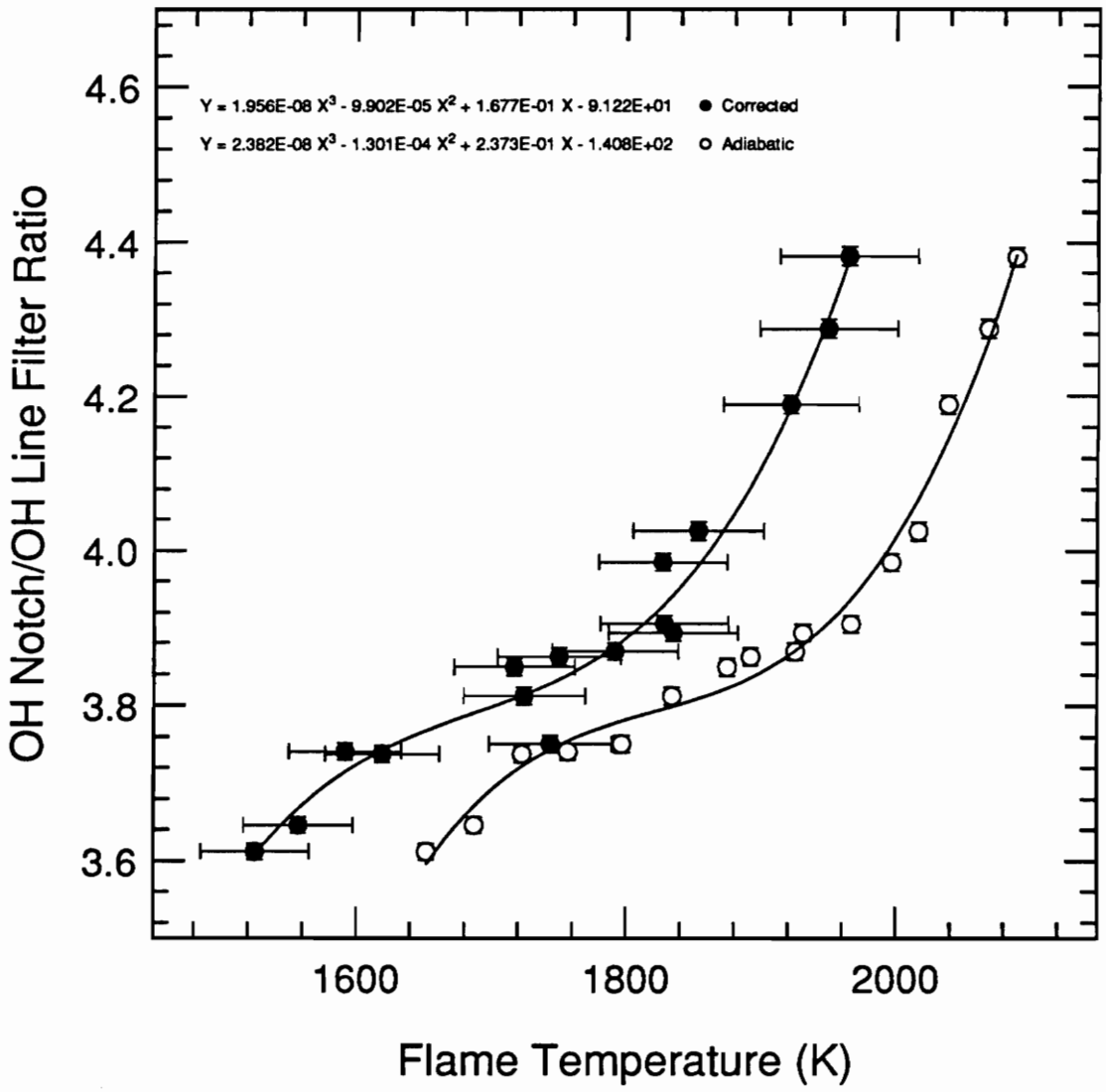

Figure 4.8: OH Notch/Line Filter Ratio as a function of both corrected and adiabatic flame temperatures of turbulent premixed methane-air flames.

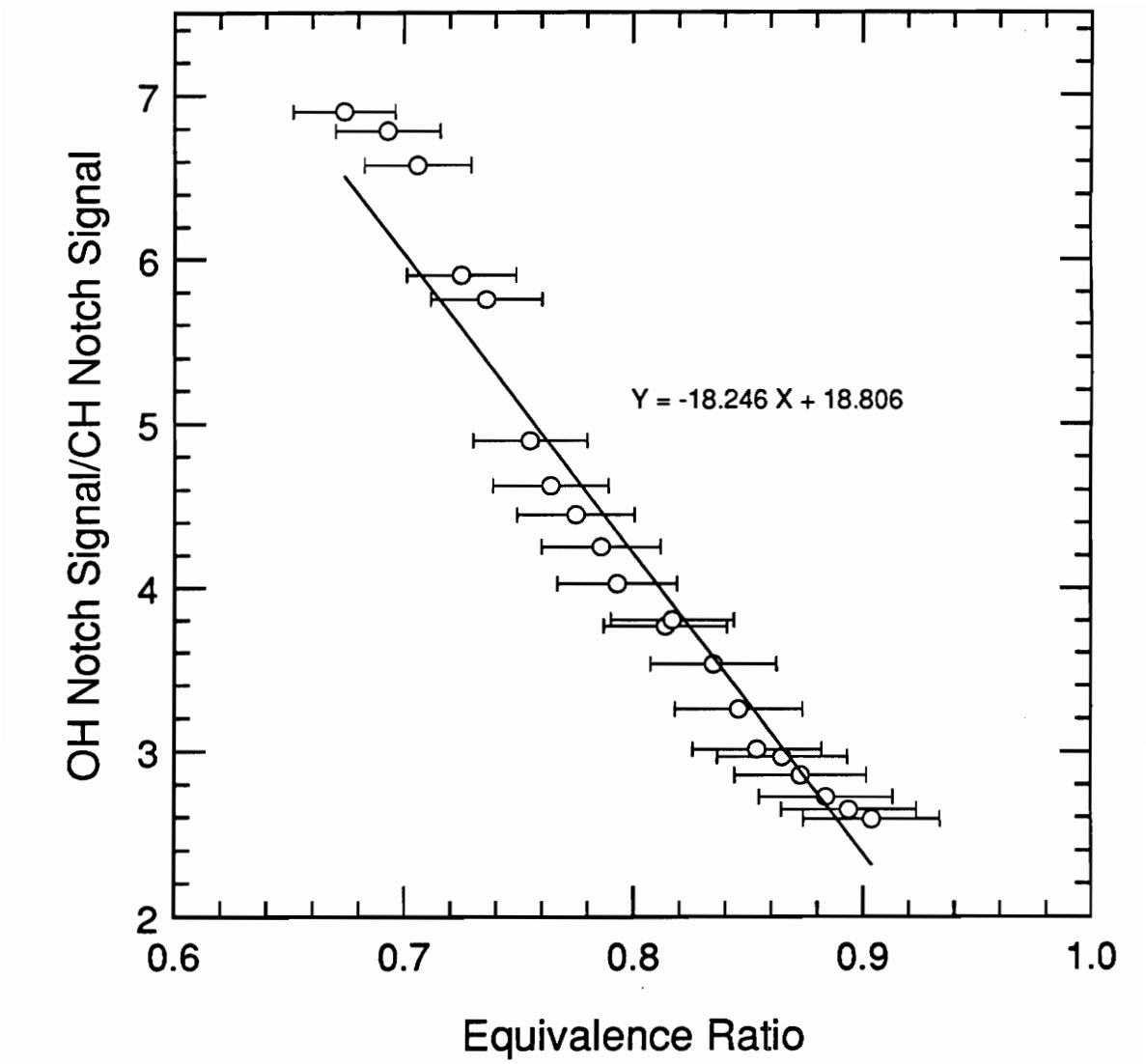

Figure 4.9: OH/CH Notch Filter Ratio as a function of equivalence ratio for turbulent premixed methane-air flames with Reynolds numbers of 7000.

correlation with similar trends (the use of different hardware configurations limits the usefulness of direct comparisons). The level of turbulence in flames with Reynolds numbers of 7000 is not strong enough to directly affect flame chemistry. The increased turbulence might affect quantities such as flame speed and perhaps the size and effective thickness of the flame's reaction zone, but these affects were not enough to greatly influence chemiluminescent emission levels over a broad range of wavelengths.

Figure 4.10 shows OH N/LFR as a function of both corrected and adiabatic flame temperatures for turbulent premixed methane-air flames with Reynolds numbers of 7000. This plot is comparable to Figure 4.8, which shows the same quantities plotted for flames with Reynolds numbers of 3000. The same trend of an initially small slope increasing greatly with temperature is again witnessed in Figure 4.10, but although the rate of increase is similar, the range is slightly greater for flames with higher levels of turbulence (compare the range of OH N/LFR values for Figures 4.8 and 4.10). Johnsson's laminar flame studies [26] show the same trend as well, but again differences in hardware preclude direct comparisons of results. Figure 4.10 also shows an increase in the slope of the correlation at about 1700 K, 100 K earlier than Figure 4.8. It is also interesting to note that the change in the second derivative of the correlation seen in Figure 4.8 (it begins as a "concave down" curve but then changes to a "concave up" curve) is not present in the more turbulent flames of Figure 4.10. The indications are that for flames of greater turbulence, a greater resolution of flame temperatures is possible.

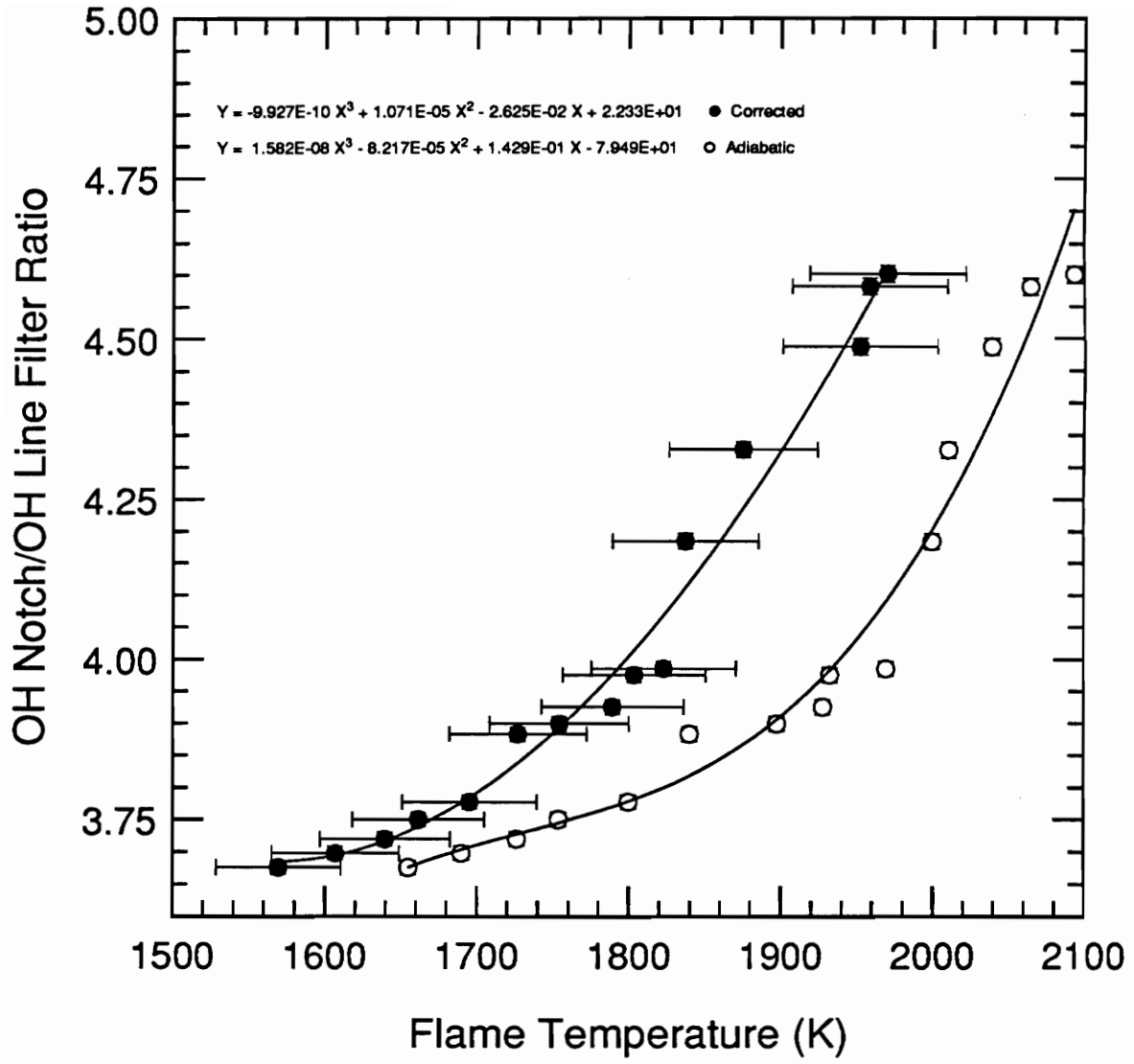

Figure 4.10: OH Notch/Line Filter Ratio as a function of both corrected and adiabatic flame temperature for turbulent premixed methane-air flames with Reynolds numbers of 7000.

5. Discussion

5.1 Introduction

In this section, the trends observed in the correlations shown in the previous section are examined in detail. Explanations for these trends are offered. Equivalence ratio correlations are discussed first, flame temperature correlations next and turbulence effects last.

5.2 Fuel-to-Air Ratio Tests

As with previous studies conducted by Johnsson [26], the observed relationship between OH/CH PHR and equivalence ratio suggests the theory that correlates the quantities is valid (first detailed by Roby [37] and referred to as the "Roby theory" hereafter). The Roby theory proposes that as a stoichiometric flame is progressively leaned out (more oxidizer with respect to fuel), the intensity of the OH chemiluminescent signal will increase relative to the CH chemiluminescent emission. The reasoning is that the production of the OH* excited radical is tied to the concentration of oxidizer. The more oxidizer present (O_2 in this case) the faster the production of OH* becomes, and the greater the intensity of the chemiluminescent emission. Of course, a physically larger flame will also produce a stronger signal, by virtue of having a greater number of OH* excited radicals to begin with, even in a stoichiometric flame. To distinguish between lean flames and large flames it is therefore necessary to normalize the correlation by ratioing the OH and CH peak signal intensities.

Figures 4.2 and 4.4 show that the relationship between OH/CH signal intensities and fuel-to-air ratio is nearly linear. This linear trend is in accordance

with the Roby theory because the wavelengths being monitored for chemiluminescent emissions are high probability areas (the "peaks" of the emissions, wavelengths where there is a high probability that chemiluminescent reactions will occupy certain energy states which will produce emissions). Because the probability that these wavelengths are well populated is high, the quantum effects of chemiluminescence on the equivalence ratio correlations are negligible. The ratios of OH/CH signal intensities *should* be varying directly with the fuel-to-air ratio of the flame; the data suggests that this is indeed occuring. The negative slope of the correlations is also in accordance with the Roby theory; the theory predicts that OH chemiluminescent emissions will increase with decreasing equivalence ratio while the CH emissions increase with increasing equivalence ratio.

Using a monochromator, equivalence ratios can be determined to within ±0.021 over a 0.67 to 0.95 range (accuracy is 97.2 percent, based on the standard percentile error of the data set, see Appendix G for details.) Using the fiber-optics and filters, equivalence ratios can be determined to within ±0.022 over a 0.66 to 0.95 range (accuracy is 97.4 percent). The ability to determine equivalence ratios so quickly and precisely without intrusive measurements is unprecedented. The application of this technology to the chemiluminescent detector system could help to develop lower emissions gas turbines with greater fuel economy.

The slope of the linear correlation of OH/CH peak signal intensities is negative and this is in accordance with the Roby theory. However, the amount of slope differs between turbulent flame and laminar flame correlations markedly.

Figure 5.1 shows the difference in slope for the OH/CH PHR correlation, OH/CH NFR correlation and the laminar flame OH/CH PHR correlation (all are quantities linked to fuel-to-air ratios) versus equivalence ratio. The reason for the difference in slopes is undetermined. It may be simply the number and density of data points involved in the correlations. It may be an effect of the secondary diffusion flames producing erroneous signals near the stoichiometric fuel-to-air ratio. More likely, it is the effect of signal attenuation by the fiber-optic lines and filters which accounts for the difference in slopes. The fiber-optic lines attenuate the chemiluminescent signal at their entrances and exits. The signal is further attenuated at the interface between the fiber-optic line and the collimating lens, again at the lens/filter interface, and yet again upon exiting the filter. Transmission losses are only one part of the attenuation. As the chemiluminescent signal traverses the distance between the flame and the PMT, it moves through several materials of differing indices of refraction (air to fiber-optic line glass to filter dielectric coating etc.) Each index of refraction shift adds noise to the signal. The filters themselves have pseudo-Gaussian transmission profiles. Since the PMT output voltage is proportional to the area under the transmission curve, the relationships between filter signals are necessarily different from the straight monochromator signals. The OH filter has a wider bandwidth than the CH filter. But the CH filter transmits more than twice the peak signal of the OH filter. The cumulative effect of these attenuations is that the correlations have different slopes. It is only important, however, that some correlation can be developed. Differences in correlations using different hardware configurations are to be expected and are only troublesome if not in accordance with theory.

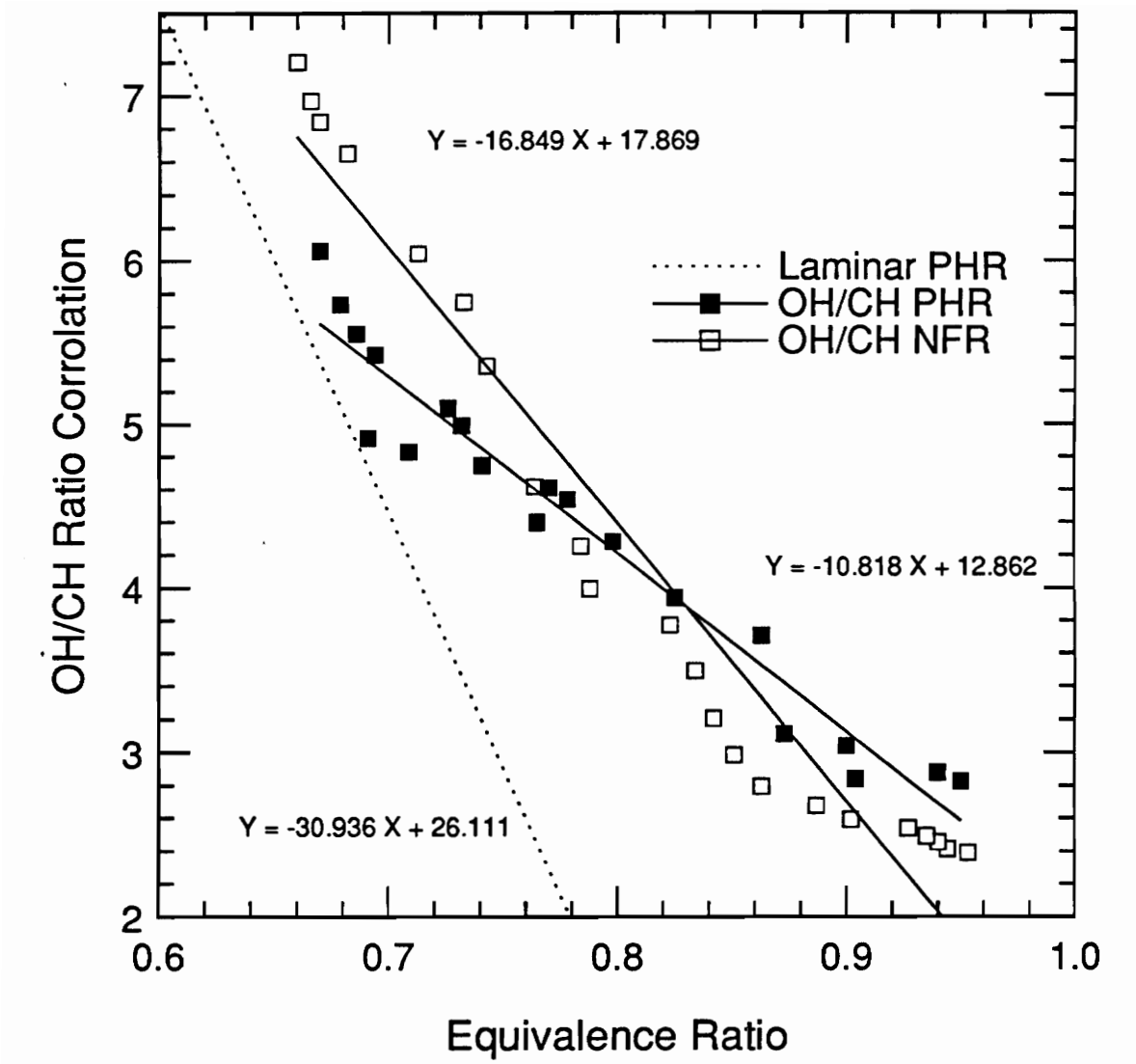

Figure 5.1: Comparison of laminar OH/CH Peak Height Ratio, turbulent OH/CH Peak Height Ratio, and turbulent OH/CH Notch Filter Ratio for premixed methane-air flames.

Calibrations of the chemiluminescent detector system would likely be necessary for differing hydrocarbon fuels. The work of Hamer [1] and Johnsson [26] shows that the H/C ratio of the fuels plays an important role in the relative proportions of OH and CH signals. Most liquid hydrocarbon fuels have an H/C ratio of 1.9 ± 0.1. Therefore, although liquid hydrocarbon fuel correlations would be different from methane correlations (methane has an H/C ratio of 4), there should not be much difference amongst the liquid fuel correlations themselves.

The success of the fiber-optic/filter set-up in achieving a similar fuel-to-air ratio correlation shows that this system can be used in the design of the chemiluminescent detector. A great deal of cost, weight and complexity is saved with the fiber-optic/filter set-up. The use of fiber-optics solves the problem of the harsh combustor environment by transporting the chemiluminescent signal away from the combustor. The filters provide more flexibility than the monochromator in the overall design and are small enough and inexpensive enough to be retro-fitted on current gas turbines.

5.3 Temperature Tests

The theory involving the relationship between the width of the chemiluminescent signal and flame temperature is somewhat more complex than the theory for equivalence ratio. As discussed in section 1.3, the development of band spectra is marked by a number of electronic transitions, each of which can be accompanied by a number of vibrational and/or rotational energy changes. Each energy change results in a specific amount of "surplus" energy, which is conserved with the emission of a photon (the chemiluminescent signal). The amount of surplus energy (this term is used only to help understand

the situation and should not be taken to represent the actual processes involved) dictates the wavelength of the chemiluminescent emission. More energetic emissions result in shorter wavelengths, usually well into the UV, while less energetic emissions are found in the visible or even infrared spectrums.

The width of the chemiluminescent signal (in wavelength numbers) is an indication of the number of possible vibration and/or rotational energy changes that are being filled by the combustion reaction. The more probable a given energy change is, the more likely it is a given excited radical will undergo that particular energy change. The more excited radicals undergo that particular energy change, the stronger the chemiluminescent signal will be at that wavelength. The head, or peak, of the OH band emission occurs around 309 nm. That is the wavelength dictated by a particular energy change which is the most probable and therefore filled by the most excited radicals. To either side of 309 nm are less probable energy changes (for the OH emission) that are filled by less and less excited radicals. This probability distribution is responsible for the multiple-head systems, like the C_2^* bands at 473.7 and 516.5 nm. Each head represents energy changes of roughly equal probability.

As the flame temperature increases, the population of vibrational energy states of the excited radicals increases dramatically. The less probable reactions become increasingly probable. More possible energy changes are filled and the intensity of the chemiluminescent emissions at off-peak wavelengths increases. It should be noted that the energy changes corresponding to the peak wavelength also increase with temperature, but the percentage increase is not as great. For instance, the chemiluminescent signal

at 309 nm may increase ten percent for a 100 K rise in combustion temperature, but the signal at 330 nm might increase tenfold for the same temperature rise. It is the increase in off-peak wavelength emissions that is indicative of a rise in combustion temperature. An examination of the spectral scan of a hotter flame will reveal that the chemiluminescent signal appears "wider" than the scan of a colder flame. However, a physically larger flame will also generate a wider signal, again because of the greater number of excited molecules available. To guard against the possibility of mistaking a hotter flame for a larger one (and vice versa) the width of the chemiluminescent signal should be normalized with the peak height.

The OH^* emission was chosen for correlation with flame temperature. Johnsson's studies of hydrocarbon flames revealed that not all chemiluminescent signals exhibited increases in widths with increasing flame temperature [26]. The CH^* band emission showed almost no correlation with flame temperature. According to Eckbreth, the CH^* band spectra can become saturated quickly [38]. Once saturated, further increases in flame temperature produce no widening of the chemiluminescent signal. The OH^* band spectra, on the other hand, do not saturate easily [38]. The OH^* signal will continue to widen with increases in flame temperature well after the CH^* signal has ceased changing. Another factor for the choice of the OH^* excited radical is that its production is independent of fuel composition. The H/C ratio of the fuel has little effect on the production of OH^* excited radicals; that is, all hydrocarbon fuels produce large amounts of OH^* excited radicals. The OH^* emission is also deeper in the UV and therefore less susceptible to background radiation noise.

The OH FWHH parameter can predict flame temperature over a wide range of operation. For flame temperatures from 1500 to 1800 K, the resolution of the OH FWHH is poor. Flame temperature can only be determined to within ±142.68 K (accuracy, based on standard percentile error, is 91.1 percent) in this range of temperatures. However, most gas turbine combustors do not operate with flames this cool. From 1800 to 2100 K, the ability of the correlation to determine flame temperatures increases to within ±41.26 K (accuracy is 97.8 percent). The slope of the correlation becomes steeper and steeper at an ever increasing pace after 1800 K. For flames above 2100 K, the accuracy of the OH FWHH correlation will doubtless improve even further.

The accuracy of the OH N/LFR correlation using fiber-optics and filters demonstrates the usefulness of this configuration to the chemiluminescent detector system. Resolution of temperatures in the 1500 to 1800 K range is improved, with temperature determinations to within ±45.56 K (accuracy is 97.4 percent). For flames above 1800 K, temperature can be determined to within ±18.95 K (accuracy is 99.0 percent). Again, for still hotter flames the ability to determine flame temperature is expected to improve further.

It should be noted that the non-linear shape of the various correlations, laminar OH FWHH, turbulent OH FWHH, turbulent OH N/LFR, and the OH N/LFR for flames with Reynolds number of 7000 (discussed below) is in accordance with the chemiluminescent theory of temperature detection. It is the quantum effects at the off-peak wavelengths which determines the shape of the correlations. Probability distributions are responsible for the non-linear trends.

5.4 Turbulence Intensity Tests

The levels of turbulence in an actual gas turbine combustor are many times those seen in the experiments conducted for this research. Reynolds numbers of 100,000 and more are not uncommon. At such high levels of turbulence, the chemistry of the flame itself is altered. The eddies and currents in the flow are on such a fine scale that the kinetic rates of the combustion reaction are speeded up and the reaction zone or flame front is no longer a well defined quantity. Since the effects of extreme turbulence on chemiluminescent reactions do not readily correspond to any simple theory or calculation, only thorough experimentation will reveal what the effects really are. Today there are many theories as to what really happens to flames under the influence of high turbulence. But as early as 1957 Gaydon and other recognized that there are at least these two main effects [9]:

> "Flame propagation depends on conductive heat transfer and diffusion of active species, and under laminar flow conditions the burning velocity is a well defined quantity. Under turbulent flow conditions there is a considerable increase in effective burning velocity .... Turbulence may have two main effects; it may break up the flame front (wrinkled flame concept) so that its area is increased and the volume rate of consumption of gas mixture shows a corresponding increase; or it may, by stirring within the reaction zone, cause increased heat transfer and radical diffusion and so alter the structure of the flame front itself. The first effect certainly occurs, but there has been some uncertainty about the importance of the second effect ...."

Figures 4.4 and 4.9 (repeated below for convenience) show OH/CH Notch Filter Ratios plotted as a function of equivalence ratio for flames with Reynolds numbers of 3000 and 7000, respectively. As mentioned in section 3.4, these levels of turbulence were chosen because they lie respectively within the

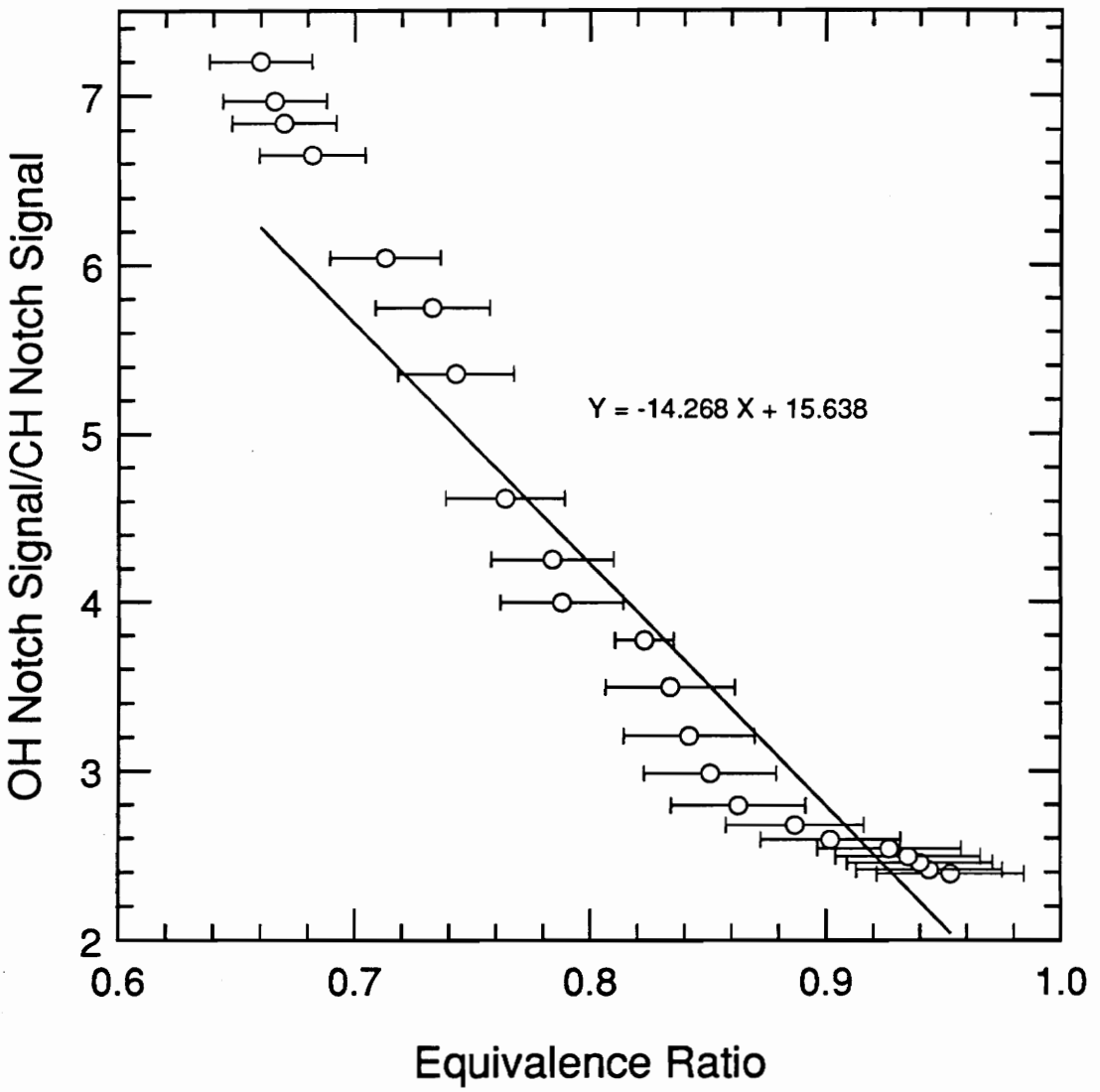

Figure 4.4: OH/CH Notch Filter Ratio for turbulent premixed methane-air flames.

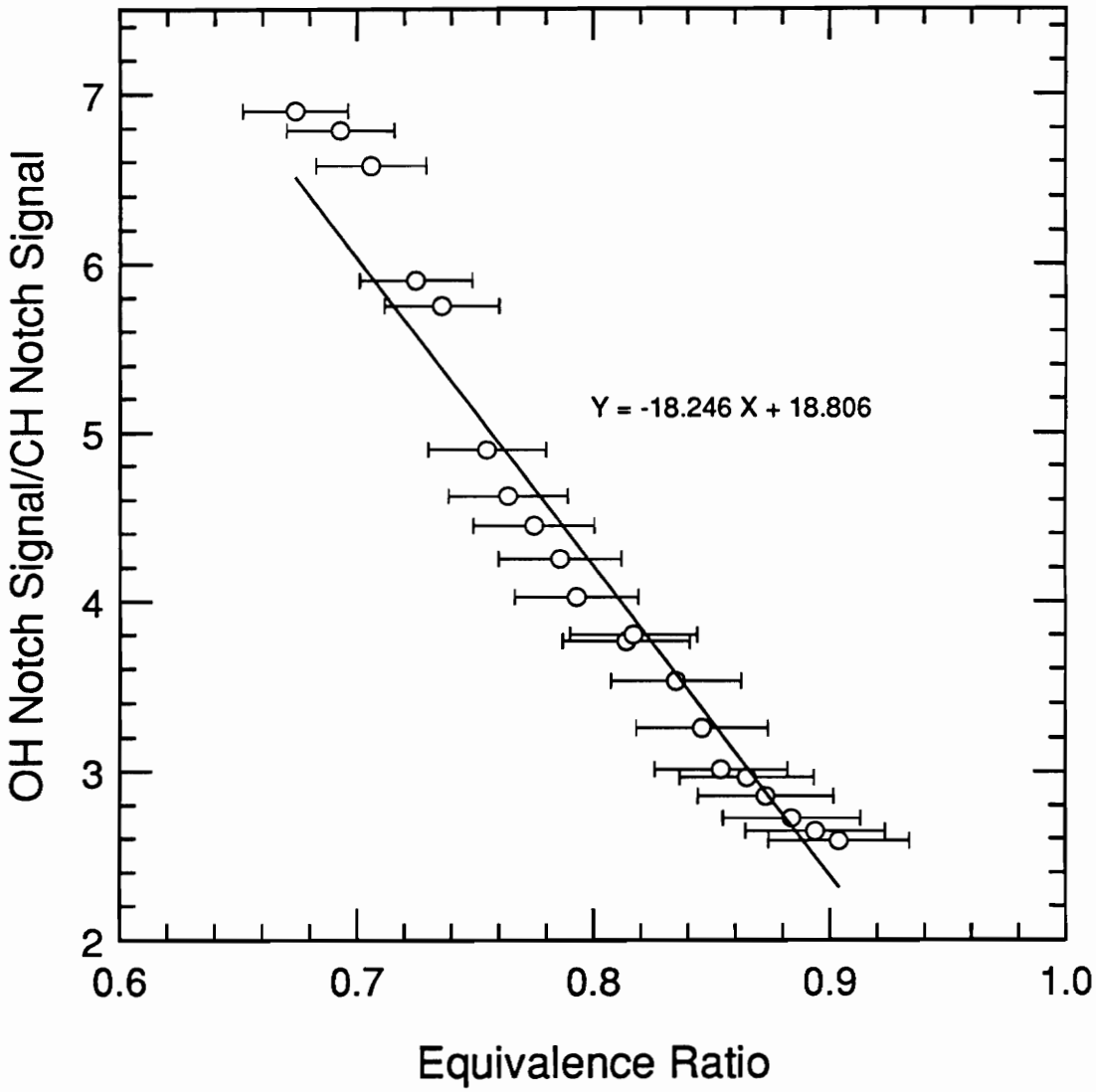

Figure 4.9: OH/CH Notch Filter Ratio as a function of equivalence ratio for turbulent premixed methane-air flames with Reynolds numbers of 7000.

wrinkled laminar and intermediate turbulence flow regimes. Analysis of the two OH/CH NFR plots shows that there is little if any effect of increased turbulence on the fuel-to-air ratio correlation. However, this conclusion does not mean that turbulence itself has no effect on the chemiluminescent processes used in developing the fuel-to-air ratio correlation, only that the additional turbulence from a Reynolds number of 3000 to a Reynolds number of 7000 produced no noticeable effects. Additional experiments at higher and higher levels of turbulence are the only sure method of determining the effects of turbulence on the chemiluminescent reactions used in the fuel-to-air ratio correlation.

Although additional turbulence produced little or no effect on the fuel-to-air correlation, it did appear to have an effect on the temperature correlation. Figures 4.8 and 4.10 (repeated below for convenience) are plots of OH N/LFR for flames of Reynolds numbers of 3000 and 7000, respectively. Additional turbulence seems to have increased the resolution of flame temperatures, particularly below 1800 K.

An examination of the data used to make Figures 4.8 and 4.10 reveals that the OH Notch Filter values did not change much from flames with Reynolds numbers of 3000 to flames with Reynolds numbers of 7000. Most of the difference between the two correlations is due to changes in the OH Line Filter values. This result may be because the OH Notch Filter signal is broadband (compared to the OH Line Filter signal). Perhaps the effects of additional turbulence are more noticeable in an examination of narrow bandwidths; or, more likely, the turbulence effects are confined to the wavelengths passed by the OH Line Filter. This latter approach assumes that the effects of the turbulence

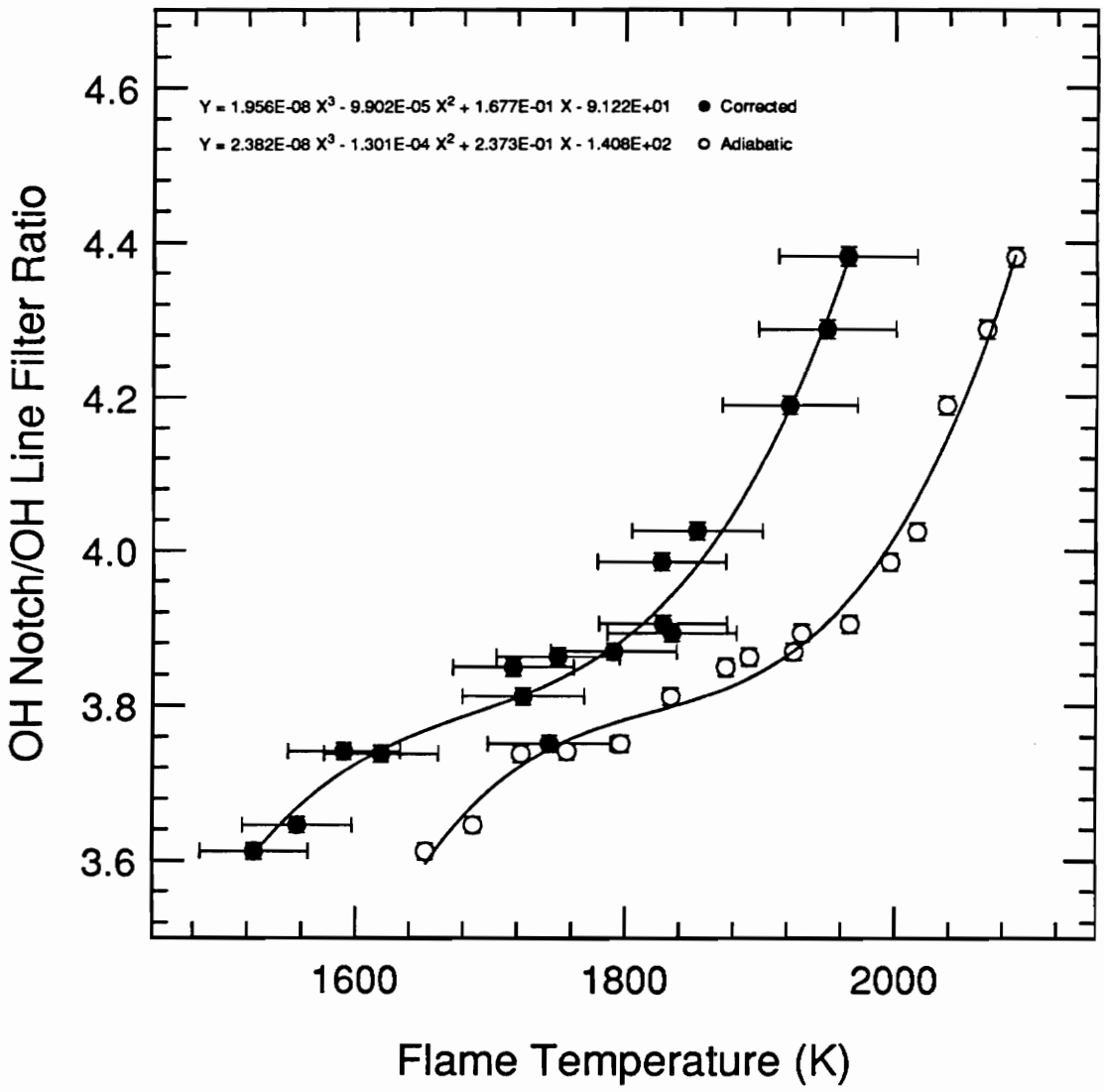

Figure 4.8: OH Notch/Line Filter Ratio as a function of both corrected and adiabatic flame temperatures of turbulent premixed methane-air flames.

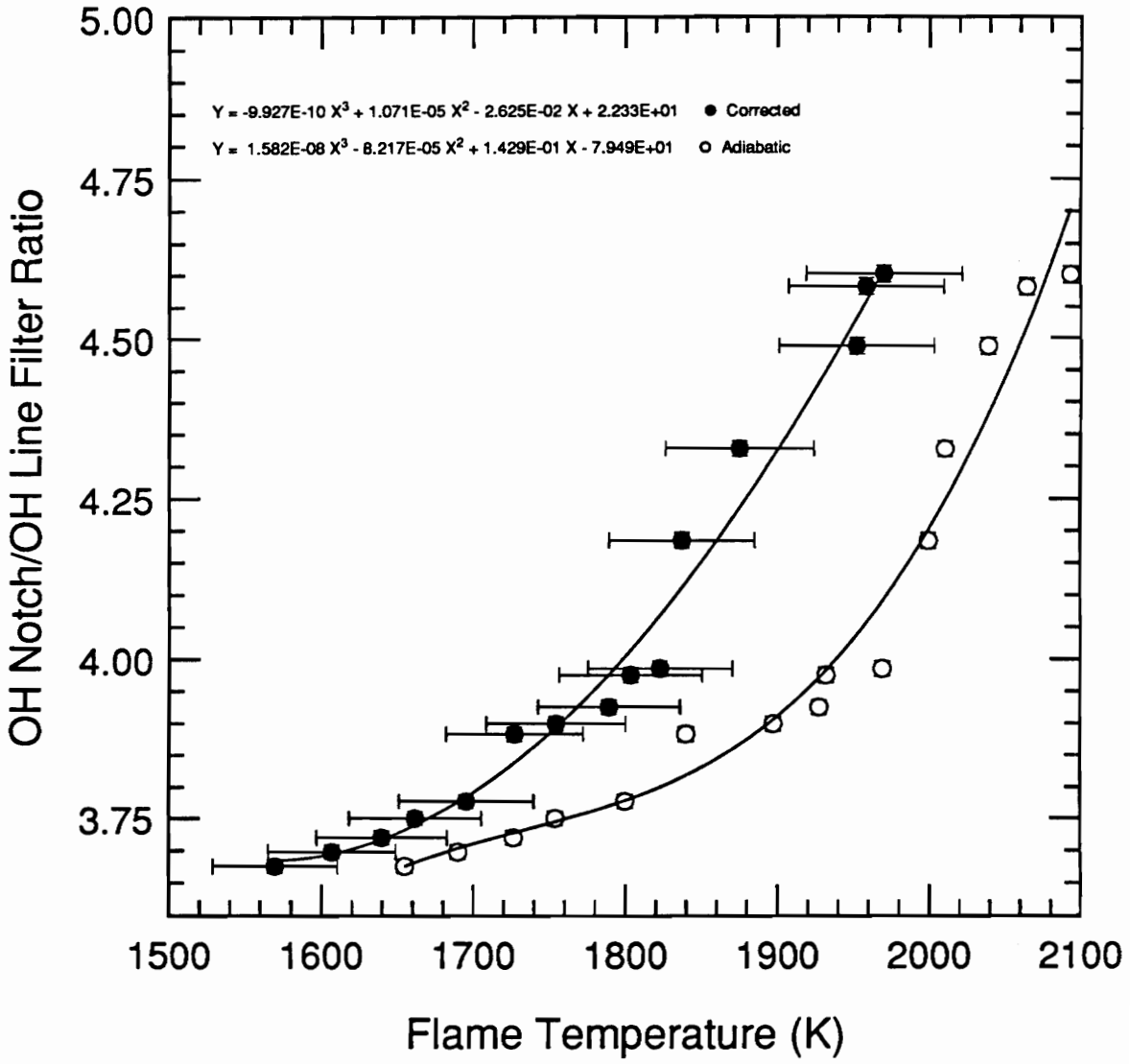

Figure 4.10: OH Notch/Line Filter Ratio as a function of both corrected and adiabatic flame temperature for turbulent premixed methane-air flames with Reynolds numbers of 7000.

are prevalent where there are the most molecules taking part in the reactions. Since the OH Line Filter monitors a wavelength where there is a high probability distribution (i.e., the "head" of the chemiluminescent signal), there are more molecules being observed and therefore it is more likely the effects of increased turbulence (quantum effects like probability distribution of chemiluminescent emissions) will be noticed. Again, further experimentation at higher levels of turbulence are needed to substantiate any assumptions.

To validate the theories of the effects of high turbulence on chemiluminescent emissions proposed in this thesis, further research is necessary. Until such research is performed, the effects of turbulence can only be guessed at. However, it is believed that extreme levels of turbulence, sufficient to alter flame chemistry, will substantially affect chemiluminescent reactions and thus affect the correlations derived from them. Just exactly how the correlations will be affected is a subject for continued discussion. Ideally, the experiments carried out for this research will be duplicated with higher and higher levels of turbulence. The procedures outlined in this thesis should be followed so as to isolate the effects of increasing turbulence on chemiluminescent emissions. What was learned from the research done in this work is that low levels of turbulence addition have little or no effect on broadband chemiluminescent emissions and serve to slightly attenuate narrowband chemiluminescent emissions.

5.5 Effects of Assumptions

All the experiments performed for this research were conducted at atmospheric pressure (anywhere from 690 to 720 mm Hg in Blacksburg). At the

high pressures (ten atmospheres or more) involved in gas turbine combustion, a peculiar phenomenon known variously as Lorentz or collision broadening occurs.

When pressures are increased, the collision rates among the molecules in a given area are increased as well (as long as the temperature is above absolute zero). Because of the increased rate of collisions, there are more reactions which take place that give rise to chemiluminescent emissions. Since band spectra emissions depend on a number of probable chemiluminescent reactions for their shape, the bands will broaden under the influence of increased pressures. This broadening occurs because certain less probable energy states will become increasingly probable with elevated pressures. The effect is similar to the "filling in" of energy states observed with elevated temperatures (see section 5.3).

The effect of Lorentz broadening in non-linear in nature and becomes increasingly important at higher pressures. Since modern gas turbine combustors operate at many times atmospheric pressure, Lorentz broadening is a non-trivial effect and must be accounted for. However, Lorentz broadening tends to affect IR emissions more than UV emissions (shorter wavelength emissions are more energetic in nature and thus less affected by an additional number of collisions) so perhaps the effect upon the correlations developed in this thesis will be less than expected.

The elevated combustion temperatures of actual gas turbines give rise to another spectral phenomenon: Doppler broadening. The effect is analogous to the Doppler shift commonly experienced with moving producers of sound (trains,

cars, planes, etc.) and used in radio astronomy to determine interstellar distances.

The molecules of an chemiluminescent signal emitting gas are not stationary, but move. The molecules do not move very far, but they do move quite rapidly. And it is the speed of the emitter and not the distance traveled which determines a Doppler shift. Because the chemiluminescent signal is emitted from a moving object, it has its wavelength shifted by a small amount as viewed by an outside observer who is not moving with respect to the object. The formula for determining the Doppler shift is as follows:

$$\lambda_f = \lambda_i\left(1+\frac{v}{c}\right) \qquad [42]$$

where λ_f is the final wavelength, λ_i is the emitting wavelength, v is the speed of the emitter molecule, and c is the speed of light.

The Doppler shift is caused by the random thermal motion of the gas molecules and always results in a chemiluminescent emission with a slightly greater wavelength than it normally has [9]. Consequently, the entire emission is shifted to slightly higher wavelengths. However, not all parts of a band spectrum are shifted by the same amount. The broadening has a Gaussian distribution of intensity centered on the "peak" or central spectral line of the emission; to either side of the peak the intensity of the broadening falls off exponentially. So where there is an abundance of chemiluminescence, the shift is more noticeable. At wavelengths with only a few chemiluminescent emissions, the shift is less noticeable. The majority of the chemiluminescent emissions occur in the center

wavelengths of the band spectrum (at the "peak" of "head") since these are the wavelengths corresponding to more probable energy states. The Doppler shift alters the width of the band spectrum emission more at the center wavelengths and less at the outer wavelengths. The result is an emission profile which looks less like a "spike" and more like a "hill". This is called Doppler broadening.

Doppler broadening is directly proportional to the square root of flame temperature and inversely proportional to square root of the molecular weight of the molecules in question. Therefore, the effects of Doppler broadening are increasingly important at high temperatures (which also have lower molecular weight hydrocarbon species). Compression heating raises the combustion temperatures of the fuel and air mixture several hundred degrees Kelvin. Advances in turbine material science technology will doubtless push combustion temperatures even higher (better thermodynamic efficiency is gained with higher combustion temperatures). If temperatures continue to rise, Doppler broadening will become more and more important to chemiluminescent detector technologies.

The effects of Doppler and Lorentz broadening cannot be ignored. They can significantly affect chemiluminescent emissions. They will certainly change the temperature and equivalence ratio correlations developed in this thesis. However, the effect of band spectrum broadening is entirely beneficial to the chemiluminescent detector concept. More broadening should extend the range and improve the resolution of the temperature correlation discussed in this research. Broadening should, in effect, serve to increase the slope of the

correlation by increasing the intensity of the OH Notch Filter Signal (or by increasing the width in the OH FWHH correlation).

An assumption was made regarding the consistency of the flowrates during the experiments. The duration of the scan was on the order of five minutes. During that time, the gas line pressure fluctuated slightly, although it was compensated for at the rotameter when detected. The fluctuations were minor, perhaps only ± ½ of the minimum gradation of the rotameter. The assumption of constant flowrates regards this drift in flowrates as insignificant.

Temperature measurements with a thermocouple assumed the only heat loss was through radiative heat transfer at the bead. Obviously, this was not the only source of heat loss (the reason adiabatic flame temperatures were also included in correlations; the actual flame temperature was between the corrected flame temperature and the adiabatic flame temperature, probably closer to the former). Conduction of heat to the burner, radiation to surroundings (not insignificant, as temperatures in the laboratory could rise ten degrees Fahrenheit in half an hour of continuous testing), and catalysis at the thermocouple (especially with the presence of additional H_2 from the secondary attachment flame; platinum catalysis of the $H + H \rightarrow H_2$ exothermic reaction leads to heat addition directly at the thermocouple bead and artificially high temperature readings) are all sources of error in the temperature measurement. However, the chemiluminescent flame temperature correlation may be more accurate than the thermocouple in any case, which renders error analysis of the reference temperature academic.

A more detailed analysis of all possible sources of error in this research is given in Appendix G. The effects of the assumptions above are reviewed in detail, as are many other sources of error. Methods of reducing the errors are discussed, along with the consequences of such actions.

6. Summary and Conclusions

6.1 Summary

6.1.1 Fuel-to-Air Ratio Measurement

This thesis describes research done on turbulent, premixed methane-air-nitrogen flames to determine if the laminar flame correlations between chemiluminescent signals and equivalence ratio were relevant in the turbulent flow regime. Theory predicted that the ratio of the peak signal intensities of the OH* and CH* emissions would vary with the equivalence ratio of the flame. Experimental results showed a nearly linear correlation between OH/CH Peak Height Ratio and equivalence ratio. Experiments also showed that a fiber-optic/filter set-up could successfully predict equivalence ratio by using the similar OH/CH Notch Filter Ratio parameter as a correlation.

6.1.2 Flame Temperature Measurement

This thesis also describes tests done on turbulent, premixed methane-air-nitrogen flames to determine if the laminar flame correlations between chemiluminescent signals and flame temperature held in the turbulent flow regime. Theory predicted that the width of the OH* chemiluminescent signal with respect to its height would increase with temperature. Experimental results showed a non-linear correlation between the Full Width at Half Height of the OH* chemiluminescent signal and flame temperature. A similar correlation was found to exist for calculated adiabatic flame temperature. Tests also showed that a fiber-optic/filter set-up could successfully predict flame temperature by using the similar OH Notch/Line Filter Ratio correlation.

6.1.3 Effects of Turbulence

One of the experimental goals of this thesis was to determine the effects of increasing turbulence of the reactions involved in chemiluminescent emissions. In particular, the effects of increased turbulence on the OH/CH NFR and OH N/LFR correlations was investigated. Flames with Reynolds numbers of 7000 was analyzed to form correlations to compare with the correlations from flames with Reynolds numbers of 3000. Experimental results showed that there was little or no effect of increased turbulence on the OH/CH NFR correlation and a small attenuation of the Line Filter signal in the OH N/LFR correlation. No attempt was made to measure turbulence effects with different hardware configurations, nor were experiments carried out with still higher levels of turbulence. Although it was concluded that the effects of small levels of turbulence addition had only minor effects on the developed correlations, it is believed that higher levels of turbulence addition will significantly alter chemiluminescent emissions.

6.2 Conclusions

A chemiluminescent detector has been developed that can sense flame ignition, blowoff, temperature and equivalence ratio. This detector has an extremely fast response time, has a reliable and repeatable signal and would be inexpensive to install and maintain. More importantly, the detector uses current "off-the-shelf" technology; making it inexpensive to design and manufacture as well.

The fuel-to-air ratio and flame temperature testing revealed that the theories and correlations developed for laminar flames could be extended with success to turbulent flames. Equivalence ratios can be determined to within ±0.021 with the OH/CH PHR correlation. The temperature of the flame could be determined to within ±41.26 K over a small range of combustion temperatures. The two correlations agree with theory and seem to be independent of one another. The use of fiber-optic/filter hardware only improved the correlations. Equivalence ratios could be determined to within ±0.022, about the same as with the bulkier and more expensive lens/monochromator hardware, and flame temperature could be determined to within ±18.95 K with the more practical and rugged fiber-optic/filter hardware.

Small levels of turbulence addition did not seem to significantly affect chemiluminescent emissions. Much higher levels of turbulence, like those found in actual gas turbine combustors, may significantly affect chemiluminescent emissions. Since there is no readily applicable theory on the effects of turbulence on chemiluminescence, only careful experimentation can be sure to reveal these effects. The investigation of the effects of turbulence on chemiluminescence in this research can only be considered preliminary. Further experimentation with much higher levels of turbulence is required to complete the exercise.

The chemiluminescent detector developed in this research has a great deal of potential. Enormous benefits can be reaped from the application of the chemiluminescent detector to modern gas turbine equipment. However, to take advantage of this potential and explore the possibilities of its application, more

research needs to be done on the chemiluminescent detector. The technology is well within reach, what remains is to harness that technology into a working prototype and thence into production.

6.3 Recommendations for Future Work

The next logical step is to perform research with the chemiluminescent detector in an actual gas turbine combustor environment. Only here can the effects of extreme turbulence, high pressure and elevated combustion temperatures be evaluated. The procedure developed in this thesis (outlined in section 1.4) should be imitated; that is, the effects of each experimental variable should be considered in isolation. Comparisons should be made with existing equivalence ratio and flame temperature monitoring technology to see how the chemiluminescent detector "measures up". It is believed that the chemiluminescent detector is more efficient and certainly more cost effective than any fuel/air flowrate measuring system (which provide no temperature data) and may be even more accurate than any of the assorted exhaust thermocouple schemes being employed today. A fully automated testing procedure needs to be developed to increase the rate at which data points can be taken (each data point in the plots of this thesis represents many hours of experimentation). A large database is necessary to make correlations and conclusions statistically significant.

Research should continue with the fiber-optic/filter hardware described in this thesis. The harsh combustor environment absolutely favors the use of fiber-optics over a spatially dependent lens system. Not only is the fiber-optic set-up flexible, rugged, compact, lightweight, and inexpensive, but it was able to

achieve the best correlations for flame temperature. The attractiveness of eliminating the PMT for a photodiode should not be overlooked. Although the photodiode was unusable in laboratory experiments (light levels are too low for a clean signal), it should be useful in actual gas turbine conditions (where light levels are a thousand times the laboratory signal). Although the photodiode has a slower time response than the PMT (but still much faster than the chemiluminescent reactions), it is certainly more rugged than the fragile photomultiplier tube and less expensive, too.

The detector should be installed on the individual cans of a multiple "cannular" gas turbine combustor to evaluate the ability of the detector to sense individual can temperatures and equivalence ratios. After many hours of experimentation, the physical durability of the detector could be evaluated, as well as the consistency of the signal over extended periods of use. Reliability of the detector in the presence of oil, soot, and foreign material certainly is of interest.

It is possible that the detector can be used to provide information on anomalous combustor operation. The data provided by the detector can be compiled into a database of chemiluminescent signals corresponding to known defective combustor conditions. This database can then be used in an intelligent neural network to diagnose anomalous combustor operation without physically inspecting the combustor (and incurring the costs involved therein). After the chemiluminescent detector has proved itself in the field, this diagnostic ability will surely be of use to the companies financially responsible for combustor maintenance and repair.

Of course, the intended application of the chemiluminescent detector is in an active gas turbine combustor control system. Such a control system would use the detector to provide input on combustor operating parameters in real time and make adjustments to keep the combustor operating at optimum efficiency. The power of the gas turbine could be maximized, or the fuel economy, or the emissions output, depending on operational requirements. This control system is not unlike the modern electronic fuel injection systems now being employed on many spark ignition internal combustion engines in the automotive industry. Although fuel injection does not inherently provide more power or better emissions than carburetion, it allows the manufacturer to tune the engine for its intended usage. The result is greater flexibility; the ability to get the most out of any given engine is vastly improved. It is the same for an active control system for gas turbine combustors -- each gas turbine can be "tuned" to its intended usage and therefore operate more efficiently with less expense and pollution. True, the addition of an active control system adds a small cost to the operation and maintenance of the gas turbine, but one has only to look to the advances the automotive industry has made in the areas of power, fuel economy, and emissions to realize that the cost is more than justified.

REFERENCES

1. Hamer, A. J., The Use of Chemiluminescence for Light-Off Detection of Flames, M.S. Thesis, Virginia Tech, Blacksburg, Virginia, 1989.

2. Walsh, E. J., "Gas Turbine Multiple-Combustion System", GER-3435A, Gas Turbine Division, General Electric Company, Schenectady, New York, 1984.

3. Blevins, L. G., Effects of High Levels of Steam Addition on NO_x Reduction in Laminar Opposed Flow Diffusion Flames, M.S. Thesis, Virginia Tech, Blacksburg, Virginia, 1992.

4. Kuo, K. K., Principles of Combustion, John Wiley and Sons, New York, New York, 1986.

5. Walsh, E. J., Ibid.

6. Morey, W. W., Quentin, G. H., and Angello, L. A., "Fiber Optic Probe for Flame Monitoring in Gas Turbine Combustors", American Society of Mechanical Engineers 89-GT-49, Gas Turbine and Aeroengine Congress and Exposition, Toronto, Canada, June 4-8, 1989.

7. Cohen, L. M., Gat, N., and Witte, A. B., "Start-of Ignition Sensor for a Diesel Engine", *Combustion Science and Technology*, vol. 42, pp. 211-6, 1985.

8. Zoia, D., and Inoue, M., "Combustion Sensors: Push for New Technology Is Growing", WARD'S Auto World, Detroit, Michigan, September, 1988.

9. Gaydon, A. B., The Spectroscopy of Flames, Second Edition, Chapman and Hall, New York, New York, 1974.

10. Gaydon, A. B., and Wolfhard, H. G., Flames -- Their Structure, Radiation, and Temperature, Fourth Edition, The Chaucer Press, Bungay, Suffolk, England, 1979.

11. Peeter, J., Lambert, J., Hertoghe, P., and van Tiggelen, A., "Mechanism of C_2^* and CH^* Formation in a Hydrogen-Oxygen Flame Containing Hydrocarbon Traces", Thirteenth Symposium (International) on Combustion, The Combustion Institute, p. 321, 1971.

12. Schott, G. L., *Journal of Chemical Physics*, vol. 32, p. 170, 1960.

13. Lyon, R. K., and Kydd, P. H., *Journal of Chemical Physics*, vol. 34, p. 1069, 1961.

14. Glover, J. H., "Chemiluminescence in Gas Analysis and Flame-Emission Spectrometry", *Analyst* 100: 449-64, 1975.

15. Stedman, D. H., and Fraser, M. E., "Analytical Applications of Gas Phase Chemiluminescence", Chemi- and Bioluminescence, Burr, J. G., ed., Marcel Dekker, Inc., New York, New York, 1985.

16. Fontjin, A., ed., Gas-Phase Chemiluminescence an Chemi-Ionization, North-Holland, New York, New York, 1985.

17. Peeter, J., Lambert, J., Hertoghe, P., and van Tiggelen, A., Ibid.

18. Heffington, W., Parks, G., Sulzman, K., and Penner, S., "Studies of Methane-Oxidation Kinetics", Sixteenth Symposium (International) on Combustion, The Combustion Institute, p. 997, 1977.

19. Bowman, C. T. , and Seery, D., "Chemiluminescence in the High-Temperature Oxidation of Methane", *Combustion and Flame*, vol. 12, p. 611, 1968.

20. Kaskan, W., "The Source of the Continuum in Carbon Monoxide-Hydrogen-Air Flames", *Combustion and Flame*, vol. 3, p. 39., 1959.

21. Gaydon, A., "The Use of Shock Tubes for Studying Fundamental Combustion Processes", Eleventh Symposium on Combustion, The Combustion Institute, p. 321, 1971.

22. Porter, R., Clarke, A., Kaskan, W., and Brown, W., "A Study of Hydrocarbon Flames", Eleventh Symposium on Combustion, The Combustion Institute, p. 907, 1967.

23. Child, E., and Wohl, K., "Spectrophotometric Studies of Laminar Flames -- I, The Decay of Radical Radiation", Seventh Symposium on Combustion, The Combustion Institute, p. 215, 1959.

24. Kashida, R., and Wohl, K., "Spectrophotometric Studies of Laminar Flames -- II, The Flame Front", Seventh Symposium on Combustion, The Combustion Institute, p. 221, 1959.

25. Beyler, C. L., Flame Structure and Stabilization in Premixed Swirl-Stabilized Combustion, M. S. Thesis, Cornell University, Ithaca, New York, 1981.

26. Johnsson, E. L., The Use of Chemiluminescence for Detection of Ignition, Temperature, and Fuel-to-Air Ratio of Flames, M. S. Thesis, Virginia Tech, Blacksburg, Virginia, 1991.

27. Vandsburger, U., Burner for Gaseous Premixed Turbulent-Flowing Mixtures, Shop Drawings and Schematics, Virginia Tech Mechanical Engineering Department Shop, Blacksburg, Virginia, 1991.

28. Oriel Catalog, vol. III, *Optics and Filters*, pp. 1-2 to 1-14, The Oriel Corporation, Stratford, Connecticut, 1990.

29. The Temperature Handbook, vol. 28, p. Z-18, Omega Engineering, Inc., Stamford, Connecticut, 1992.

30. Thermocouple Radiation Correction FORTRAN Program, TCOUPLE.FOR, Sandia National Laboratories, from Mitchell, R. E., Private Communication, Blacksburg, Virginia, 1991.

31. Data Transferal BASIC Program, JIMTRAN.BAS, from Hamer, A. J., and Johnsson, E. L., Private Communication, Blacksburg, Virginia, 1991.

32. Data Plotting Program, PROPLOT, version 1.01, from Eskin, L. D., and Seitzman, J. M., Cogent Software, 1987.

33. Heywood, J. B., Internal Combustion Engine Fundamentals, McGraw-Hill Publishing Company, New York, New York, 1988.

34. White, F. M., Fluid Mechanics, Second Edition, McGraw-Hill Book Company, New York, New York, 1986.

35. Wilke, C. R., *Journal of Chemical Physics*, vol. 18, pp. 517-9, 1950.

36. Chemical Equilibrium Solver Program, STANJAN, version 3.89, from Reynolds, W. C., Stanford University, Stanford, California, 1987.

37. Roby, R. J., Private Communication, Blacksburg, Virginia, 1991.

38. Eckbreth, A. C., Laser Diagnostics for Combustion Temperature and Species, Abacus Press, Cambridge, Massachusetts, 1988.

39. Treager, I. E., Aircraft Gas Turbine Engine Technology, Second Edition, New York, New York, McGraw-Hill Book Company, 1979.

40. Yates, T. C., and Smith, T. S., "Pumping Systems and Flow Interfaces for Rapid Response Electronic Reheat Controls", AGARD Conference Proceedings, No. 421, Advanced Technology for Aero Gas Turbine Components, Paris, France, May 4-8, 1987.

41. Vleghert, J. P. K., "Deterioration in Service of Engine Transient Behavior", AGARD Conference Proceedings, No. 324, Engine Handling, Marathon, Greece, October 11-14, 1982.

42. Bauerfeind, I. K., "Some General Topics in the Field of Engine Handling", AGARD Conference Proceedings, No. 324, Engine Handling, Marathon, Greece, October 11-14, 1982.

43. Stetson, H. D., "Designing for Stability in Advanced Turbine Engines", AGARD Conference Proceedings, No. 324, Engine Handling, Marathon, Greece, October 11-14, 1982.

44. Skirak, C. A., De Hoff, R. L., and Hall, W. E., "Design, Evaluation, and Test of an Electronic, Multivariable Control for the F100 Turbofan Engine", AGARD Conference Proceedings, No. 274, Advanced Control Systems for Aircraft Powerplants, DFVLR, Cologne, Germany, October 1-2, 1979.

Appendix A:

Applications to Afterburners

Afterburning engines require the use of variable area exhaust nozzles to control airflow. During normal afterburner operation, the nozzle is enlarged to allow a larger volume of air to flow through the engine and reduce back pressure to prevent compressor stall. Afterburners are typically used for short periods to increase thrust and accelerate the aircraft; the time required to initiate afterburner operation and accelerate to full thrust augmentation is very short. Afterburner ignition must be confirmed before the nozzle can be widened; if the nozzle opens and afterburner ignition fails, the compressor/fan stalls and engine failure may result [39]. A device to sense afterburner ignition and subsequent flame blowout is a necessity for proper afterburner performance.

While the ideal situation would be to open the nozzle up just after the afterburner ignites, there is short delay associated with the hydromechanical actuators of the nozzle system [40]. However, widening the nozzle too early in the afterburner lighting process can be just as disastrous as widening the nozzle after afterburner combustion has been established. Widening the nozzle too early results in an immediate loss in thrust and, more importantly, an increase in airflow velocity in the vicinity of the flameholder region, which could make afterburner ignition impossible. Vleghert [41] states:

> "Preferably the afterburner should light up on a small amount of fuel, then -- once alight -- it can be opened smartly to [the maximum]....Nowadays a delay -- and sometimes a ramp function is built in which under normal conditions prevents maximum afterburner fuel flow at light-up. If ignition is delayed, however, a hard light results. Control would be greatly eased with an [afterburner] flame detector, which inhibits fuel flow increase until light-up has occurred. So far, however, reliability of such an installation has been a problem."

In addition to afterburner blowout problems, the stability of afterburner combustion is another concern. A stable afterburner flame is desired to avoid the constant changes in nozzle geometry that would be necessary otherwise. And while the consequences of unsteady afterburner combustion are not as severe as afterburner blowout, they are hardly welcome. Pressure waves caused by unsteady afterburner combustion can travel upstream through the engine, adversely affecting compressor/fan performance and possibly leading to stall or surge. There are several factors that can affect the stability of afterburner combustion.

In modern high-bypass ratio afterburning engines, gas stream mixers are omitted from the design to save weight. Consequently, the afterburner must burn a large part of the fuel in the cold stream at relatively low pressures -- a problem that contributes to combustion instability. According to Bauerfeind [42]:

> "While the earlier low bypass ratio engines normally employed a gas stream mixer arrangement, the modern high bypass ratio engines (above 0.6) have no such arrangement mainly in order to save structural weight and length. This means that a large portion of the fuel has to be burnt in the cold stream at comparatively low pressure levels. This entails potential problems when lighting the fuel on afterburner selection and when lighting across the individual zones during an 'acceleration' of the afterburner towards maximum boost."

High altitude can also contribute to afterburner combustion instability. As pressures and temperatures decrease with increasing altitude, the combustion stability margin decreases as well [43]. The fuel scheduling accuracy is also adversely affected by high altitude operation, due to lower fuel flowrates and lower ambient pressures. With fuel flow becoming more unstable and the combustion stability margin shrinking, high altitude afterburner operation can

lead to combustion instability and thence to stall or surge of the compressor/fan. Currently, active control systems are used to dampen the effects of unstable afterburner combustion.

One such control system was developed by Skirak, De Hoff, and Hall [44] for the Pratt and Whitney F100 turbofan. Monitoring several engine variables, this digital control system was designed to suppress pressure disturbances caused by afterburner ignition. In six of eight flight conditions tested, their control system was successful in suppressing disturbances caused by the initiation of the afterburner system. The control system did not sense enough of a pressure difference in the two failures (45,000 feet and 50,000 feet at Mach 0.9) to properly suppress the disturbance. However, the viability of an active feedback system to monitor and control combustion and pressure stability while the afterburner is in operation has been proven by Skirak, De Hoff, and Hall. And clearly a faster, more sensitive combustion detector would be of benefit to the design. Quite possibly, a detector based on the chemiluminescent signals of combustion could be used to fill this role.

Appendix B:

Rotameter Calibrations

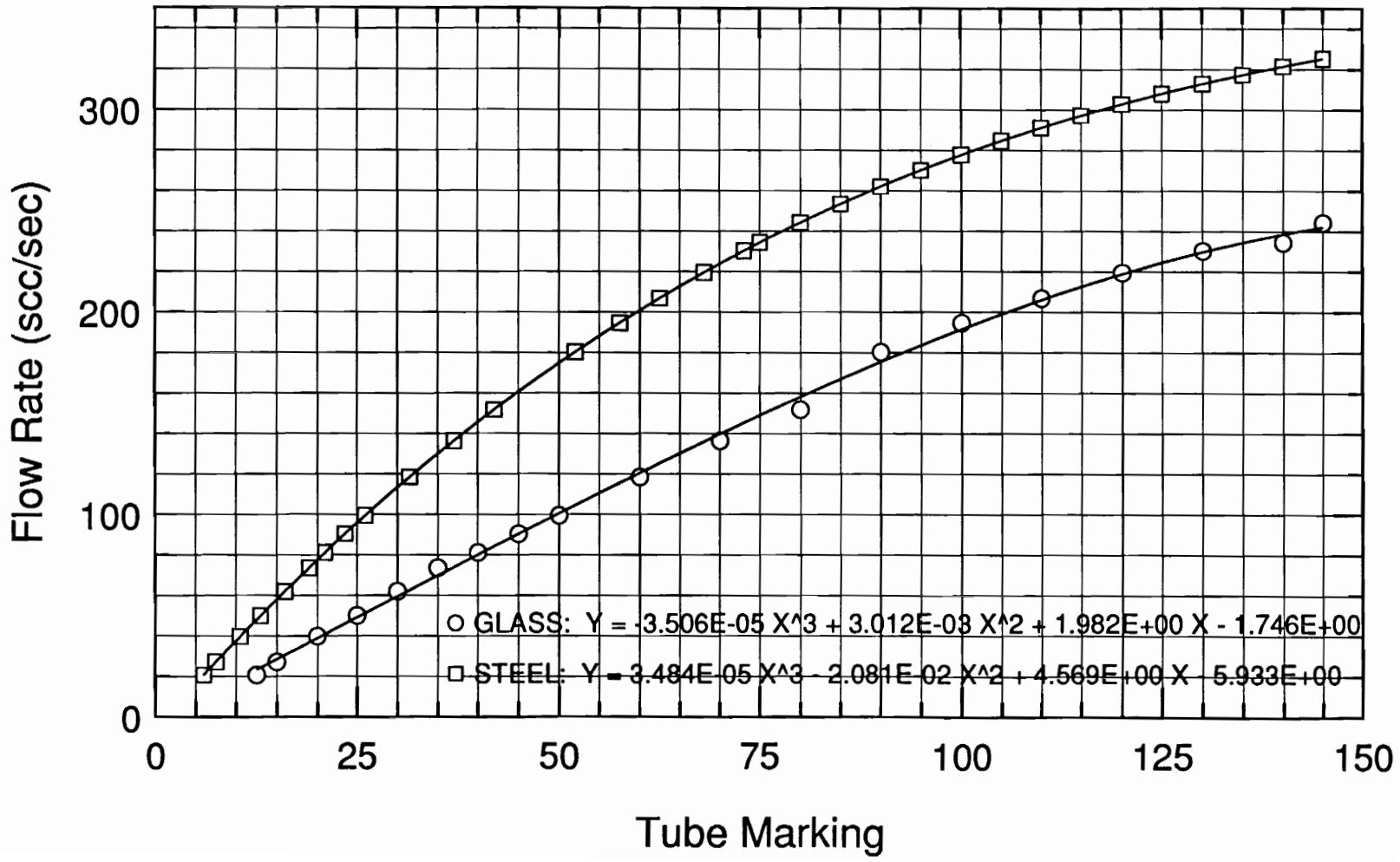
Tube 604#3, Methane @ 40 psig, 760 mm Hg & 273.15 K
Flow Rate (scc/sec)
300
200
100
0
0
25
50
75
100
125
150
Tube Marking
GLASS: Y = -3.506E-05 X^3 + 3.012E-03 X^2 + 1.982E+00 X - 1.746E+00
STEEL: Y = 3.484E-05 X^3 - 2.081E-02 X^2 + 4.569E+00 X - 5.933E+00

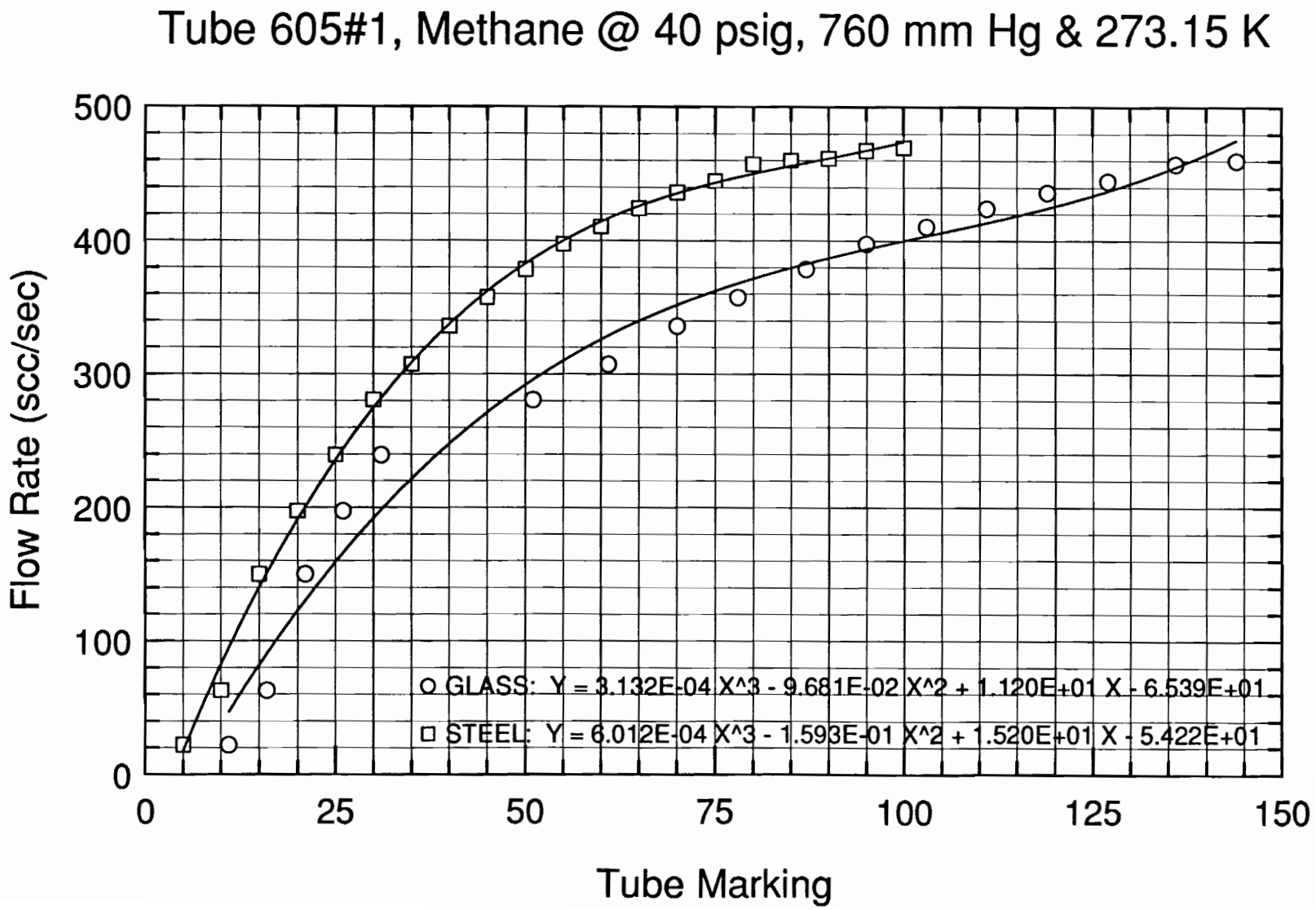
Tube 605#1, Methane @ 40 psig, 760 mm Hg & 273.15 K
Flow Rate (scc/sec)
500
400
300
200
100
0
0
25
50
75
100
125
150
Tube Marking
GLASS: Y = 3.132E-04 X^3 - 9.681E-02 X^2 + 1.120E+01 X - 6.539E+01
STEEL: Y = 6.012E-04 X^3 - 1.593E-01 X^2 + 1.520E+01 X - 5.422E+01

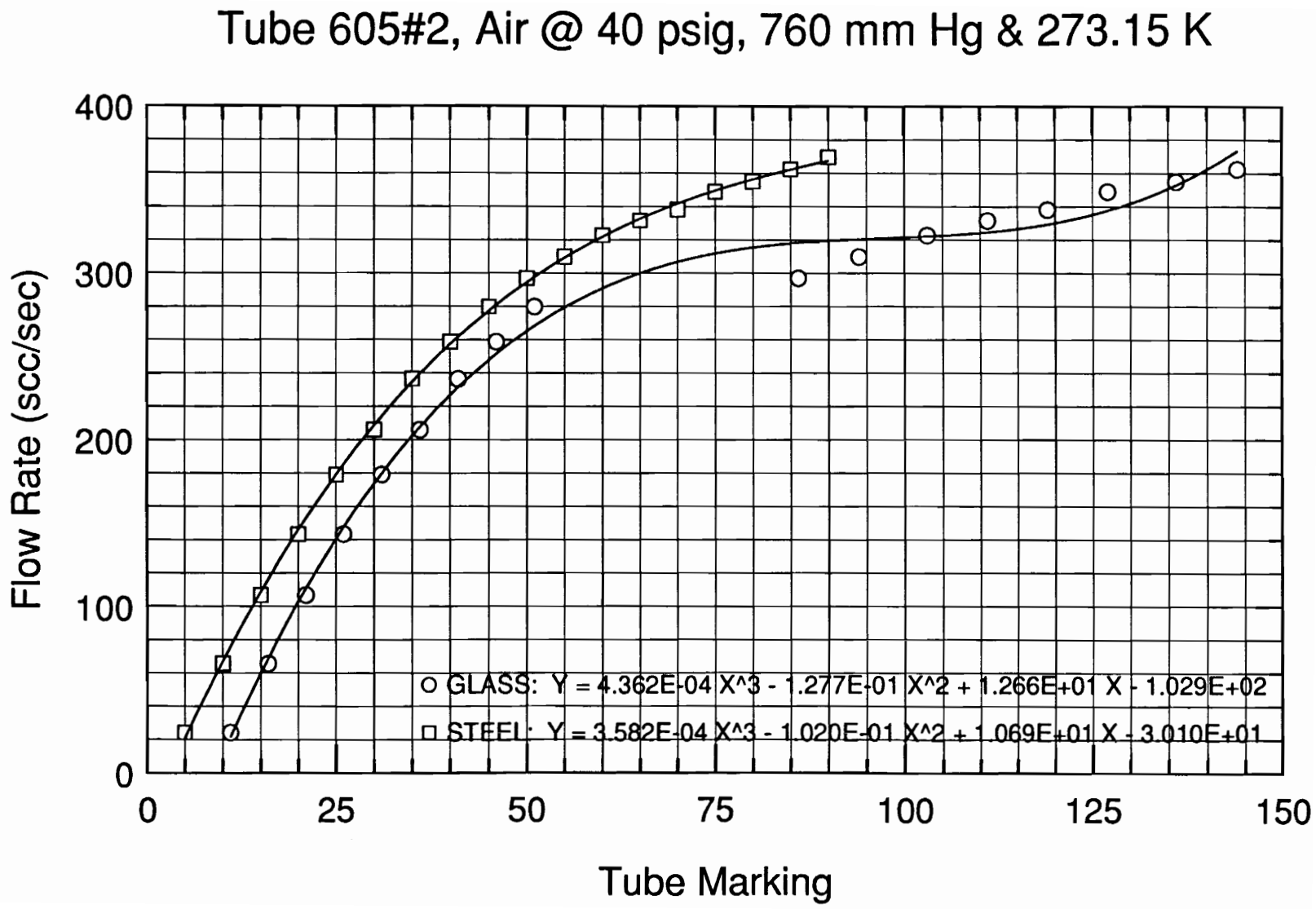
Tube 605#2, Air @ 40 psig, 760 mm Hg & 273.15 K
Flow Rate (scc/sec)
400
300
200
100
0
0
25
50
75
100
125
150
Tube Marking
GLASS: Y = 4.362E-04 X^3 - 1.277E-01 X^2 + 1.266E+01 X - 1.029E+02
STEEL: Y = 3.582E-04 X^3 - 1.020E-01 X^2 + 1.069E+01 X - 3.010E+01

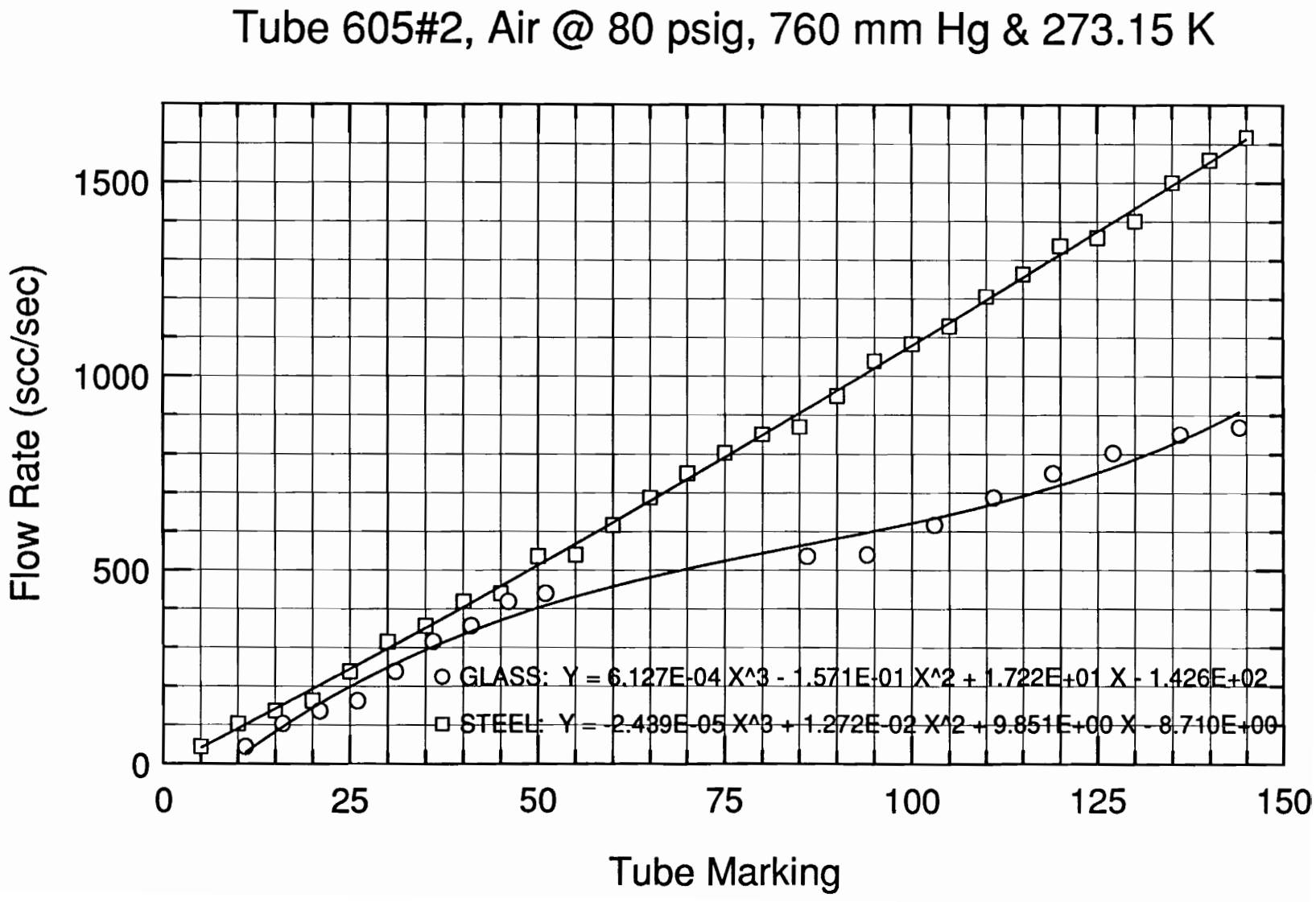
Tube 605#2, Air @ 80 psig, 760 mm Hg & 273.15 K
Flow Rate (scc/sec)
1500
1000
500
0
0
25
50
75
100
125
150
Tube Marking
GLASS: Y = 6.127E-04 X^3 - 1.571E-01 X^2 + 1.722E+01 X - 1.426E+02
STEEL: Y = -2.439E-05 X^3 + 1.272E-02 X^2 + 9.851E+00 X - 8.710E+00

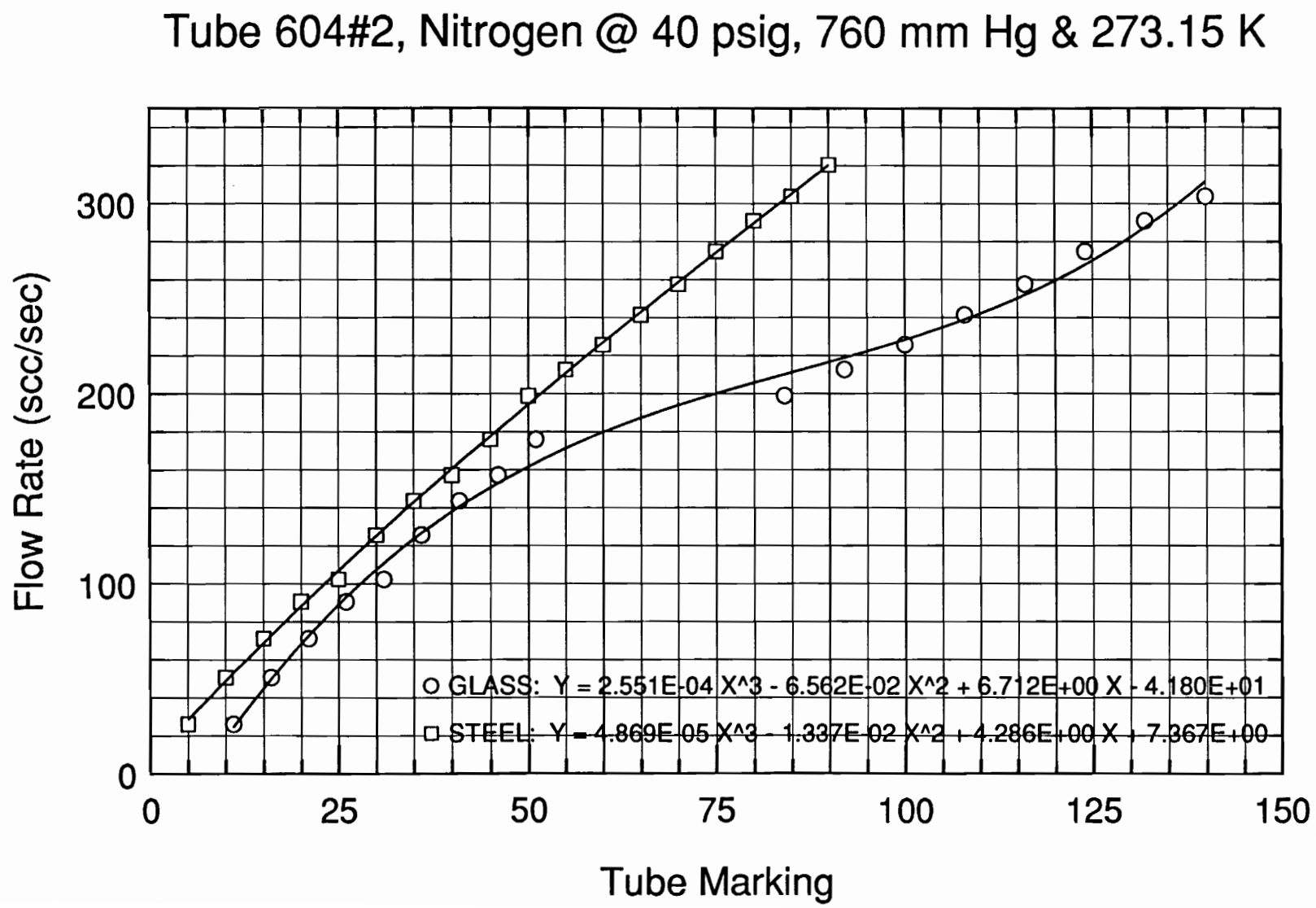
Tube 604#2, Nitrogen @ 40 psig, 760 mm Hg & 273.15 K
Flow Rate (scc/sec)
300
200
100
0
0
25
50
75
100
125
150
Tube Marking
GLASS: Y = 2.551E-04 X^3 - 6.562E-02 X^2 + 6.712E+00 X - 4.180E+01
STEEL: Y = 4.869E-05 X^3 - 1.337E-02 X^2 + 4.286E+00 X + 7.367E+00

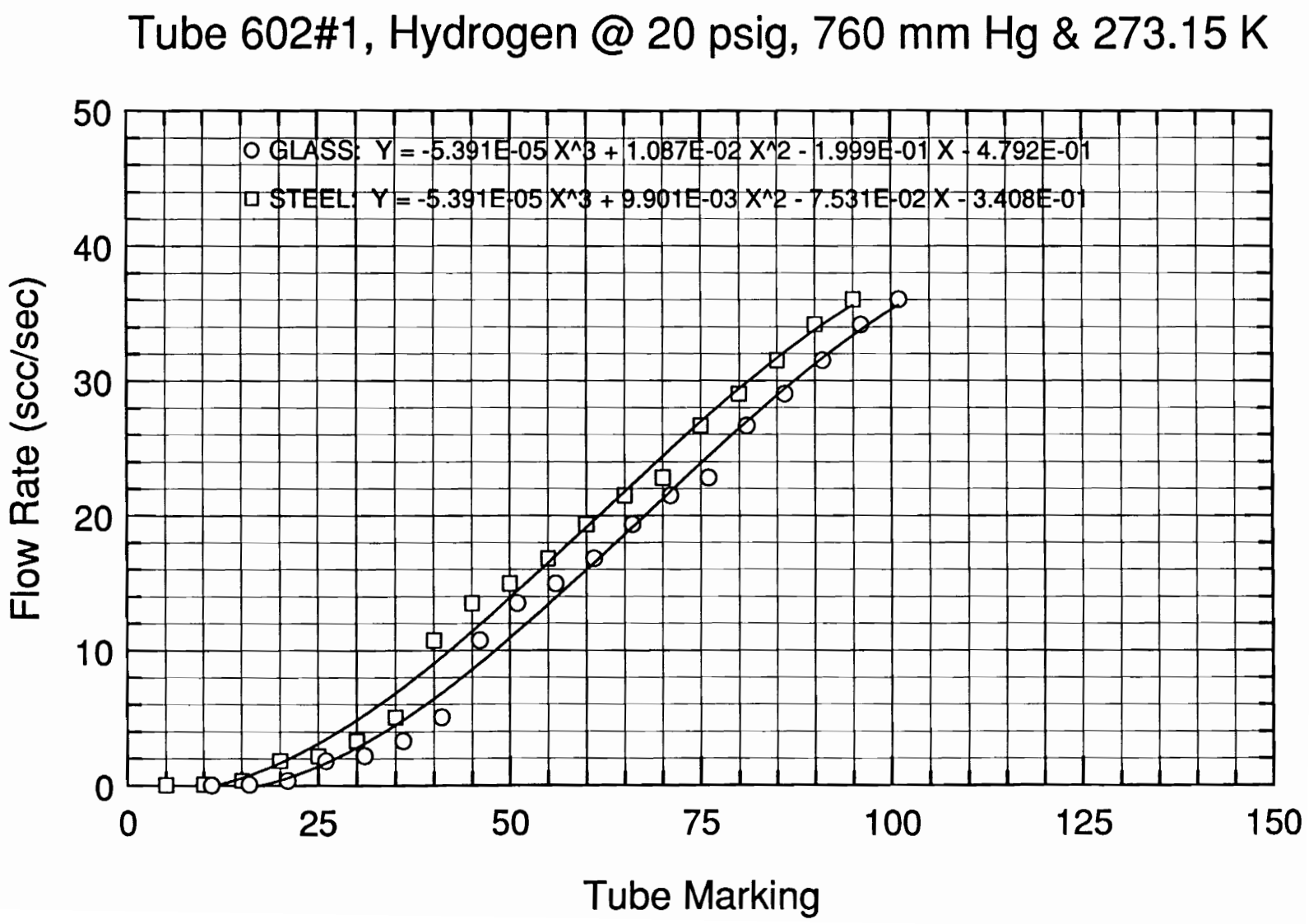
Tube 602#1, Hydrogen @ 20 psig, 760 mm Hg & 273.15 K
GLASS: Y = -5.391E-05 X^3 + 1.087E-02 X^2 - 1.999E-01 X - 4.792E-01
STEEL: Y = -5.391E-05 X^3 + 9.901E-03 X^2 - 7.531E-02 X - 3.408E-01
Flow Rate (scc/sec)
0
10
20
30
40
50
0
25
50
75
100
125
150
Tube Marking

Appendix C:

Flowrate Calculation Program

FLOATPOS.FOR

```
C234567

      ZMOLFUEL = 1.
      ZMAIR = 28.962

      WRITE (*,*) 'INPUT PHI, Re, P(Pascals), AND T(Kelvin)'
      READ (*,*) PHI, RE, P, T
      WRITE (*,*) 'INPUT Mfuel, RHOfuel(kg/m^3), MUfuel(kg/m/s)'
      READ (*,*) ZMFUEL, RHOFUEL, ZMUFUEL
      WRITE (*,*) 'INPUT # MOLES AIR/MOLE FUEL IN STOICHIOMETRIC MIX'
      READ (*,*) ZMOLAIR

      RHOAIR = .003483*P/T
      ZMUAIR = (3.3E-7)*T**.7
      RATIOACT = PHI*ZMOLFUEL*ZMFUEL/ZMOLAIR/ZMAIR
      RATIOVOL = RATIOACT*RHOAIR/RHOFUEL
      XFUEL = 1./((ZMFUEL/ZMAIR/RATIOACT)+1.)
      XAIR = 1.-XFUEL
      RHOMIX = (XFUEL*RHOFUEL)+(XAIR*RHOAIR)
      PHI121 = (8.)**(-.5)*(1.+(ZMFUEL/ZMAIR))**(-.5)
      PHI122 = (1.+(ZMUFUEL/ZMUAIR)**.5*(ZMAIR/ZMFUEL)**.25)**2.
      PHI12 = PHI121*PHI122
      PHI211 = (8.)**(-.5)*(1.+(ZMAIR/ZMFUEL))**(-.5)
      PHI212 = (1.+(ZMUAIR/ZMUFUEL)**.5*(ZMFUEL/ZMAIR)**.25)**2.
      PHI21 = PHI211*PHI212
      ZMUMIX1 = XFUEL*ZMFUEL/(XFUEL+XAIR*PHI12)
      ZMUMIX2 = XAIR*ZMUAIR/(XFUEL*PHI21+XAIR)
      ZMUMIX = ZMUMIX1+ZMUMIX2
      QMIX = .014962*ZMUMIX/RHOMIX*RE
      QMIX = (QMIX*1.E+6)*(273.15/T)**.5
      QAIR = QMIX/(1.+RATIOVOL)
      QFUEL = QMIX-QAIR

      WRITE (*,*)
      WRITE (*,*) 'Qair is ',QAIR,' standard cc/sec'
      WRITE (*,*) 'Qfuel is ',QFUEL,' standard cc/sec'

      END
```

Appendix D:

Thermocouple Bead Radiation Correction Program

TCOUPLE.FOR

```
C     **** THERMOCOUPLE RADIATION CORRECTION PROGRAM ****
C          ORIGINALLY FOR HYDROGEN/OXYGEN/ARGON FLAMES;
C          ADAPTED FOR METHANE/OXYGEN/NITROGEN FLAMES
C          REVISED BY:          R. ROBY, 8-24-84
C          FURTHER REVISIONS BY: J. HUNDERUP, 2-2-90
C                                R. JOHNSSON, 2-5-90, 9-10-90
C                                J. REANEY, 3-13-92
C
C     THIS ROUTINE DETERMINES THE GAS TEMPERATURE AT THE LOCATION
C     OF A Pt-Pt10%Rh THERMOCOUPLE BEAD BY MAKING A RADIATION
C     CORRECTION TO THE THERMOCOUPLE BEAD TEMPERATURE.
C
C     TG = TC + SIGMA*EMISS*D*(TC^4-TW^4)/LAMDA/NU
C
C     WHERE:  TG = CORRECTED GAS TEMPERATURE
C             TC = THERMOCOUPLE BEAD TEMPERATURE
C             SIGMA = STEFAN-BOLTZMANN CONSTANT, CAL/SQCM/SEC/K
C             EMISS = THEMOCOUPLE WIRE EMISSIVITY
C             D = BEAD DIAMETER, CM
C             TW = TEMPERATURE OF SURROUNDINGS
C             LAMDA = GAS THERMAL CONDUCTIVITY, CAL/CM/SEC/K
C             NU = NUSSELT NUMBER OF THE BEAD
C
C     DECLARATION OF VARIABLES
C
      REAL LAMDA, NU
      INTEGER FLAG
C
C     OPENING OF DATA FILE
C
      OPEN (7,FILE='TCOUPLE.DAT')
C
C     ASSIGNMENT OF VALUES TO CONSTANTS
C
      SIGMA=1.355E-12
      EMISS=0.3
      NU=2.0
      FLAG=0
C
C     WRITING OF DATAFILE TITLES
C
      WRITE (7,100)
  100 FORMAT (22X,'THERMOCOUPLE CORRECTION DATA',/,13X,'(ALL TEMPERATURE
     $S IN KELVIN; DIAMETER IN MILS)',//)
      WRITE (7,110)
  110 FORMAT (1X,'BEAD TEMP',3X,'SURROUNDINGS TEMP',3X,'BEAD DIAMETER',3
     $X,'CORRECTED GAS TEMP',/)
C
C     WRITING OF DESCRIPTION OF PROGRAM FUNCTION
```

```
C
      WRITE (*,160)
  160 FORMAT(1X,'THIS CODE MAKES RADIATION CORRECTIONS TO A THERMOCOUPLE
     $BEAD TEMPERATURE',/)
      WRITE (*,115)
  115 FORMAT (1X,'MAKE SURE CAPS LOCK IS ON FOR THE DURATION OF THIS PRO
     $GRAM!',/)
C
C     CHECK FOR SERIES TYPE DATA
C
      WRITE (*,120)
  120 FORMAT (1X,'WILL BEAD DIAMETER AND SURROUNDING TEMPERATURE BE THE
     $SAME',/,4X,'FOR ALL INPUT (Y OR N)? ',\)
      READ (*,130) IYY
  130 FORMAT (A1)
      IF (IYY.EQ.'Y') THEN
          FLAG=1
          WRITE (*,140)
  140   FORMAT (/,15X,'ENTER SURROUNDINGS TEMPERATURE (C): ',\)
          READ (*,*) TW
          WRITE (*,150)
  150   FORMAT (15X,'ENTER BEAD DIAMETER (MIL): ',\)
          READ (*,*) D
          TW=TW+273.15
          D=D*2.54E-03
      ENDIF
C
C     READING IN OF THERMOCOUPLE AND TEMPERATURE DATA
C
  300 CONTINUE
      IF (FLAG.NE.1) THEN
          WRITE (*,140)
          READ (*,*) TW
          WRITE (*,150)
          READ (*,*) D
          TW=TW+273.15
          D=D*2.54E-03
      ENDIF
      WRITE (*,170)
  170 FORMAT (15X,'ENTER BEAD TEMPERATURE (C): ',\)
      READ(*,*) TC
      TC=TC+273.15
C
C     THERMAL CONDUCTIVITY USED IS THAT FOR A MISTURE OF EQUILIBRIUM
C     PROCUCTS OF A LEAN (PHI=0.80) METHANE/OXYGEN/NITROGEN FLAME.
C     LAMDA SHOULD BE EVALUATED AT TGAS.  AN ITERATIVE PROCESS IS
C     SUGGESTED.  EXPERIENCE SHOWS THAT ONLY 3 TO 6 ITERATIONS ARE
C     REQUIRED.
C
      TG=TC
      DO 400 ITER=1,6
```

```
          LAMDA=5.0E-5*(TG/273.15)**.94
          TCORR=SIGMA*EMISS*D*(TC**4.-TW**4.)/LAMDA/NU
          TG=TC+TCORR
  400 CONTINUE
     ERROR=0.2*TCORR
C
C    PRESENTATION OF OUTPUT
C
     WRITE (*,180)
  180 FORMAT (//,20X,'CALCULATION OF TGAS',/20X,'-------------------',/)
     WRITE (*,190) TC
  190 FORMAT (15X,'THERMOCOUPLE BEAD TEMPERATURE: ',F7.2,' K')
     WRITE (*,200) TW
  200 FORMAT (15X,'SURROUNDINGS TEMPERATURE:     ',F7.2,' K')
     D=D/2.54E-3
     WRITE (*,210) D
  210 FORMAT (15X,'THERMOCOUPLE BEAD DIAMETER:   ',F7.2,' MIL')
     WRITE (*,220) TG,ERROR
  220 FORMAT (15X,'CORRECTED GAS TEMPERATURE:    ',F7.2,' +/-',F6.2,' K
    $')
C
C    INQUIRY TO USER IF THERE ARE MORE CASES TO RUN
C
     WRITE (7,230) TC,TW,D,TG,ERROR
  230 FORMAT (2X,F7.2,7X,F7.2,12X,F7.2,8X,F7.2,' +/-',F6.2)
     IF (FLAG.EQ.1) D=D*2.54E-3
     WRITE (*,240)
  240 FORMAT (/,15X,'ARE THERE MORE CASES TO RUN, Y OR N? ',\)
     READ (*,250) IYY
  250 FORMAT (A1)
     WRITE (*,*)
     IF (IYY.NE.'N') GOTO 300
     CLOSE (7)
     END
```

Appendix E:

Data Transfer Program

JIMTRAN.BAS

```
10 REM    "JIMTRAN.BAS"
20 REM
30 REM    This program transfers every nth point from a Nicolet
40 REM    digital oscilloscope recorded waveform and stores the
50 REM    data as an ASCII file to be read by plotting programs
60 REM    such as Proplot.
70 REM
80 CLS:KEY OFF
90 PRINT "You should have started GWBASIC as 'GWBASIC /C:2048'"
100 PRINT "If you did not, exit and do so.  The program will not function"
110 PRINT "correctly unless you do."
120 PRINT
130 PRINT "Also, please make sure the CAPS LOCK key is on; this program only"
140 PRINT "accepts uppercase letters for input."
150 PRINT
160 PRINT "Which channel do you wish to transfer data from: A or B";
170 INPUT A$
180 IF A$="A" OR A$="B" THEN 210 ELSE 190
190 PRINT:PRINT "I said UPPERCASE only!  Perhaps you misunderstood; please try
again."
200 B$=INKEY$:IF B$="" THEN 200 ELSE 80
210 PRINT
220 INPUT "Input start time (i.e., first data point to be read): ";STRT
230 PRINT
240 PRINT "If disk storage is desired, type name of file."
250 PRINT "(8 characters maximum; extension is preset *.DAT)."
260 PRINT "If not, simply press <ENTER> ";
270 INPUT T$
280 PRINT:PRINT "   A sampling frequency of 1 means that every point will be"
290 PRINT "   translated, a 2 means every fourth point, a 3 means every"
300 PRINT "   eighth point, and so on in powers of two."
310 PRINT:PRINT "What sampling frequency do you desire";
320 INPUT XPT
330 CLS
340 DEFINT A-Z
350 DIM N#(11)
360 OPEN "COM1:9600,S,7,1,LF" AS #1
370 PRINT #1,CHR$(1)+">";
380 PRINT #1,"K,0,131,52"
390 CLOSE
400 OPEN "COM1:9600,N,8,1" AS #1
410 PRINT #1,"C,13,13"+CHR$(10)
420 INPUT #1,E
430 PRINT #1,"C,8,1,13"
440 INPUT #1,E
450 PRINT #1,"C,4,1,13"
460 INPUT #1,E
```

```
470 IF A$="A" THEN PRINT #1,"N,0"
480 PRINT #1,"N,1"
490 INPUT #1,E
500 FOR I=1 TO 11
510 INPUT #1,N#(I)
520 NEXT I
530 INPUT #1,E
540 X=15872/2^N#(2)
550 DIM D(X)
560 PRINT "Waveform has";X;"data points."
570 PRINT "Time per point =";N#(6);"seconds."
580 PRINT "Voltage range =";N#(5)*32000;"volts."
590 PRINT
600 PRINT "Transferring data to computer now; please wait..."
610 R=X:I=0
620 IF A$="A" THEN PRINT #1,"D,6,1,0',"+STR$(X)+",1"
630 IF A$="B" THEN PRINT #1,"D,6,2,0',"+STR$(X)+",1"
640 INPUT #1,E
650 IF R<1000 THEN 680
660 IF LOF(1)>50 THEN 660
670 PRINT #1,CHR$(19);
680 WHILE LOC(1)>3:L$=INPUT$(1,1):H$=INPUT$(1,1):D(I)=CVI(L$+H$):I=I+1:WEND
690 LOCATE 7,4:PRINT "Finished with data point";I;
700 R=X-I
710 IF R>0 THEN PRINT #1,CHR$(17);:GOTO 650
720 INPUT #1,E
730 HZ#=N#(8)*65536!+N#(9)
740 IF T$="" THEN 850
750 LOCATE 9,1:PRINT "Normalizing and storing data - this will take a minute or two."
760 PRINT
770 OPEN T$+".DAT" FOR OUTPUT AS #2
780 IRATE=2^XPT
790 FOR K=0 TO X-1
800 IJL=IJL+1
810 IF IJL=16 THEN IJ=IJ+1:LOCATE 11,4:PRINT "Finished with program point";IJ;
820 IF (K-HZ#)*N#(6)<STRT THEN GOTO 840
830 IF IJL=16 THEN PRINT #2,(K-HZ#)*N#(6),(D(K)-N#(7))*N#(5):IJL=0
840 NEXT K
850 CLOSE:LOCATE 13,1:PRINT "End of program."
860 BEEP:END
```

Appendix F:

Typical PROPLOT program

```
SET PAGE FORMAT PORTRAIT
SET WINDOW X FROM 2.375 TO 7.25 Y FROM 4.0625 TO 8.9375
SET LIMITS X FROM 0.6 TO 1.0 Y FROM 2 TO 7.5
TITLE BOTTOM 'Equivalence Ratio'
TITLE LEFT 'OH/CH Ratio Corrolation'
SET ORDER X Y
SET SYMBOL '3P'
INSERT E:\JAMES\PLOTS\OHCHNFR1.DAT
PLOT
DRAW AXES
FIT LINE STYLE SOLID
SET ORDER X Y
SET SYMBOL '3N'
INSERT E:\JAMES\PLOTS\OHCHPHR2.DAT
PLOT POINTS 1 20
DRAW AXES
FIT LINE STYLE SOLID POINTS 1 20
FIT LINE STYLE DOTS POINTS 21 22
LEGEND 'Y = -30.936 X + 26.111' 2.8 4.5 SIZE 1.4
LEGEND 'Y = -10.818 X + 12.862' 5.6 5.9 SIZE 1.4
LEGEND '3 OH/CH PHR' 5.2 7.3
CASE 'N'
LEGEND 'Y = -16.849 X + 17.869' 3.8 8.2 SIZE 1.4
LEGEND '3 OH/CH NFR' 5.2 7.1
CASE 'P'
STAMP BOTTOM FILE
```

Appendix G:

Uncertainty Analysis

Introduction

This appendix presents an uncertainty analysis of the experimental measurements of equivalence ratio, corrected flame temperature, chemiluminescent signal peak heights, full width at half-heights, and integrated filter signal strengths of the turbulent, premixed methane-air-nitrogen flames discussed in this research. Root mean square addition is used for propagation of errors associated with single measurements. This method assumes that errors are independent of each other and normally distributed throughout the scale of the measurement.

Equivalence ratio uncertainty

The uncertainty in the calculation of equivalence ratio involves several factors. There is uncertainty involved in both the fuel and air volume flowrates, each of which contains uncertainty concerning ambient pressure and temperature measurements. Following the algorithm for computing fuel and air flowrates given in section 3.2 (also the algorithm for program FLOATPOS.FOR given in Appendix B), it is clear that the volumetric fuel-to-air ratio is dependent on the density measurements of both the fuel and the air, each of which is dependent on ambient pressure and temperature readings. The uncertainty associated with the volumetric fuel-to-air ratio is therefore:

$$Error_{(F/A)_{vol}} = \sqrt{(Error_{\rho_{air}})^2 + (Error_{\rho_{fuel}})^2}$$

where $$Error_{\rho_{air}} = \sqrt{(Error_{pressure})^2 + (Error_{temperature})^2}$$

and $$Error_{\rho_{fuel}} = \sqrt{(Error_{pressure})^2 + (Error_{temperature})^2}$$

The barometric pressure readings were read off a 152.4 millimeter (six inch) full scale mercury barometer marked off in millimeters. It is assumed that the scale could be accurately read in increments equal to one-half the smallest division. This meant that the accuracy of the pressure reading was ±0.5 mm or 0.328 percent of full scale. Likewise, the ambient temperature readings were read off a sixty-five degree Kelvin thermometer marked off in one degree Kelvin increments. One-half of the smallest division is one-half degree Kelvin and thus the accuracy of the temperature measurement is ±0.5 K or 0.769 percent of full scale. Therefore the total uncertainty involved with the volumetric fuel-to-air measurement may be calculated as follows:

$$
\begin{aligned}
Error_{\rho_{air}} &= Error_{\rho_{fuel}} \\
&= \sqrt{(Error_{pressure})^2 + (Error_{temperature})^2} \\
&= \sqrt{(0.00328)^2 + (0.00769)^2} \\
&= \underline{0.836\%}
\end{aligned}
$$

$$
\begin{aligned}
Error_{(F/A)_{act}} &= \sqrt{(Error_{\rho_{air}})^2 + (Error_{\rho_{fuel}})^2} \\
&= \sqrt{(0.00836)^2 + (0.00836)^2} \\
&= \underline{\underline{1.183\%}}
\end{aligned}
$$

Other factors affecting equivalence ratio uncertainty are fuel-air mixture viscosities and densities. The mixture viscosity measurement is dependent upon component viscosity measurements which are in turn dependent on ambient temperature readings. The mixture density measurement is also dependent on component densities which are in turn dependent on pressure and temperature readings. Thus:

$$Error_{\mu_{mix}} = \sqrt{(Error_{\mu_{air}})^2 + (Error_{\mu_{fuel}})^2}$$
$$= \sqrt{(Error_{temperature})^2 + (Error_{temperature})^2}$$
$$= \sqrt{(0.00769)^2 + (0.00769)^2}$$
$$= \underline{1.088\%}$$

$$Error_{\rho_{mix}} = \sqrt{(Error_{\rho_{air}})^2 + (Error_{\rho_{fuel}})^2}$$
$$= \sqrt{(0.00836)^2 + (0.00836)^2}$$
$$= \underline{1.183\%}$$

The volume flowrate of the fuel-air mixture is dependent on the viscosity and density measurements of the mixture. Therefore the uncertainty involved with the volume flowrate for the mixture can be calculated as follows:

$$Error_{Q_{mix}} = \sqrt{(Error_{\mu_{mix}})^2 + (Error_{\rho_{mix}})^2}$$
$$= \sqrt{(0.01088)^2 + (0.01183)^2}$$
$$= \underline{\underline{1.607\%}}$$

Finally, the required volume flowrate of air is dependent on the volume flowrate of the mixture and the volumetric fuel-to-air ratio. Actual volume flowrates of air are also dependent on the accuracy of the rotameters. Since the rotameters are divided into 150 gradations, their accuracy is ±0.5 gradations or 0.333 percent of full scale. Therefore the uncertainty associated with the volume flowrate of air is as follows:

$$Error_{Q_{air}} = \sqrt{(Error_{Q_{mix}})^2 + (Error_{(F/A)_{mix}})^2 + (Error_{rotameter})^2}$$
$$= \sqrt{(0.01607)^2 + (0.01183)^2 + (0.00333)^2}$$
$$= \underline{2.023\%}$$

The required volume flowrate of fuel is derived from the required volume flowrate of air and the volume flowrate of the mixture. The actual volume flowrate of fuel is also dependent on the rotameter. Therefore the uncertainty associated with the volume flowrate of fuel is as follows:

$$Error_{Q_{fuel}} = \sqrt{(Error_{Q_{air}})^2 + (Error_{Q_{mix}})^2 + (Error_{rotameter})^2}$$
$$= \sqrt{(0.02023)^2 + (0.01607)^2 + (0.00333)^2}$$
$$= \underline{2.605\%}$$

Of course, the uncertainty involved with the measurement of equivalence ratio is dependent on the volume flowrates of both fuel and air. Thus, the total uncertainty involved with the calculation of equivalence ratio is:

$$Error_{\phi} = \sqrt{(Error_{Q_{air}})^2 + (Error_{Q_{fuel}})^2}$$
$$= \sqrt{(0.02023)^2 + (0.02605)^2}$$
$$= \underline{3.298\%}$$

Corrected flame temperature uncertainty

The corrected flame temperature uncertainty depends on two main factors: the uncertainty of the oscilloscope reading the thermocouple voltages and the uncertainty of the radiation correction program.

The oscilloscope is digital in nature; that is, it interprets an analog electrical signal as a discrete digital value. The uncertainty of this conversion is

a direct function of the size of the digitizing scale (the minimum distance, in volts, between two discrete signals). The oscilloscope has a minimum voltage scale of ±100 millivolts; however, the signal may be magnified up to 256 times. Therefore the uncertainty is one-half of the minimum gradation; ±0.390625 millivolts or 0.195 percent.

The radiation correction program used to convert measured thermocouple bead temperatures to corrected flame temperatures is dependent upon bead diameter and the temperature of the surroundings. The program assumes that the bead is spherical. The uncertainty of the measurement of the bead diameter is a function of the accuracy of the microscope used to measure bead diameters. The image of the bead could be measured accurately to the nearest half-centimeter on a thirty centimeter scale and with an eighty power microscope magnifying the bead, the uncertainty is ±0.0625 millimeters or 1.667 percent of full scale. Thermocouple beads tended not to be perfectly spherical, with an average eccentricity of 0.98. Therefore the uncertainty in assuming a spherical bead is about two percent.

The corrected flame temperature uncertainty can thus be calculated as follows:

$$
\begin{aligned}
Error_{T_{corrected}} &= \sqrt{(Error_{Voltage})^2 + (Error_{RadiationCorrection})^2} \\
&= \sqrt{(Error_{Voltage})^2 + (Error_{BeadDiameter})^2 + (Error_{Eccentricity})^2} \\
&= \sqrt{(0.00195)^2 + (0.01667)^2 + (0.02)^2} \\
&= \underline{2.611\%}
\end{aligned}
$$

Chemiluminescent signal peak height uncertainty

The chemiluminescent signal peak height uncertainty is simply the uncertainty associated with the oscilloscope voltage readings. As mentioned above, the full scale range is 200 millivolts (±100 mV) and one-half the minimum gradation is ±0.391 millivolts or 0.195 percent.

The total uncertainty associated with the OH/CH PHR correlation is dependent on the uncertainties of both the OH peak height signal and the CH peak height signal and is calculated as follows:

$$\begin{aligned} Error_{PHR} &= \sqrt{2(Error_{Voltage})^2} \\ &= \sqrt{2(0.00195)^2} \\ &= \underline{0.276\%} \end{aligned}$$

Full width at half height uncertainty

The uncertainty in the measurement of the width of the chemiluminescent signal is dependent on three factors: the uncertainty of the oscilloscope, the uncertainty of the monochromator, and the uncertainty of the synchronization of the two devices.

The uncertainty of the oscilloscope along the timescale axis was one-half of twenty milliseconds over a range of 317.44 seconds (20 ms/point with 15,872 data points). The accuracy is ±10 milliseconds or 0.00315 percent of full scale. The uncertainty of the monochromator was determined by the exit slight width (a narrow exit slit allowed fewer wavelengths of light to pass). The exit slit width corresponded to about 1.5 nanometers for these experiments. The range was 264.53 nanometers (the monochromator scans at 50 nm/min for 317.44 seconds). The monochromator's accuracy was therefore ±0.75 nm or 0.284

percent of full scale. The uncertainty of the synchronizing operation was determined by the reaction time of the human operator; not more than 0.5 seconds between the time the monochromator passed 270 nm and when the oscilloscope began recording. The accuracy was therefore ±0.25 seconds over the 317.44 seconds scan range, or 0.0788 percent of full scale.

The uncertainty of the width of the chemiluminescent signal can be calculated as follows:

$$\begin{aligned} Error_{\lambda width} &= \sqrt{(Error_{Time})^2 + (Error_{Monochromator})^2 + (Error_{Synchronization})^2} \\ &= \sqrt{(0.0000315)^2 + (0.00284)^2 + (0.000788)^2} \\ &= \underline{0.294\%} \end{aligned}$$

The calculation of half heights involves the uncertainty of the oscilloscope voltage readings in two places. Thus the total half height uncertainty can be calculated as follows:

$$\begin{aligned} Error_{HalfHeight} &= \sqrt{2(Error_{Time})^2} \\ &= \sqrt{2(0.00195)^2} \\ &= \underline{0.276\%} \end{aligned}$$

And therefore the total uncertainty involved with the calculation of full width at half height can be calculated as follows:

$$\begin{aligned} Error_{FWHH} &= \sqrt{(Error_{\lambda width})^2 + (Error_{HalfHeight})^2} \\ &= \sqrt{(0.00294)^2 + (0.00276)^2} \\ &= \underline{\underline{0.404\%}} \end{aligned}$$

Integrated filter signal strength uncertainty

The uncertainty of the integrated filter signal strengths is dependent on the uncertainty of the oscilloscope along the voltage axis and the uncertainty of the oscilloscope along the timescale axis.

The uncertainty of the oscilloscope along the voltage axis is given above as ±0.391 millivolts or 0.195 percent of full scale. The uncertainty of the oscilloscope along the timescale axis is given above as ±10 milliseconds or 0.00315 percent of full scale.

There is a further uncertainty involved in the OH N/LFR correlation, which concerns the accuracy of the monochromator. As stated above the monochromator has an accuracy of ±0.75 nm or 0.00284 percent of full scale.

The total uncertainty associated with the OH/CH NFR is dependent on the uncertainties of both the OH filter and the CH filter and is calculated as follows:

$$\begin{aligned} Error_{NFR} &= \sqrt{2(Error_{Voltage})^2 + 2(Error_{Time})^2} \\ &= \sqrt{2(0.00195)^2 + 2(0.0000315)^2} \\ &= \underline{0.195\%} \end{aligned}$$

The total uncertainty associated with the OH N/LFR is dependent on the uncertainties of the OH filter and the monochromator and is calculated as follows:

$$\begin{aligned} Error_{N\,/\,LFR} &= \sqrt{(Error_{Voltage})^2 + (Error_{Time})^2 + (Error_{Monochromator})^2} \\ &= \sqrt{(0.00195)^2 + (0.0000315)^2 + (0.00284)^2} \\ &= \underline{0.284\%} \end{aligned}$$

Standard percentile error of the data set

In section 5, accuracy figures are given for equivalence ratio and flame temperature predictions. These accuracy figures are based on standard percentile errors derived from the data sets. The standard percentile error is a measure of the statistical accuracy of a curve fit to a data set and is not a representation of the uncertainty associated with the measurement and/or collection of the data.

For each data set, there are independent and dependent values. For example, equivalence ratio correlations have OH/CH PHRs as the independent value. The dependent value is the predicted equivalence ratio, calculated from a linear regression of the data set. This dependent value differs from the known equivalence ratio, which is calculated from fuel and air flowrates beforehand. The amount by which the predicted value differs from the known value is the error (E), or the percent error (%E) on a percentile basis. Each set of data points in the set has an associated error value. The standard error is defined as follows:

$$StandardError = \pm\sqrt{\frac{1}{n-1}\sum_{1}^{n}(E)^2}$$

Likewise, the standard percentile error is defined as:

$$StandardPercentileError = \sqrt{\frac{1}{n-1}\sum_{1}^{n}(\%E)^2}$$

where n is the number of data points in the data set in both cases.

VITA

Born James Ernest Reaney, October 24, 1968, Kanagawa-ken, Japan. Son of Chun Cha and Leland Ernest Reaney, Jr. Moved to Seoul, Korea shortly thereafter, then Bangkok, Thailand in 1970. Sister Jennifer Elizabeth Reaney was born in January 1972 in Thailand. Moved to Indianapolis, Indiana in 1972. Moved to Heidelberg, Germany in summer 1973. Began elementary school at Patrick Henry Village Elementary School I in fall 1973. Began third grade at PHV Elementary School II. Moved to Queens, New York in winter 1975-6 and completed third through sixth grades at P.S. 209. Began intermediate school at J.H.S. 194 in fall 1979. Completed seventh grade and began eighth before moving to Seoul, Korea again in December 1980. Completed eighth, ninth, and tenth grades at Seoul American High School. Moved to St. Louis, Missouri in June 1984. Completed eleventh grade at Hazelwood Central High School. Moved to Dale City, Virginia in June 1985. Completed senior high school and received high school diploma from Osbourn Park High School in June 1986.

Army brat and damn proud of it.

Moved to Blacksburg, Virginia in September 1986 and began studies in Mechanical Engineering at Virginia Tech which led to a Bachelor of Science degree in December 1990. Began graduate studies in Mechanical Engineering at Virginia Tech in January 1991 which culminated in a Master of Science degree and this thesis in August 1992. Picked up minors in Mathematics and English

along the way, and will have completed a Bachelor of Arts degree in Philosophy by May 1993.

James will pursue a PhD in Mechanical Engineering at Virginia Tech beginning in the Fall of 1992. He plans to complete his degree by the end of summer 1995. By that time, he will have lived in Blacksburg for eight years, by far the longest in one location. He plans to secure a job in the combustion field, and possibly teach his own students at a major university one day. He will not live anywhere he has lived before unless absolutely necessary. He plans to travel frequently.

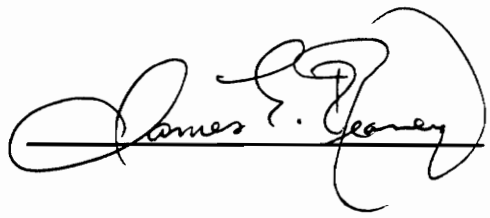

James E. Reaney